

INFORMATION TO USERS

This manuscript has been reproduced from the microfilm master. UMI films the text directly from the original or copy submitted. Thus, some thesis and dissertation copies are in typewriter face, while others may be from any type of computer printer.

The quality of this reproduction is dependent upon the quality of the copy submitted. Broken or indistinct print, colored or poor quality illustrations and photographs, print bleedthrough, substandard margins, and improper alignment can adversely affect reproduction.

In the unlikely event that the author did not send UMI a complete manuscript and there are missing pages, these will be noted. Also, if unauthorized copyright material had to be removed, a note will indicate the deletion.

Oversize materials (e.g., maps, drawings, charts) are reproduced by sectioning the original, beginning at the upper left-hand corner and continuing from left to right in equal sections with small overlaps. Each original is also photographed in one exposure and is included in reduced form at the back of the book.

Photographs included in the original manuscript have been reproduced xerographically in this copy. Higher quality 6" x 9" black and white photographic prints are available for any photographs or illustrations appearing in this copy for an additional charge. Contact UMI directly to order.

UMI[®]

Bell & Howell Information and Learning
300 North Zeeb Road, Ann Arbor, MI 48106-1346 USA
800-521-0600

Novel Graphical Approaches in QCD and the Wess-Zumino Model

by

Omid Hamidi-Ravari

Department of Physics, McGill University

Montréal, Canada

July 1997

A Thesis submitted to the Faculty of Graduate Studies and Research in
partial fulfillment of the requirements for the degree of Doctor of Philosophy

© Omid Hamidi-Ravari, 1997



National Library
of Canada

Acquisitions and
Bibliographic Services

395 Wellington Street
Ottawa ON K1A 0N4
Canada

Bibliothèque nationale
du Canada

Acquisitions et
services bibliographiques

395, rue Wellington
Ottawa ON K1A 0N4
Canada

Your file Votre référence

Our file Notre référence

The author has granted a non-exclusive licence allowing the National Library of Canada to reproduce, loan, distribute or sell copies of this thesis in microform, paper or electronic formats.

The author retains ownership of the copyright in this thesis. Neither the thesis nor substantial extracts from it may be printed or otherwise reproduced without the author's permission.

L'auteur a accordé une licence non exclusive permettant à la Bibliothèque nationale du Canada de reproduire, prêter, distribuer ou vendre des copies de cette thèse sous la forme de microfiche/film, de reproduction sur papier ou sur format électronique.

L'auteur conserve la propriété du droit d'auteur qui protège cette thèse. Ni la thèse ni des extraits substantiels de celle-ci ne doivent être imprimés ou autrement reproduits sans son autorisation.

0-612-36979-X

Canada

Abstract

Quantum Chromodynamics is the underlying theory of hadrons and their interactions. In deriving results from this theory one relies on perturbative calculations. Sometimes indirect methods have been explored to circumvent direct calculation of pure gluonic amplitudes. For example, it has been shown that supersymmetric extension of QCD along with supersymmetric Ward identities can be used to establish relations between amplitudes with the same total number of particles but a different number of gluons. Such relations are used here to connect pure gluonic and pure fermionic amplitudes in the case of 4-pt and 6-pt functions. These relations offer an indirect way of calculating tree level pure gluonic amplitudes since these amplitudes are identical in supersymmetric and non-supersymmetric QCD. The aforementioned relations however, provide no insight into the relation between Feynman diagrams of the amplitudes involved. In this regard, we investigate the relation between individual Feynman diagrams in the Wess-Zumino model.

Another calculational difficulty arises when one is concerned with high energy scattering in QCD. In the high energy regime, because the effective coupling constant is relatively large, it is necessary to sum up an infinite number of diagrams. This is made even more difficult due to the cancellations in certain color channels that occurs at any perturbative order. The new non-abelian cut diagram technique provides considerable assistance by giving the result with the cancellations already built into its rules. Sixth-order calculations are carried out to show the efficiency of this technique. Finally, we consider the question of diagrams with fermion loops that need regularization because of their UV divergence. We find that regularization leads to an enhancement in their high energy behavior.

Résumé

La chromodynamique quantique (QCD) est la théorie décrivant les hadrons ainsi que leurs interactions. Les résultats obtenus dans le cadre de cette théorie font appel à des calculs perturbatifs. Afin d'éviter un calcul direct des amplitudes purement gluoniques, des méthodes indirectes ont été développées. Par exemple, il a été prouvé que l'extension supersymétrique de QCD avec une version supersymétrique des identités de Ward peut être utilisée afin d'établir des relations entre des amplitudes avec un nombre identique de particules mais un nombre différent de gluons. De telles relations sont utilisées ici afin de relier des amplitudes purement gluoniques et purement fermioniques dans les cas de fonction à quatre et six points. Ces relations nous offrent une méthode de calcul indirect des amplitudes gluoniques au niveau des arbres, ces dernières étant identiques dans le cas supersymétriques ou non. Elles ne conviennent par contre aucune intuition en ce qui concerne les diagrammes de Feynman correspondant. Nous recherchons donc l'existence de relations au niveau des diagrammes de Feynman dans le cadre du modèle de Wess et Zumino.

Un autre problème calculatoire apparaît lorsque l'on étudie la diffusion à haute énergie en QCD. A ces énergies, vu l'importance de la constante de couplage effective, il est nécessaire de sommer un nombre infini de diagrammes. Le problème est de plus compliqué par l'existence d'annulation dans certains canaux de couleur à chaque ordre de la série de perturbation. La nouvelle technique des diagrammes non-abéliens tronqués est d'une aide précieuse car elle prend en compte automatiquement ces annulations. Des calculs jusqu'au sixième ordre ont été effectués afin de démontrer l'efficacité de cette méthode. Pour terminer, nous considérons le cas des diagrammes avec des boucles de fermions qui nécessitent une régularisation due à des divergences ultraviolettes. Nous trouvons que la regularization mène à une augmentation de $\ln(s)$ dans leur comportement à haute énergie.

Acknowledgements

I would like to take this opportunity to thank my supervisor, professor C.S. Lam, for his support and patience during the course of this work. His guidance, suggestions and explanations kept me on track and corrected my mistakes and for that I am deeply grateful. I also learned a great deal from the courses I had with my supervisor and professors R.C. Myers, C.P. Burgess and N. de Takacsy to each of whom I feel indebted.

I would also like to thank my friends S. M. Zebarjad, M. R. Garousi, M. Sabouri and M. Dezfouli for countless things too numerous to mention. I also thank my office mates Jason Breckenridge and Y.J. Feng for bearing with me for the past four years. I hope I have not bored Jason with my silly computer questions. I would specially like to thank him for taking his time to read and correct the English mistakes of the original draft. I would also like to thank Philippe Page for his kind help in translating the abstract into French.

My gratitudes are due to the Ministry of Culture and Higher Education of Iran for the scholarship that made my PhD studies possible. I also thank the Carl Reinhardt McGill Major Fellowship for the support during the last year of my studies.

Last but not least, I would like to thank my family for all the moral support they gave me. Having to live apart for the past five years has not been easy on me as it wasn't on them. Their believing in me was the sole driving force at times when the challenge seemed invincible. I hope to have lived up to their expectations. I would like to dedicate this thesis to my parents as a token of my appreciation.

Statement of Original Contributions

Supersymmetric Ward identities are among the techniques used to calculate pure gluonic amplitudes more effectively at tree level. Using these identities we present an independent derivation of the relation between pure gluonic and pure fermionic amplitudes in the 4-pt function case. In this thesis we also derive such a relation in the 6-pt function case which is a new result. Such relations reduce the difficulty of perturbative calculations of pure gluonic amplitudes at tree level to a minimum and are of interest to QCD practitioners. We also carry out a graphical analysis of the Supersymmetric Ward identities in the Wess-Zumino model which show that such relations also exist among individual Feynman diagrams. This analysis sheds light on the inner mechanism of supersymmetric Ward identities.

In high energy near forward scattering in QCD, cancellation of leading (and sometimes subleading) factors of logarithms of energy takes place. In perturbative calculations this leaves us with a vanishing result in the leading log approximation. The new cut-diagram technique [22] effectively deals with this problem. We will present a sixth-order quark-quark scattering calculation [35] which will demonstrate the power of the new technique. Lastly we will compute the high energy behavior of three of the eighth-order QCD diagrams which contain fermion loops and were previously considered in the context of QED [19]. The study of these diagrams is necessary in order to extend the perturbative calculations beyond the well known sixth-order results.

Contents

Abstract	i
Résumé	ii
Acknowledgements	iii
Statement of Original Contributions	iv
1 Introduction	1
2 Supersymmetry	4
2.1 Supersymmetry algebra	6
2.2 Vector Multiplet and supersymmetric Ward identities	7
2.3 A detailed example	14
3 Supersymmetric relations among Feynman diagrams	18
3.1 Wess-Zumino model and basic diagrammatic identities	19
4 High energy scattering	30
4.1 Regge theory	34
4.2 Dispersion relations	37
4.3 The BFKL equation	41

5	Calculating high energy scattering amplitude using non-abelian cut diagrams	48
5.1	High energy kinematics	49
5.2	Abelian cut diagrams	50
5.3	Non-abelian cut diagrams	53
5.4	Lightcone integration	55
5.4.1	The '+' integration	55
5.4.2	The '-' integration	57
5.5	Review of the sixth-order calculations	59
5.6	Sixth-order cut diagram calculations	66
5.6.1	Diagrams A_c , $B1_c$ and $B2_c$	68
5.6.2	Diagrams $\overline{C1}_c$ and $\overline{C2}_c$	70
5.6.3	Diagrams $C3_c$, $C4_c$, $C7_c$, $C8_c$, $C11_c$ and $C12_c$	72
5.6.4	Diagrams $C15_c - C20_c$	73
5.6.5	A recap of the final results	75
5.7	Discussion	76
6	Eighth-Order Diagrams with 4-point fermion loops	78
6.1	Fermion loop subdiagrams	79
6.2	8th-order Calculations	87
A	Conventions and some fine details	101
A.1	Spinor helicity technique	101
A.1.1	Off-shell Fierz identities	104
A.2	Supersymmetry conventions	106
A.3	Some fine details	107
B	Color oriented vertices	111

C Color decomposition of cut and ordinary Feynman diagrams	113
D Dimensional Regularization formulas	117
Bibliography	118

List of Figures

2.1	Color-oriented 4-pt diagrams.	15
3.1	Vertex factors of massless WZ model.	20
3.2	Designation of external states.	20
3.3	Relation 1A.	21
3.4	Relation 1B.	22
3.5	Relation 2A.	23
3.6	Relation 2B.	23
3.7	Relation 3A.	25
3.8	Relation 3B.	25
3.9	Sewing 3-pt functions	26
3.10	Moving the dot from an internal to an external line	26
3.11	A derived relation among 4-pt functions.s	26
3.12	A 4-pt example. SUSY factors;(A1)-[k1], (B1)-[k3], (C1)-[k2] .	28
3.13	An 8-pt example	28
4.1	Elastic scattering in s and t -channels.	35
4.2	The complex l -plane. Regge poles are indicated by dots. (a) Contour C_1 encircles the positive l axis (b) After opening the contour.	36
4.3	Integration contour in (a) s -plane (b) z_t -plane.	40

4.4	The BFKL ladder. Thin lines and thick lines represent elementary and reggeized gluons respectively.	43
5.1	(a) External momenta (b) An electron (quark) \rightarrow electron (quark)	49
5.2	(a) A one loop Feynman diagram (b) its flow diagram	57
5.3	(a) A two-loop Feynman diagram, (b) and (c) its flow diagrams	57
5.4	Quark-quark scattering in QCD up to 6th order. The thick lines at the top and bottom of each diagram are the q-lines, and the thin lines are gluon lines	60
5.5	Color basis.	66
5.6	Space-time cut diagrams	67
5.7	Color cut diagrams	67
5.8	Flow diagrams	69
5.9	Factorization formula applied to $C15_c$	74
6.1	8th-order diagrams.	81
6.2	Fourth-order subdiagrams	83
B.1	Color-oriented vertices.	112
C.1	(a) Triple-gluon color factor, (b),(c) Two identities involving $3g$ vertex.	114
C.2	Two different forms of $if_{bad}t_a t_b = ct_d$	114
C.3	Final set of graphical relations.	115
C.4	A sample calculation of the color of a Feynman diagram.	115
C.5	A sample calculation of the color of a cut diagram.	116

Chapter 1

Introduction

The advancement of physics as an exact science occurs along two interacting directions. The first direction is that of observation and experiment. At this stage one makes measurements of various physical quantities relevant to a certain phenomenon. The results of these measurements are then analyzed, tabulated and plotted against one or more basic physical quantities. At the second stage one faces the challenge of describing this body of data and facts using models and theories constructed for that purpose. A model or a theory is almost always a mathematical construct that attempts to give a clear picture, at least in an algebraic or prescriptive way, of how the phenomenon occurs and progresses. By its nature, the extraction of results from theories involves calculations that are, with the exception of simple models, complicated, and very often an exact result is simply not obtainable. Therefore, a better understanding of a phenomenon depends on how much calculational power, analytic or numerical, one has at one's disposal to tackle the theory that explains that phenomenon.

One such case is that of Quantum Chromodynamics (QCD). This theory is believed to be the underlying theory of hadrons and their interactions. As with any other quantum field theory, an essential tool for extracting results

from QCD is the perturbation technique. This technique, however, is not free of limitations. Due to the complexity of QCD, improved calculational methods to deal with its various aspects are of prime importance.

It is the purpose of this thesis to consider the basics of two of these techniques and to examine examples where they can be applied. The first technique has to do with supersymmetry. By considering the supersymmetric extension of QCD along with supersymmetric Ward identities one is able to relate pure gluonic amplitudes to amplitudes that have fewer numbers of gluons and hence obtain an indirect way of determining tree-level pure gluonic amplitudes. This method works since tree-level pure gluonic amplitudes are identical in supersymmetric and non-supersymmetric QCD. The ensuing simplification is a result of reducing the number of gluons which have complicated self-interaction vertices. We will derive relations connecting the 4-pt and 6-pt pure gluonic amplitudes to the 4-pt and 6-pt pure fermionic ones. We will also address a related question regarding the relation between individual Feynman diagrams in a supersymmetric relation among scattering amplitudes, i.e. supersymmetric Ward identities.

The second technique proves to be suitable for high energy scattering calculations at low momentum transfer, $-t \ll s$ with s the square of energy in the center of mass system. In this energy regime the effective coupling constant, $g^2 \ln(s)$, carries an energy dependent factor and therefore is not necessarily small. This compels one to sum an infinite number of Feynman diagrams each calculated in the leading $\ln(s)$ approximation. It then turns out that the leading contributions to certain color channels at any order of perturbation cancel out. This obliges one to calculate each diagram to its non-leading contribution, which is an enormous task. The technique of non-abelian cut diagrams, introduced recently, is an improved calculational

method that gives the result for the sum of diagrams at each order of perturbation with all the cancellations already built into its rules. As a result what one calculates is directly the result after the cancellations have been done. We will work out in detail the quark-quark scattering up to sixth-order using this new technique to demonstrate its efficiency.

In the high energy perturbative calculations, diagrams containing fermion loops are believed to make only non-leading contributions. In the context of QCD such diagrams suffer from UV divergences that must be handled before high energy calculations can be carried out. We find that as a result of regularization the high energy behavior of such diagrams demonstrates an enhancement in energy dependence over similar situations in QED.

The outline of the thesis is as follows. In chapter 2 after a quick review of the essentials of supersymmetry, the supersymmetric Ward identities will be used to work out the relation between the 4-pt and 6-pt pure gluonic and pure fermionic amplitudes. In chapter 3 a further endeavor will be undertaken which will result in establishing relations among individual Feynman diagrams. Chapter 4 contains a brief review of the historical development of the high energy scattering experiments that demonstrated the growth of the total hadronic scattering cross section with energy along with some of the theoretical ideas developed to explain them. In chapter 5 the newly developed non-abelian cut diagram technique will be introduced and applied to quark-quark scattering up to sixth-order. Finally, in chapter 6, the high energy behavior of diagrams containing fermion loops that require regularization will be addressed.

Chapter 2

Supersymmetry

In this part of the thesis we will consider a particular aspect of supersymmetry (SUSY) [1]. No doubt much can be said about mathematical construction of SUSY, its group theoretical content, and how it has been employed fruitfully in various quantum field theories. Out of all that, what is of interest to us here is how different SUSY scattering amplitudes are related and in what ways such relations can be exploited. Before getting too specific let us have a general look at SUSY.

Supersymmetry is a symmetry between fermions (matter) and bosons (carriers of interactions). Since fermions generally have half-odd-integer spin and bosons have integer spin, SUSY must change the spin content of the fields describing these particles. In a SUSY quantum field theory one generally talks about a supermultiplet, i.e., a set of fields with spins differing by $1/2$ which transform into each other under SUSY transformations. Examples are scalar multiplet consisting of a Majorana (self-conjugate) fermion and a complex scalar field or a vector multiplet consisting of a spin one vector field and a Majorana fermion. The particles (fields) transforming into each other under SUSY are called superpartners. We will review the Wess-Zumino model based on scalar multiplet as well as vector model in the next two

sections.

Despite its great beauty, to date, SUSY remains as a model since none of the predicted SUSY partners of the known particles have yet been observed. Whether or not SUSY is a true symmetry of nature, one can still benefit from it in a different way. The reason for this inherent potential lies in the fact that in a SUSY theory gauge bosons (relatively complicated objects with regard to their interactions) are related to fermions (less involved in their interactions). Through the use of Supersymmetric Ward Identities (SWI) [2, 3] one can establish a relation between an amplitude with external gauge bosons and one that has some of those bosons replaced by fermions. This is a well known technique and has been used in the calculation of primitive color oriented gluon amplitudes [4]. In these works one pair of gluons is replaced with a pair of gluinos (gluino is the SUSY partner of gluon). One can, however, repeat this process in succession and replace as many gluon pairs as possible which will proportionally reduce the amount of necessary subsequent diagrammatic calculations. Here we consider cases where one can find explicit relations between pure gluon and pure gluino amplitudes. These turn out to be two special cases of the 4-pt and the 6-pt function amplitudes.

The fact that SWI relate different SUSY amplitudes does not tell how individual diagrams are related. A natural question is whether or not one can establish relations between individual Feynman diagrams in a quest to find a more effective way of calculating Feynman diagrams. We will address this question in the Wess-Zumino model in chapter 3. As will be seen, this is done effectively by introducing a dot (to be explained later) that sits on an external line of the diagram of interest. By moving this dot through the diagram to all the allowed external legs one can generate a unique set of diagrams that sum to zero. Each of the diagrams in this relation belong to an amplitude

that are altogether related by SUSY Ward identities. Establishing a similar relation in SUSY Yang-Mills theory is more involved and is the substance for a future work.

2.1 Supersymmetry algebra

In order to derive SWI we would need some familiarity with SUSY itself. A thorough discussion of the SUSY algebra will pull us away from our main purpose so we will review only those essential elements that we will be using later. Our consideration is restricted to $N = 1$ supersymmetry, i.e., the simplest case where one only has one supersymmetric generator Q as opposed to extended supersymmetry where one has several generators, Q^A , $A = 1, \dots, N$.

In its simplest form, SUSY is an extension of the Lie algebra of the Poincare group to a Graded Lie Algebra (GLA) via introducing a self-conjugate spinor ¹, Q_α , of spin $\frac{1}{2}$. The (anti) commutations relations of the SUSY algebra are [5, 6],

$$\begin{aligned} [Q_\alpha, M^{\mu\nu}] &= i(\sigma^{\mu\nu} Q)_\alpha, \\ [Q_\alpha, P^\mu] &= 0, \\ \{Q_\alpha, \bar{Q}_\beta\} &= 2(\gamma_\mu)_{\alpha\beta} P^\mu, \end{aligned} \tag{2.1.1}$$

where μ and ν are space-time and α and β spinor indices. In these relations $M^{\mu\nu}$ are the generators of Lorentz boosts and P^μ are the generator of translation. Because of the spinorial nature of Q_α this algebra involves both commutators and anticommutators. By introducing a pair of anticommuting parameters $\bar{\xi}_\alpha$ and η_β the last relation in (2.1.1) may be written as a

¹For a list of our conventions see App. A.2.

commutator relation,

$$\bar{\xi}_\alpha \{Q_\alpha, \bar{Q}_\beta\} \eta_\beta = [\bar{\xi}Q, \bar{Q}\eta] = 2\bar{\xi}\gamma_\mu\eta P^\mu \quad (2.1.2)$$

This fact is related to the property that a GLA over complex numbers can actually be converted into an ordinary Lie algebra over a Grassmann algebra [7]

$$\{\theta^a, \theta^b\} = 0 \quad \forall \theta^i \in \{\theta^j\}, j = 1, \dots, N.$$

2.2 Vector Multiplet and supersymmetric Ward identities

In this section we will focus our attention on the SUSY extension of pure Yang-Mills (YM) gauge theory. Our aim is to extend the results of the previous works [3, 8] and to relate the scattering amplitudes involving only gluons to those which involve only gluinos (fermions). One can do this in certain cases.

The SUSY extension of the classical Lagrangian for the pure YM theory in Wess-Zumino gauge is given by [6]

$$\mathcal{L} = -\frac{1}{4}F^{(a)\mu\nu}F_{\mu\nu}^{(a)} + \frac{1}{2}i\bar{\lambda}^a\gamma^\nu\mathcal{D}_\nu\lambda^a + \frac{1}{2}D^aD^a, \quad (2.2.3)$$

$$F_{\mu\nu}^a = \partial_\mu A_\nu^a - \partial_\nu A_\mu^a + gf^{abc}A_\mu^bA_\nu^c,$$

$$\mathcal{D}_\nu\lambda = \partial_\nu\lambda^a + gf^{abc}A_\nu^b\lambda^c, \quad (2.2.4)$$

where all spinor indices have been suppressed. The Lagrangian \mathcal{L} involves the gluon field represented by the spin-1 vector A_μ^a , the gluino field represented by the spin $\frac{1}{2}$ Majorana field λ^a and the auxiliary real field D^a , with a the gauge group index. Note that all these particles belong to the same adjoint representation of the gauge group $SU(N)$. The auxiliary field D^a has no observable physical effect because it has no kinetic term in \mathcal{L} . The reason for

introducing it is the original desire to have unconstrained SUSY invariance. The Lagrangian in (2.2.3) is invariant, $\delta\mathcal{L} = 0$, under SUSY transformations defined by,

$$\begin{aligned}\delta\lambda^a &= -\frac{1}{2}i\sigma^{\mu\nu}\xi F_{\mu\nu}^a - \gamma_5\xi D^a \\ \delta A_\mu^a &= i\bar{\xi}\gamma_\mu\lambda^a \\ \delta D^a &= -i\bar{\xi}\gamma^\mu\gamma_5\mathcal{D}_\mu\lambda^a\end{aligned}\tag{2.2.5}$$

where ξ is the infinitesimal spinor. Taking \mathcal{L} as describing a quantum field theory then $\delta\Phi \equiv i[\bar{\xi}Q, \Phi]$ where Q is the SUSY generator and Φ stands for any of the fields λ^a , A_μ^a or D^a . In order to find the SUSY relations among on-shell scattering amplitudes we would need the transformations of on-shell particle creation and annihilation operators. These are not difficult to find, (see App. (A.3)) and the result is

$$\begin{aligned}[\hat{Q}, \hat{\Lambda}_\pm^\dagger(p)] &= \pm\sqrt{2}N_\pm(p, k)\hat{g}_\pm^\dagger(p) & ; & \quad [\hat{Q}, \hat{g}_\pm^\dagger(p)] = \pm\sqrt{2}N_\mp(p, k)\hat{\Lambda}_\pm^\dagger(p) \\ [\hat{Q}, \hat{\Lambda}_\pm(p)] &= \pm\sqrt{2}N_\mp(p, k)\hat{g}_\pm(p) & ; & \quad [\hat{Q}, \hat{g}_\pm(p)] = \mp\sqrt{2}N_\pm(p, k)\hat{\Lambda}_\pm(p)\end{aligned}\tag{2.2.6}$$

where $\hat{Q} \equiv \bar{\xi}Q$, $\hat{\Lambda}^\pm$ and \hat{g}^\pm are the fermion (gluino) and gluon annihilation operators and the constants $N_\pm(p, k)$ are defined by

$$N_+ = \theta [kp] \quad ; \quad N_- = \bar{\theta} \langle kp \rangle\tag{2.2.7}$$

in which θ and $\bar{\theta}$ are two anticommuting constants and²

$$[kp] \equiv \bar{u}_+(k)u_-(p) \quad ; \quad \langle kp \rangle \equiv \bar{u}_-(k)u_+(p) \cdot$$

These commutation relations are sufficient for us to work out supersymmetric Ward identities. Consider a product of a number of on-shell creation and

²For a more thorough description of the notations see App. A.1

annihilation operators. Due to the fact that the generator of supersymmetry annihilates the supersymmetric vacuum, the commutator of \widehat{Q} and any combination of these on-shell operators will have a vanishing vacuum expectation value. If Φ_i represents any of these operators, then we obtain the following Supersymmetric Ward Identity (SWI) [2, 3],

$$0 = \langle 0 | [\widehat{Q}, \prod_{i=1}^n \Phi_i] | 0 \rangle = \sum_{i=1}^n \langle 0 | \Phi_1 \cdots [\widehat{Q}, \Phi_i] \cdots \Phi_n | 0 \rangle \quad (2.2.8)$$

This equation is nothing but a relation among supersymmetric amplitudes. As a warm up exercise we first go over some of the well known results. For brevity we will drop the $\widehat{}$ over the operators and assume all the particles to be out-going. So our notation in the following will be $\widehat{g}^\pm(p_i) = g_i^\pm$, and similarly for other operators. Consider the following choice of operators,

$$0 = \langle 0 | [Q, \Lambda_1^+ g_2^+ \cdots g_n^+] | 0 \rangle = N_-(p_1, k) M(g_1^+, g_2^+, \cdots, g_n^+) \\ + N_+(p_2, k) M(\Lambda_1^+, \Lambda_2^+, \cdots, g_n^+) + \cdots + N_+(p_n, k) M(\Lambda_n^+, g_2^+, \cdots, \Lambda_n^+) \quad (2.2.9)$$

Notice the sign flip of the SUSY factors $[-N_+(p_i, k)]$ in all but the first term because this factor carries the noncommuting constant θ that produces a minus sign when moved past Λ_1^+ . Since for a massless fermion all fermion-vector couplings are helicity conserving, all the terms on the second line will vanish since two out-going fermions of the same helicity are equivalent to a helicity flipped in \rightarrow out pair of fermions. As a consequence the first term having only gluons must vanish too. This result is usually put as follows: maximal helicity violation is forbidden. This fact holds true to any order of perturbation and is also true at tree level in a non-supersymmetric theory.

Let us consider another example and start from the same string of operators but with one negative helicity gluon,

$$0 = \langle 0 | [Q, \Lambda_1^+ g_2^- g_3^+ \cdots g_n^+] | 0 \rangle = \cdots$$

$$N_-(p_1, k)M(g_1^+, g_2^-, \dots, g_n^+) + N_-(p_2, k)M(\Lambda_1^+, \Lambda_2^-, \dots, g_n^+) \quad (2.2.10)$$

where we have dropped all the vanishing terms possessing two fermions with the same helicity. Here we still have the option of choosing k . If we let $k = p_1$ the first term will vanish and for the equality to hold the second term must vanish also. So an amplitude with a pair of fermions and any number of gluons with the same helicity vanishes. If we let $k = p_2$ the second term will vanish and therefore an all gluon amplitude with only one nonidentical gluon helicity will vanish.

A non-vanishing example would be the following. Let us start with the same string of operators as (2.2.8) but with two negative helicity gluons,

$$\begin{aligned} 0 = \langle 0 | [Q, \Lambda_1^+ g_2^- g_3^- g_4^+ \dots g_n^+] | 0 \rangle = & N_-(p_1, k)M(g_1^+, g_2^-, g_3^-, \dots, g_n^+) \\ & + N_-(p_2, k)M(\Lambda_1^+, \Lambda_2^-, g_3^-, \dots, g_n^+) + N_-(p_3, k)M(\Lambda_1^+, g_2^-, \Lambda_3^-, \dots, g_n^+) \end{aligned} \quad (2.2.11)$$

Now if we simply let $k = p_3$ we will obtain

$$M(g_1^+, g_2^-, g_3^-, g_4^+, \dots, g_n^+) = -\frac{\langle 32 \rangle}{\langle 31 \rangle} M(\Lambda_1^+, \Lambda_2^-, g_3^-, \dots, g_n^+) \cdot \quad (2.2.12)$$

As can be seen, a single application of (2.2.8) has the potential of relating amplitudes with one pair of fermions to an all-gluon amplitude. Similar examples with different initial helicity structures can be worked out. In all of them the pure gluonic amplitude will be related to a sum of amplitudes with one pair of gluons replaced by gluinos. What we would like to do is to make multiple use of (2.2.8) and try to replace all gluons with fermions. This will only be possible in amplitudes with an even number of particles.

We will start by considering the simplest case of four particles. In this case it turns out that we need two initial combinations. These are

$$S_1 = \Lambda_1^+ g_2^+ g_3^- g_4^- \quad ; \quad S_2 = \Lambda_1^+ \Lambda_2^+ \Lambda_3^- g_4^- \cdot \quad (2.2.13)$$

Taking the vacuum expectation value of the commutator of each of these combinations with Q will give

$$\begin{aligned} \langle k_1 1 \rangle M_1 - \langle k_1 3 \rangle M_2 - \langle k_1 4 \rangle M_3 &= 0, \\ \langle k_2 1 \rangle M_4 - \langle k_2 2 \rangle M_2 - \langle k_2 4 \rangle M_5 &= 0, \end{aligned} \quad (2.2.14)$$

where M_i are amplitudes defined by

$$\begin{aligned} M_1 &\equiv M_1(g_1^+, g_2^+, g_3^-, g_4^-), \\ M_2 &\equiv M_2(\Lambda_1^+, g_2^+, \Lambda_3^-, g_4^-), \\ M_3 &\equiv M_3(\Lambda_1^+, g_2^+, g_3^-, \Lambda_4^-), \\ M_4 &\equiv M_4(g_1^+, \Lambda_2^+, \Lambda_3^-, g_4^-), \\ M_5 &\equiv M_5(\Lambda_1^+, \Lambda_2^+, \Lambda_3^-, \Lambda_4^-). \end{aligned} \quad (2.2.15)$$

Note that these equations have each been derived separately and thus are independent. The two different values k_1 and k_2 reflect this independence. Now if we let $k_1 = p_4$ and $k_2 = p_1$ we will get,

$$\langle 4 1 \rangle M_1 - \langle 4 3 \rangle M_2 = 0 \quad ; \quad \langle 1 2 \rangle M_2 + \langle 1 4 \rangle M_5 = 0 \quad (2.2.16)$$

from which we conclude,

$$M_1(g_1^+, g_2^+, g_3^-, g_4^-) = \frac{\langle 4 3 \rangle}{\langle 1 2 \rangle} M_5(\Lambda_1^+, \Lambda_2^+, \Lambda_3^-, \Lambda_4^-). \quad (2.2.17)$$

A similar result has been derived in [8]. There are two conclusions we can draw from this result. From a calculational point of view, it is far more simpler to calculate an all fermion 4-point amplitude than to calculate one with external gluon lines due to the complexity of the three and four gluon vertices. Secondly, this result shows at a glance the gauge independence of the amplitude M_1 from the gauge dependencies of external gluons since on the right hand side everything is explicitly gauge independent.

This result may seem like pure luck, and in general it is not *a priori* clear that one can get such relations when more particles are involved. To examine the possibility we have to consider six-point functions. Here again one is seeking an equation relating an amplitude with six external gluons to one that has six external fermions (gluinos). It turns out that this case is quite a bit more laborious than the 4-point case. The reason for this is that in each application of (2.2.8), one obtains a relation between amplitudes that in general have $2m$ fermions and l gluons and those that have $2(m-1)$ fermions and $(l+2)$ gluons. For $m=3$ and $l=0$ the all-fermion amplitude will appear together with the amplitudes having four fermions and two gluons. Then it is necessary to repeat the procedure starting with a different initial operator combination so as to get relations between $(4\Lambda, 2g)$ and $(2\Lambda, 4g)$ type amplitudes. Repeating this once again finally establishes relation between the $(2\Lambda, 4g)$ type and the $(6g)$ amplitudes. Once these equations are laid out one has to solve the linear system of equations for the desired relation.

To begin, it would be better to adopt a more economical notation. From now on the helicity index ' \pm ' will be suppressed and in order to remove the resulting ambiguity we will assume that the first three operators from the left have positive and the last three have negative helicities. The amplitude with six gluons will be denoted by G and the one with six fermions by F . A general notation for the amplitudes with two fermions (and four gluons) will be M_{ij} with i and j indicating the location of the two fermions, counted from the left. A general notation for the amplitudes with two gluons (and four fermions) will be N_{ij} with i and j locating the two gluons within the set, counted from the left. We will also use f to denote a fermion rather than Λ .

We will start by introducing the different initial operator combinations

to be used. They are

$$\begin{aligned}
S_1 &= fggggg & ; & & S_2 &= gfgggg & ; & & S_3 &= ggfggg & ; & & S_4 &= gggfgg \\
S_5 &= gffffff & ; & & S_6 &= fgffff & ; & & S_7 &= ffgfff & ; & & S_8 &= fffgff \\
S_9 &= ffgfgg & ; & & S_{10} &= ffggfg . & & & & & & & & & (2.2.18)
\end{aligned}$$

Using (2.2.8) we will get the following set of equations for S_1, \dots, S_4

$$\begin{aligned}
\langle k_1 1 \rangle G - \langle k_1 4 \rangle M_{14} - \langle k_1 5 \rangle M_{15} - \langle k_1 6 \rangle M_{16} &= 0 \\
\langle k_2 2 \rangle G - \langle k_2 4 \rangle M_{24} - \langle k_2 5 \rangle M_{25} - \langle k_2 6 \rangle M_{26} &= 0 \\
\langle k_3 3 \rangle G - \langle k_3 4 \rangle M_{34} - \langle k_3 5 \rangle M_{35} - \langle k_3 6 \rangle M_{36} &= 0 \\
[k_4 1]M_{14} + [k_4 2]M_{24} + [k_4 3]M_{34} + [k_4 4]G &= (2.2.19)
\end{aligned}$$

Similarly for S_5, \dots, S_8 we will get

$$\begin{aligned}
[q_1 1]F + [q_1 4]N_{14} - [q_1 5]N_{15} + [q_1 6]N_{16} &= 0 \\
-[q_2 2]F + [q_2 4]N_{24} - [q_2 5]N_{25} + [q_2 6]N_{26} &= 0 \\
[q_3 3]F + [q_3 4]N_{34} - [q_3 5]N_{35} + [q_3 6]N_{36} &= 0 \\
\langle q_4 1 \rangle N_{14} - \langle q_4 2 \rangle N_{24} + \langle q_4 3 \rangle N_{34} - \langle q_4 4 \rangle F &= 0(2.2.20)
\end{aligned}$$

And lastly for S_9 and S_{10}

$$\begin{aligned}
\langle k 1 \rangle M_{24} - \langle k 2 \rangle M_{14} - \langle k 5 \rangle N_{36} - \langle k 6 \rangle N_{35} &= 0 \\
\langle q 1 \rangle M_{25} - \langle q 2 \rangle M_{15} + \langle q 4 \rangle N_{36} - \langle q 6 \rangle N_{34} &= 0(2.2.21)
\end{aligned}$$

Each set of equations in (2.2.19) and (2.2.20) contain ten variables (amplitudes). By choosing two different values for each k_i and q_i , each set will have eight equations. In the set corresponding to (2.2.19), we will choose G and M_{36} as independent and will solve for the other M_{ij} in terms of these two amplitudes. In the set corresponding to (2.2.20), we will choose F and N_{36} as

independent and will solve for the other N_{ij} in terms of these two. Lastly by assigning $k = 5, 6$ and $q = 6$ in (2.2.21) we will solve for the desired relation, i.e., G in terms of F .

The calculation, although straightforward, involves lengthy matrix computations and the final result is

$$G = \frac{\langle 56 \rangle \{2[53] p_6 \cdot (p_1 + p_2) - [63]([\langle 51 \rangle \langle 16 \rangle + \langle 52 \rangle \langle 26 \rangle])\}}{[54][56] (\langle 51 \rangle \langle 62 \rangle - \langle 52 \rangle \langle 61 \rangle)} F . \quad (2.2.22)$$

It should be mentioned that the authors in [3] considered this case but did not give the relation between the six-gluon and six-fermion amplitudes. Unfortunately we have not yet found a clear interpretation of the special type of functional dependence in (2.2.22).

For higher numbers of particles one can still make multiple use of (2.2.8), but a single relation involving F and G type amplitudes alone seems unlikely due to the large number of variables which will eventually exceed the number of equations.

2.3 A detailed example

In order to see the type of calculational efficiency that relations of the form (2.2.17) can provide, we will work out the 4-pt pure fermionic and pure gluonic amplitudes. In general, instead of the whole amplitude one can consider color-oriented subamplitudes. A color-oriented amplitude is constructed from color-oriented vertices. In App.(B) we show how color-oriented vertices can be derived from normal vertices. These subamplitudes in general contain fewer number of diagrams than the complete amplitude and yet are still gauge invariant [9, 10]. With this brief introduction, the color-oriented diagrams for 4-pt pure gluonic and pure fermionic amplitudes are shown in

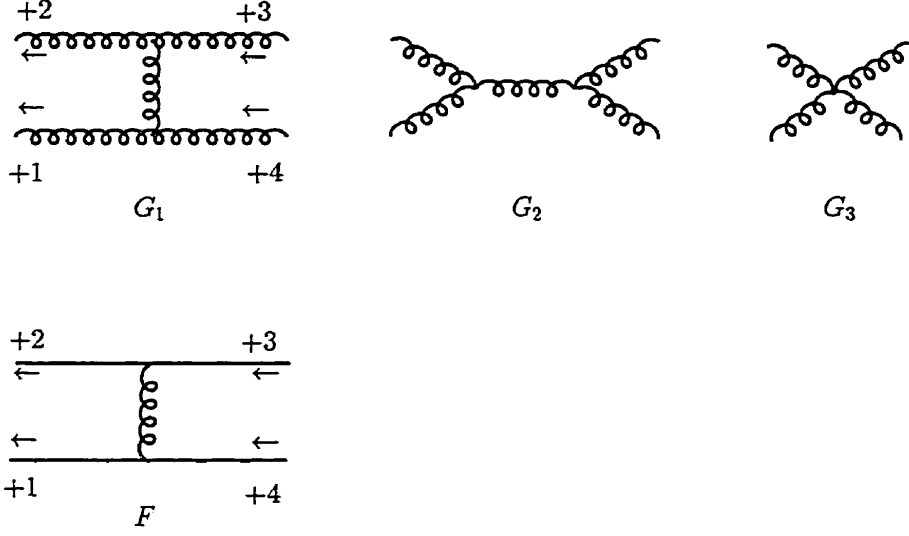


Figure 2.1: Color-oriented 4-pt diagrams.

Fig.(2.1). The expression corresponding to each of the diagrams is given below,

$$\begin{aligned}
G_1 &= \text{Tr}(t^a t^b t^c t^d) \frac{g^2}{-2p_3 \cdot p_2} \\
&\times \{ 2p_3 \cdot \epsilon_+(2)(p_4 - p_1) \cdot \epsilon_-(3)\epsilon_-(4) \cdot \epsilon_+(1) \\
&+ 2p_2 \cdot \epsilon_-(3)(p_4 + p_1) \cdot \epsilon_+(2)\epsilon_-(4) \cdot \epsilon_+(1) \\
&- \epsilon_+(2) \cdot \epsilon_-(3)\epsilon_-(4) \cdot \epsilon_+(1)(p_2 + p_3) \cdot (p_4 + p_1) \\
&- 4\epsilon_-(3) \cdot \epsilon_+(1)p_3 \cdot \epsilon_+(2)p_1 \cdot \epsilon_-(4) \\
&- 4\epsilon_-(3) \cdot \epsilon_-(4)p_3 \cdot \epsilon_+(2)p_4 \cdot \epsilon_+(1) \\
&- 4\epsilon_+(2) \cdot \epsilon_+(1)p_2 \cdot \epsilon_-(3)p_1 \cdot \epsilon_-(4) \\
&- 4\epsilon_+(2) \cdot \epsilon_-(4)p_2 \cdot \epsilon_-(3)p_4 \cdot \epsilon_+(1) \\
&+ 2\epsilon_+(2) \cdot \epsilon_-(3)(p_2 + p_3) \cdot \epsilon_+(4)p_4 \cdot \epsilon_+(1) \\
&+ 2\epsilon_+(2) \cdot \epsilon_-(3)(p_2 + p_3) \cdot \epsilon_+(1)p_1 \cdot \epsilon_-(4) \} , \quad (2.3.23) \\
G_2 &= \text{Tr}(t^a t^b t^c t^d) \frac{g^2}{2p_1 \cdot p_2} \\
&\times \{ (p_1 + p_2) \cdot (p_4 - p_3)\epsilon_+(1) \cdot \epsilon_+(2)\epsilon_-(3) \cdot \epsilon_-(4)
\end{aligned}$$

$$\begin{aligned}
& +2(p_1 + p_2) \cdot \epsilon_-(3)p_3 \cdot \epsilon_-(4)\epsilon_+(1) \cdot \epsilon_+(2) \\
& -2(p_1 + p_2) \cdot \epsilon_-(4)p_4 \cdot \epsilon_-(3)\epsilon_+(1) \cdot \epsilon_+(2) \\
& -2p_1\epsilon_+(2)(p_4 - p_3) \cdot \epsilon_+(1)\epsilon_-(3) \cdot \epsilon_-(4) \\
& -4p_1 \cdot \epsilon_+(2)p_3 \cdot \epsilon_-(4)\epsilon_+(1) \cdot \epsilon_-(3) \\
& -4p_2 \cdot \epsilon_+(1)p_4 \cdot \epsilon_-(3)\epsilon_+(2) \cdot \epsilon_-(4) \\
& +2p_2 \cdot \epsilon_+(1)(p_4 - p_3) \cdot \epsilon_+(2)\epsilon_-(3) \cdot \epsilon_-(4) \\
& +4p_2\epsilon_+(1)p_3 \cdot \epsilon_-(4)\epsilon_+(2) \cdot \epsilon_-(3) \\
& +4p_1 \cdot \epsilon_+(2)p_4 \cdot \epsilon_-(3)\epsilon_-(4) \cdot \epsilon_+(1) \} , \tag{2.3.24}
\end{aligned}$$

$$\begin{aligned}
G_3 & = Tr(t^a t^b t^c t^d) g^2 \\
& \times \{ 2\epsilon_+(1) \cdot \epsilon_-(3)\epsilon_+(2) \cdot \epsilon_-(4) \\
& -\epsilon_+(1) \cdot \epsilon_-(4)\epsilon_+(2) \cdot \epsilon_-(3) \\
& -\epsilon_+(1) \cdot \epsilon_+(2)\epsilon_-(3) \cdot \epsilon_-(4) \} , \tag{2.3.25}
\end{aligned}$$

$$F = Tr(t^a t^b t^c t^d) \frac{-g^2}{-2p_3 \cdot p_2} \langle 2 + |\gamma^\mu|3+ \rangle \langle 1 + |\gamma_\mu|4+ \rangle \tag{2.3.26}$$

For general helicity of the polarization vectors³ (not written explicitly), straightforward counting shows that G_1 and G_2 have 14 terms each and G_3 has 3 terms. The high number of terms in each diagram is due in part to the gauge dependencies of 3g and 4g vertices. Summing up the diagrams will bring about cancellation of gauge dependent terms and the result will be vastly simpler than any of the individual diagrams. Using (2.2.17) however, we can indirectly obtain the result. We will have,

$$\begin{aligned}
G_1 + G_2 + G_3 & = \frac{\langle 43 \rangle}{\langle 12 \rangle} F \\
& = \frac{\langle 43 \rangle}{\langle 12 \rangle} \left(\frac{2[21] \langle 43 \rangle}{-[23] \langle 32 \rangle} \right) \tag{2.3.27}
\end{aligned}$$

³See equation (A.1.16) for the spinor-helicity representation of the polarization vector.

As one can clearly see, the sum of 31 terms of the gluonic diagrams on the left hand side reduces to just one term. In the 6-pt function case, one of course has many more color-oriented diagrams than in the 4-pt case. Here again, by first summing the pure fermionic diagrams one calculates F and then through (2.2.22) one can indirectly find the pure gluonic 6-pt diagram.

Chapter 3

Supersymmetric relations among Feynman diagrams

In the previous chapter we saw how SWI establishes relations among scattering amplitudes. The relations found have the potential to assist one in calculating scattering amplitudes in a more efficient way. An amplitude in the perturbative language consists of the sum of Feynman diagrams that grow in complexity with the order of perturbation. The relations found using SWI relate these perturbative sums but are silent about the possible relation between individual Feynman diagrams within each of these amplitudes. One could think of this as a global picture of the relation since the role of individual diagrams is not clear. A natural question is then whether or not we can find a relation between individual Feynman diagrams of amplitudes related by SWI? Our aim in this chapter is to explore the answer to this question. For reasons that will be mentioned later such a relation is particularly difficult to find in the case of supersymmetric Yang-Mills theory. We have succeeded, however, in finding the relation between Feynman diagrams in the Wess-Zumino model (WZ) [1]. The particle multiplet of the WZ model consists of a Majorana (self-conjugate) fermion ψ , a complex scalar field ϕ and an auxiliary scalar field F . The ψ and ϕ field could both have mass m

or both be massless. In our treatment we will specialize to the massless case. We will begin with a brief review of this model.

3.1 Wess-Zumino model and basic diagrammatic identities

The WZ model is the supersymmetric extension of the complex Klein Gordon field theory in which ϕ acquires a supersymmetric partner ψ , a spin $\frac{1}{2}$ Majorana fermion. The Lagrangian describing WZ model is [1],

$$\mathcal{L} = \mathcal{L}_0 + \mathcal{L}_m + \mathcal{L}_g, \quad (3.1.1)$$

$$\begin{aligned} \mathcal{L}_0 &= \partial_\mu \phi \partial^\mu \phi^* + \frac{1}{2} i \bar{\psi} \not{\partial} \psi + F F^*, \\ \mathcal{L}_m &= -m(\phi F + \phi^* F^*) - \frac{1}{2} m \bar{\psi} \psi, \\ \mathcal{L}_g &= -g\sqrt{2} [(\phi^2 F + \phi^{*2} F^*) + \bar{\psi}(\phi P_R + \phi^* P_L)\psi], \end{aligned} \quad (3.1.2)$$

where the right P_R and left P_L projection operators are defined by,

$$P_R \equiv \frac{1}{2}(1 + i\gamma_5) \quad ; \quad P_L \equiv \frac{1}{2}(1 - i\gamma_5). \quad (3.1.3)$$

The complex scalar field F is an auxiliary field introduced to maintain unconstrained supersymmetry. Since it has no kinetic term it does not propagate and thus can be removed using its equation of motion. The resulting Lagrangian containing only the physical fields will then be

$$\begin{aligned} \mathcal{L} &= \partial_\mu \phi \partial^\mu \phi^* - m^2 \phi \phi^* + \frac{1}{2} \bar{\psi} (i\not{\partial} - m) \psi - \sqrt{2} m g \phi \phi^* (\phi + \phi^*) \\ &\quad - \sqrt{2} g \bar{\psi} [\phi P_R + \phi^* P_L] \psi - 2g^2 (\phi \phi^*)^2 \end{aligned} \quad (3.1.4)$$

This Lagrangian is invariant under SUSY transformations,

$$\delta \phi = \sqrt{2} \bar{\xi} P_R \psi = \sqrt{2} \bar{\psi} P_R \xi$$

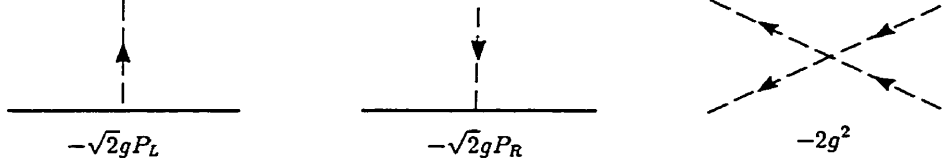


Figure 3.1: Vertex factors of massless WZ model.



Figure 3.2: Designation of external states.

$$\begin{aligned}
\delta\phi^* &= \sqrt{2}\bar{\xi}P_L\psi = \sqrt{2}\bar{\psi}P_L\xi \\
\delta\psi &= -\sqrt{2}\left[i\bar{\not{\partial}} + m + \sqrt{2}g(\phi P_L + \phi^*P_R)\right](\phi P_L + \phi^*P_R)\xi \\
\delta\bar{\psi} &= -\sqrt{2}\bar{\xi}(\phi P_L + \phi^*P_R)\left[-i\overleftarrow{\not{\partial}} + m + \sqrt{2}g(\phi P_L + \phi^*P_R)\right] \quad (3.1.5)
\end{aligned}$$

Using a similar method to that explained in App. (A.3) we can write down the SUSY transformations of the on-shell operators. They are

$$\begin{aligned}
[Q, \Lambda_+^\dagger(p)] &= +N_-(k, p)a^\dagger(p) \quad ; \quad [Q, \Lambda_-^\dagger(p)] = -N_+(k, p)b^\dagger(p) , \\
[Q, a^\dagger(p)] &= +N_+(k, p)\Lambda_+^\dagger(p) \quad ; \quad [Q, b^\dagger(p)] = -N_-(k, p)\Lambda_-^\dagger(p) , \\
[Q, \Lambda_+(p)] &= -N_+(k, p)a(p) \quad ; \quad [Q, \Lambda_-(p)] = +N_-(k, p)b(p) , \\
[Q, a(p)] &= +N_-(k, p)\Lambda_+(p) \quad ; \quad [Q, b(p)] = -N_+(k, p)\Lambda_-(p) , \quad (3.1.6)
\end{aligned}$$

where the constants N_+ and N_- are defined by

$$N_+(k, p) = i\sqrt{2}\theta[kp] \quad ; \quad N_-(k, p) = i\sqrt{2}\bar{\theta} \langle kp \rangle . \quad (3.1.7)$$

In (3.1.6) $a(p)$ and $b(p)$ are the annihilation operators of the scalar particle and its antiparticle.

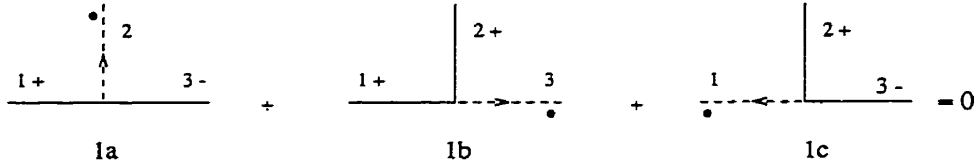


Figure 3.3: Relation 1A.

From now on we specialize to massless, $m = 0$, WZ model. Using the Lagrangian (3.1.2) one can easily extract the vertex factors which are shown in Fig.(3.1). The dashed line represents the boson particle. It indicates a boson, type a , if the momentum and the arrow are parallel and an anti-boson, type b , if they are anti-parallel. The fermion line does not carry an arrow since it represents a Majorana fermion. In writing down the expression associated with a Feynman diagram however, this seems to pose an ambiguity since one is not guided naturally to the right order of gamma matrices. This ambiguity can be removed by associating an arbitrary, but fixed, direction with the fermion line. Figure (3.2) shows the way external states will be assigned. Since the fermion-boson vertices carry projection operators $P_{R,L}$ the helicity of the states on opposite sides of the vertex must be different.

In order to find the relation between Feynman diagrams we need to consider some basic relations. These relations can best be presented using the *dot* convention. We place a dot on a fermion (boson) line to indicate that it is a supersymmetrically transformed line. Thus removing a dot from a fermion (boson) line will change it back to a boson (fermion). There is a factor associated with the dot depending on where it is. These factors can be read from the right-hand sides of commutation relations (3.1.6). For example, if the dot is on a positive helicity fermion line with a momentum pointing outward (away from the vertex) it represents $+N_-(k, p)$ or a dot on an incoming a type fermion is $+N_-(k, p)$ and is $-N_+(k, p)$ on an outgoing

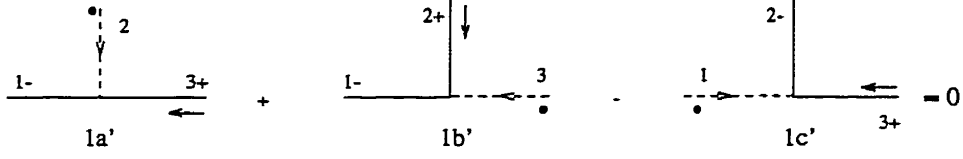


Figure 3.4: Relation 1B.

one. With this brief introduction we can now consider the basic relations. They are as follows:

- **Relation 1.**

Referring to Fig.(3.3) with $p_{in} = p_3$ and $p_{out} = p_1 + p_2$ and following the rule for writing the associated expression we have,

$$\begin{aligned}
 1a &= (-1) \langle k + \not{p}_2 | p_{b+} \rangle \langle p_a - \not{p}_1 P_L \not{p}_3 | p_{c+} \rangle , \\
 1b &= \langle k + \not{p}_3 | p_{c+} \rangle \langle p_a - \not{p}_1 P_L \not{p}_2 | p_{b+} \rangle , \\
 1c &= \langle k + \not{p}_1 | p_{a+} \rangle \langle p_b - \not{p}_2 P_L \not{p}_3 | p_{c+} \rangle , \tag{3.1.8}
 \end{aligned}$$

where all common factors including the denominator of the propagators have been dropped. The SUSY factor in these expressions are the ones that contain k . If the boson line arrows were pointing inward as in Fig.(3.4) then the corresponding helicities should become negative in these factors. The momenta p_a , p_b and p_c could be any of the on-shell momenta of the external lines that appear in the momentum expansion of that particular line. The (-1) factor in $1a$ is due to the anti-commutativity of the SUSY factor θ (suppressed in the above relations) and appears because in factoring out it passes by an odd number of fermion lines. Using off-shell Fierz relations, see App. (A.1.1), it is straightforward to see that,

$$\text{Relation 1A:} \quad 1a + 1b + 1c = 0 . \tag{3.1.9}$$

In case any of the three lines is an external on-shell line, say p_2 for instance, then in the above amplitudes \not{p}_2 must be dropped and that has to accompany

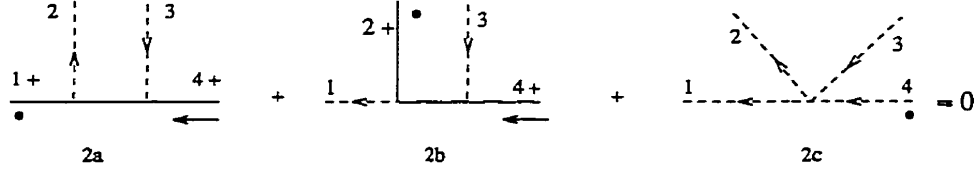


Figure 3.5: Relation 2A.

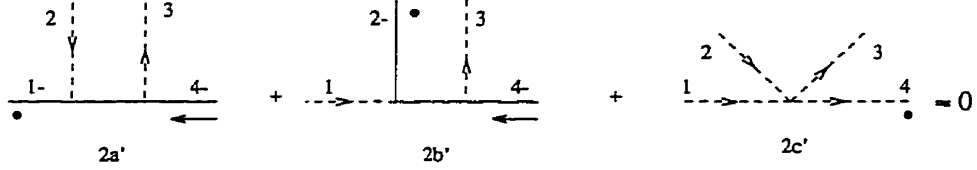


Figure 3.6: Relation 2B.

a helicity flip in the corresponding state as well as momentum change, in this case $|p_b = p_2 - \rangle$.

Similarly for Fig(3.4) we have

$$\begin{aligned}
 1'_a &= - \langle k - |p_2|p_b - \rangle \langle p_a + |p_1 P_R p_3|p_c \rangle , \\
 1'_b &= \langle k - |p_3|p_c - \rangle \langle p_a + |p_1 P_R p_2|p_b - \rangle , \\
 1'_c &= \langle k - |p_1|p_a \rangle \langle p_b + |p_2 P_R p_3|p_c - \rangle , \tag{3.1.10}
 \end{aligned}$$

from which it follows

$$\text{Relation 1B: } 1'_a + 1'_b + 1'_c = 0 . \tag{3.1.11}$$

• Relation 2

This relation is depicted pictorially in Fig.(3.5). The momentum configuration is $p_{in} = p_3 + p_4$ and $p_{out} = p_1 + p_2$ where all p_i can in general be off-shell. The corresponding expressions for these diagrams, ignoring all common factors, are

$$2a = \langle k - |p_1 P_L (p_1 + p_2) P_R p_4|p_d - \rangle ,$$

$$\begin{aligned}
2b &= \langle k - |\not{p}_2 P_L (\not{p}_1 + \not{p}_2) P_R \not{p}_4 | p_d^- \rangle , \\
2c &= \langle k - |\not{p}_4 | p_d^- \rangle (p_1 + p_2)^2 .
\end{aligned}
\tag{3.1.12}$$

From these expressions it follows that

$$\text{Relation 2A:} \quad 2a + 2b + 2c = 0 .
\tag{3.1.13}$$

The amplitudes given above also yield the on-shell results if any of the momenta go on-shell. For example, if all p_i except p_4 are taken to be on-shell then

$$\begin{aligned}
2a &= - \langle k1 \rangle [12] \langle p_2 - |\not{p}_4 | p_d^- \rangle , \\
2b &= - \langle k2 \rangle [21] \langle p_1 - |\not{p}_4 | p_d^- \rangle , \\
2c &= \langle k - |\not{p}_4 | p_d^- \rangle [12] \langle 21 \rangle ,
\end{aligned}
\tag{3.1.14}$$

which will satisfy (3.1.13) provided we write $p_4 = p_1 + p_2 - p_3$ and use Fierz relations. For Fig(3.6) the corresponding amplitudes (the primed ones) can be obtained from (3.1.12) by flipping the helicities of the states and changing the lable $L \leftrightarrow R$ on the projection operators. For the resulting $2'_{a,b,c}$ expressions it follows that

$$\text{Relation 2B:} \quad 2'_a + 2'_b - 2'_c = 0 .
\tag{3.1.15}$$

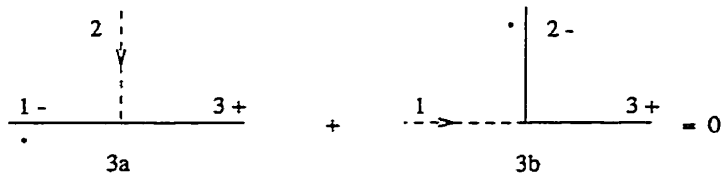


Figure 3.7: Relation 3A.

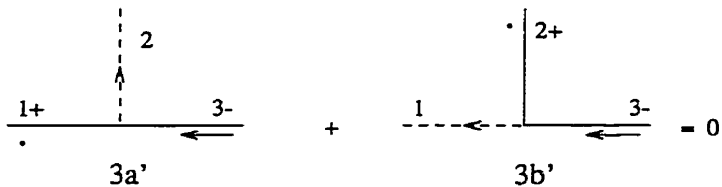


Figure 3.8: Relation 3B.

• **Relation 3.**

Another relation that can be easily checked is depicted in Fig.(3.7). Assuming p_3 is an on-shell fermion line we have,

$$3a = \langle k + \not{p}_1 P_R | 3+ \rangle \quad ; \quad 3b = \langle k + \not{p}_2 P_R | 3+ \rangle , \quad (3.1.16)$$

where again the common SUSY factor of $-\sqrt{2i\bar{\theta}}$ has been dropped. Using Fierz identities it follows that

$$\text{Relation 3A:} \quad 3a+3b = [k, 1+2] \langle 1+2, 3 \rangle = [k3] \langle 33 \rangle = 0 . \quad (3.1.17)$$

In (3.1.16), if we change the helicity of the fermion line which should accompany a change in the direction of arrow on the boson line, only the type of brackets will change, i.e., $[..] \leftrightarrow \langle .. \rangle$. The resulting graphical relation is shown in Fig(3.8).

Now let us consider how these graphical relations may be used to relate more complex diagrams. The strategy for obtaining such relations is the following. By joining elementary pieces together and by moving the dot from internal lines to external ones, diagrams with more external lines can

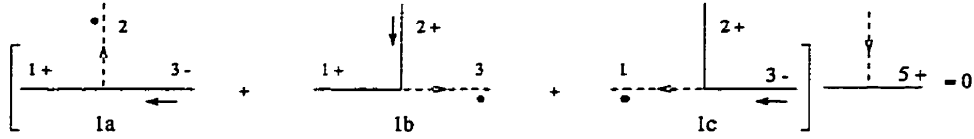


Figure 3.9: Sewing 3-pt functions

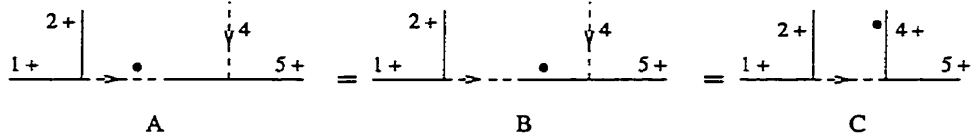


Figure 3.10: Moving the dot from an internal to an external line

be constructed. Along with constructing bigger diagrams one also obtains relations among them. Consider the following example. We can start from relation 1A and sew on an extra piece as shown in Fig(3.9). As one can see, the first and the third grafted diagrams are normal ones (note that in the grafting process one has to strip off the helicity state $|p_c+ \rangle$ from the common line 3) but the second one looks odd. To get a sensible diagram we first notice that line 3 has, from (3.1.8) and after attaching the extra piece, the SUSY factor $\langle k + |p_3 P_R|5+ \rangle$. All we need to do is to move the dot across to the negative helicity outgoing fermion of the grafted piece which will generate the same SUSY factor, from (3.1.16), Fig.(3.10). The last step is to use relation 3A to move the dot to the external line 4. Putting all three terms together the final result is as shown in Fig.(3.11). As a further check we can directly verify the validity of the relation of Fig(3.11). Assuming all

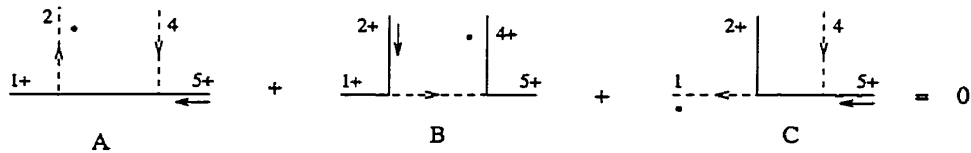


Figure 3.11: A derived relation among 4-pt functions.s

external lines are on-shell, the expressions associated with each term are,

$$A = [k_1][12] \langle 25 \rangle ; B = -[k_4][12] \langle 45 \rangle ; C = -[k_1][21] \langle 15 \rangle . \quad (3.1.18)$$

Using Fierz identities it follows that $A + B + C = 0$. One can proceed further and sew on more and more pieces and create complicated diagrams and relations.

There is an even easier way to obtain such relations. This shorter technique was actually derived from considering several examples. We first explain the rule and will then give examples. We notice that there are two types of SUSY factors, one having square brackets $[..]$ and one having angle brackets $\langle .. \rangle$. With this in mind let us start from an arbitrary diagram with on-shell external lines and choose the dot to be on one of the external lines. Based on the type and momentum direction of the line carrying the dot the SUSY factor will either be square or angle brackets. As a rule the dot can only go to those external lines whose resulting SUSY factor will be the same in type as the original line. In order to reach these external lines one has to move the dot along some internal fermion or boson lines. At tree level there is only one path to take for each destination. Passing the dot along an internal line should bring about a particle type change from fermion \leftrightarrow boson. When the dot is moved along a fermionic line of the diagram between two fermion-boson vertices, the fermion propagator shrinks and produces a four-boson vertex. This occurs every other time a fermion propagator is reached. The sum of diagrams created in this way will be zero.

Our first example is shown in Fig.(3.12). The momenta are chosen as $p_{in} = p_3 + p_4$ and $p_{out} = p_1 + p_2$. We start with the dot on line 1 with negative helicity. In this case the dot can go to either Λ_{+out} or Λ_{-in} particle types which are lines 2 and 3. It is straightforward to verify the relation

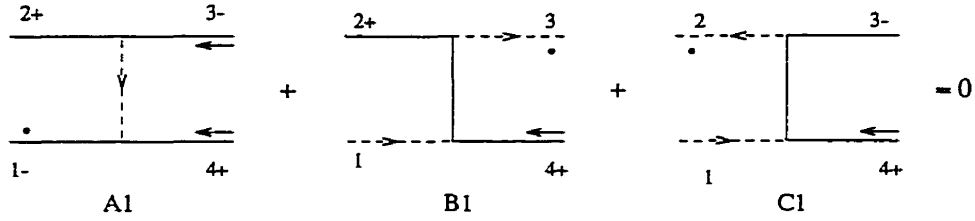


Figure 3.12: A 4-pt example. SUSY factors; (A1)-[k1], (B1)-[k3], (C1)-[k2]

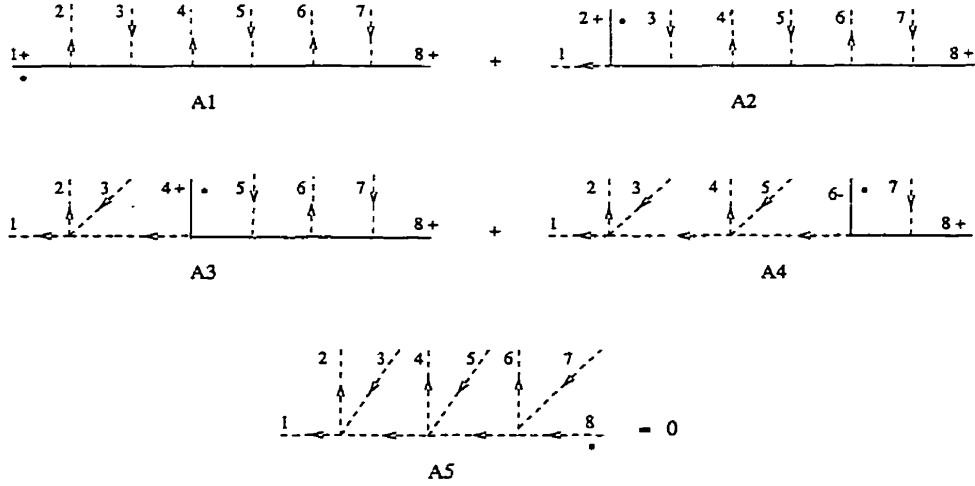


Figure 3.13: An 8-pt example

depicted in Fig.(3.12). The expressions for the three terms are

$$A1 = -[k1] \langle 14 \rangle [23] ; \quad B1 = [k3][23] \langle 34 \rangle ; \quad C1 = -[k2][32] \langle 24 \rangle \quad (3.1.19)$$

where we have again ignored all common factors. Now using momentum conservation we have

$$\begin{aligned} [k2] \langle 24 \rangle &= \langle +k | \not{p}_2 | 4+ \rangle \\ &= \langle k + | \not{p}_3 + \not{p} - \not{p}_1 | 4+ \rangle \\ &= [k3] \langle 34 \rangle - [k1] \langle 14 \rangle . \end{aligned}$$

Replacing this in $C1$ it follows that $A1 + B1 + C1 = 0$. As an example illustrating shrinking of fermion propagators consider Fig(3.13). The 'in' and 'out' momenta are $p_{in} = p_8 + p_7 + p_6 + p_5$, $p_{out} = p_1 + p_2 + p_3 + p_4$. The

expressions for the diagrams are

$$\begin{aligned}
A_1 &= \langle k1 \rangle [12] \langle 2, 1+3 \rangle [1+3, 2+4] \langle 2+4, 1+3-5 \rangle [1+3-5, 7] \langle 78 \rangle , \\
A_2 &= \langle k2 \rangle [21] \langle 1, 2+3 \rangle [2+3, 1+4] \langle 1+4, 2+3-5 \rangle [2+3-5, 7] \langle 78 \rangle , \\
A_3 &= \langle k4 \rangle [4, 1+2+3] \langle 1+2+3, 4-5 \rangle [4-5, 7] \langle 78 \rangle (p_1+p_2)^2 , \\
A_4 &= - \langle k6 \rangle [67] \langle 78 \rangle (p_1+p_2)^2 (p_1+p_2+p_3+p_4)^2 , \\
A_5 &= \langle k8 \rangle (p_1 + p_2)^2 (p_1 + p_2 + p_3 + p_4)^2 (p_7 + p_8)^2 .
\end{aligned} \tag{3.1.20}$$

From the Fierz identities it follows then that

$$A_1 + A_2 + A_3 + A_4 + A_5 = 0 . \tag{3.1.21}$$

These examples serve to illustrate that in the WZ model one is able to dig further down from what SWI provides and find relations among individual diagrams. A further question is whether such relations exist in other theories such as supersymmetric Yang-Mills theory. In a (SUSY) gauge theory each complete amplitude is a gauge invariant unit but each diagram is gauge dependent. The complete amplitude can be split into the so called primitive color subamplitudes each of which contain fewer number of diagrams which are still gauge invariant. Further gauge invariant splittings are impossible. If one attempts to relate diagrams within subamplitudes of the same color (coming from different processes) we will end up with a gauge dependent relation. As a result of the gauge dependence, physical diagrams (made up of regular vertices) will not add up to zero, leaving left over pieces. Therefore, one is obliged to introduce nonphysical vertices. So the conclusion is that in gauge theories, gauge invariance forces diagrams to be split into gauge invariant subamplitudes. Attempts to split the gauge invariant unit will result in nonphysical vertices.

Chapter 4

High energy scattering

Until 1972 it was a commonly held belief in the physics community that the total scattering cross section approaches a constant as the square of the total center of mass energy, s , tends to infinity. Around that time the ISR [11, 12] experiments found evidence that this belief is not strictly true and a rise in the total hadronic scattering cross section was observed. Subsequent analysis of the data established the growth of the total cross section as $\sigma_{tot} \propto s^{0.08}$ [13]. Since then other scattering experiments have verified this observation. Recently, scattering experiments at HERA [14] have revealed an even stronger growth for γ^*p total cross section $\sigma_{tot} \propto s^{0.5}$. These growths are generally believed to be due to the exchange of a composite object, called the *pomeron*, between the colliding hadrons. The gentler growth is due to the so called *soft* or non-perturbative pomeron and the steeper one due to the *hard* or perturbative pomeron.

The rise of the total cross section at high energies can be looked upon from two different perspectives. First, according to the Froissart-Martin [15, 16] theorem at asymptotic high energies the total cross section cannot grow faster than $\sigma_{tot} \propto \ln^2(s)$. The observed power growth is not necessarily a threat since the present day energies available are believed not to

be high enough to meet the requirement of the theorem. One possibility is that at yet higher energies multiple gluon exchanges will take place which will dampen the growth. This point is not of primary concern at the moment. On the theoretical side however, the situation is different. Here there are two approaches. First is the Regge phenomenological approach which is based on general unitarity, analyticity and crossing symmetry properties of scattering amplitudes [17]. In Regge theory, based on assumptions regarding singularities of the partial-wave amplitude, one finds the general dependence of the scattering amplitude, $A(s, t)$, on s . According to Regge theory the high energy behavior of $A(s, t)$ is dominated by the poles of the partial wave amplitude, see section 4.1. In the simplest case one assumes that the singularities of the partial wave amplitude are simple poles. Then the scattering amplitude exhibits an asymptotic power growth, $A(s, t) \sim s^{\alpha_P(t)}$, if $\alpha_P(t)$ is the *pomeron* pole. The pomeron pole is one of a series of possible poles in the complex angular momentum plane generally referred to as Regge poles. The pomeron pole provides the leading contribution to the total cross section. From the optical theorem one would then have,

$$\sigma_{tot} = \frac{1}{s} \text{Im}A(s, t = 0) \propto s^{\alpha_P(0)-1} .$$

As one can see, if $1 < \alpha_P(0)$ the result will violate the Froissart bound. Nonetheless at present day energies, this model fits the data. From the collected scattering results, the effective pomeron trajectory has been found to be $\alpha_P(t) = 1.08 + 0.25t$ [13]. There are other possibilities as well. These are due to Regge cuts. These cuts will generally produce $\ln(s)$ factors in the amplitude.

The second approach is via the perturbative QCD calculations. In 1975 Low and Nussinov [18] proposed a perturbative model of the pomeron in

which the pomeron is simply the color-singlet component of a two-gluon exchange in QCD. Diagrammatic calculations in the leading log approximation (LLA) have been carried out to substantiate this proposal [19, 20] and to study other aspects of the high-energy near-forward scattering. A characteristic feature of these calculations is the necessity to sum up an infinite number of diagrams. The reason is that even if $g^2 \ll 1$, the effective coupling at high energy is $g^2 \ln(s)$ which may be of the order of unity and hence an infinite number of diagrams must be summed up. Dealing with such a huge number of diagrams is an enormous task and compels one to work in LLA. This turns out not to be sufficient. The reason is the common cancellation of leading $\ln(s)$ factors which occurs in certain color channels of the sum of diagrams at each order of perturbation. Because of this one needs the sub-leading contributions of a diagram. This fact in itself is a calculational hardship and complicates matters. Here a calculational method that would give the leading contribution of the sum of diagrams at each order of perturbation would simplify the calculations considerably. There is another point to notice. A priori one cannot dismiss non-leading terms, whether they are non-leading contributions of a leading diagram or leading contribution of a non-leading diagram, since it is quite possible that the sum of non-leading terms may overrun the sum of leading terms.

The result of finite order diagrammatic calculations [19] seems to indicate that the high-energy near-forward scattering is governed by multiple reggeized gluon exchanges, supplemented by elementary gluon production from the reggeons and by s -channel unitarity [21]. The emergence of reggeon exchange out of perturbative calculations is particularly interesting and is consistent with the Regge theory result.

There is another important development in this area. A case where the

leading log factors do not cancel is in the sum, in LLA, of a reggeized gluonic ladder with an effective vertex for elementary gluon production. The sum leads to the BFKL equation, see section 4.2. The color singlet solution of this equation is the hard pomeron and the color-octet is the reggeon. The pomeron solution results in a cross section that violates the Froissart bound. Here there is a possibility that non-leading diagrams, i.e., those with multiple gluon exchange as well as those containing fermion loops, may be of importance.

Recently a new way of calculating sums of Feynman diagrams at a given order of perturbation was proposed [22]. The new technique exploits non-abelian cut diagrams as opposed to standard Feynman diagrams. A non-abelian cut diagram is in fact an extract of the sum of a number of standard diagrams and as such contains a number of cancellations already built in. This greatly simplifies the calculations. We will examine this new technique in chapter 5.

As was mentioned above, restoration of unitarity and fulfilling the requirement of the Froissart bound would demand resummation of multi-gluon exchange diagrams. Some recent studies have been conducted in this direction [23, 24]. The question of the role of fermion loops in the context of the BFKL equation has also been the subject of some recent articles [25]. The study of the contribution of diagrams containing fermion loops to the high energy behavior of electron-electron scattering amplitude was pioneered by Cheng and Wu [26]. In QED such amplitudes are free of UV divergence. Similar diagrams occur when considering quark-quark scattering in QCD. In QCD however, these diagrams are UV divergent and therefore regularizing them is necessary. In chapter 6 we will examine this point and will calculate three eighth-order diagrams containing fermion loops in quark-quark scat-

tering. We find that as a result of regularization, the high energy behavior of such diagrams exhibits an enhancement in their energy dependence as compared to QED diagrams.

The outline of the present chapter is as follows. The elements of Regge theory will be reviewed in section 4.1. Section 4.2 will be a review of the BFKL equation.

4.1 Regge theory

In 1959 Regge [27] showed the advantage of viewing the angular momentum l as a complex variable. He showed that for a wide class of potentials the only singularities of scattering amplitudes in the complex angular momentum plane were poles, now known as Regge poles. If these poles occur for positive integer values of l they correspond to bound states or resonances. Regge's considerations were non-relativistic but it was later shown that the theory of complex angular momentum, Regge theory, can also be used in high energy particle physics. Below we will review the complex momentum approach as is used in the high energy particle scattering.

Consider an elastic scattering process [28] (a) : $A(p_1) + B(p_2) \rightarrow A(p'_1) + B(p'_2)$ progressing in the s -channel, $0 < s, t < 0, u < 0$, as shown in Fig.(4.1). The goal is to find out how the scattering amplitude $A(s, t)$ behaves as s , the center of mass (CM) energy, grows very large. To this end we first consider the crossed process (b) : $B(p_2) + \overline{B(-p'_2)} \rightarrow A(p'_1) + \overline{A(-p_1)}$. The amplitude for (b) can be obtained from $A(s, t)$ by analytic continuation to the t -channel physical region where $0 < t, s < 0, u < 0$. Now, using t -channel partial waves we can expand $A(s, t)$ as follows,

$$A(s, t) = A_+(s, t) + A_-(s, t) , \quad (4.1.1)$$

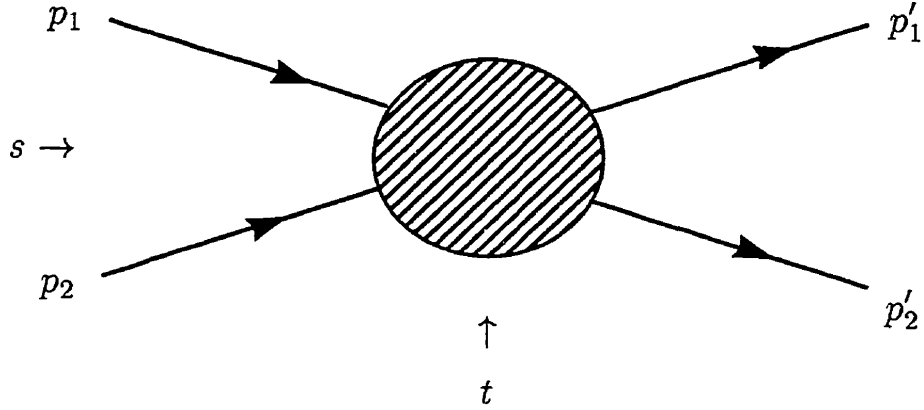


Figure 4.1: Elastic scattering in s and t -channels.

$$A_{\pm}(s, t) = \frac{1}{2} \sum_{l=0}^{\infty} (2l+1) A_{\pm l}(t) [P_l(-z_t) \pm P_l(z_t)], \quad (4.1.2)$$

where l is the angular momentum, $A_{\pm l}(t)$ is the positive (negative) signature (to be explained below) t -channel partial wave, P_l is the Legendre polynomial, $z_t = -\cos(\theta_t)$ with θ_t the scattering angle in the CM of process (b). The relation between Mandelstam variables in t -channel physical region are,

$$s = \frac{-t}{2} (1 - \cos \theta_t) \quad ; \quad u = \frac{-t}{2} (1 + \cos \theta_t) . \quad (4.1.3)$$

Note that we can move back to s -channel physical region by allowing $1 < |z_t|$ and $t < 0$. The reason for splitting $A(s, t)$ into positive and negative signature parts as in (4.1.1) is as follows. Suppose that particle A is its own antiparticle $A = \bar{A}$. Then the amplitude for the t -channel process (b) has a $s \leftrightarrow u$ symmetry. Since only $P_l(z_t)$ with even l has such a symmetry, $P_{l=\text{even}}(-z_t) = P_{l=\text{even}}(z_t)$, one would expect that only $P_{l=\text{even}}(z_t)$ should be present in the expansion. Equation (4.1.2) implements this requirement. After this brief digression let us take another step and think of $P_l(z_t)$ and $A_{\pm l}(t)$, originally defined for positive integers, as analytic functions of l . In this extension $P_l(z_t)$ will no longer be a polynomial but rather a hypergeometric function with a branch cut going from (-1) to $-\infty$. The situation

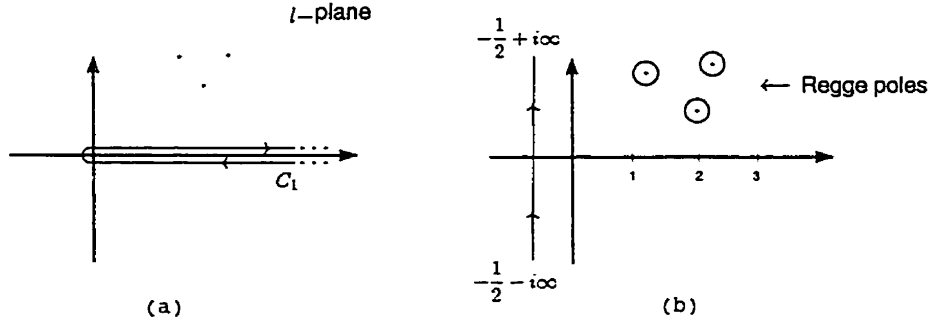


Figure 4.2: The complex l -plane. Regge poles are indicated by dots. (a) Contour C_1 encircles the positive l axis (b) After opening the contour.

with $A_{\pm l}(t)$ is more subtle. We assume that it has only isolated singularities and thus makes the analytic continuation in the complex l plane plausible. Also we assume that $A_{\pm l}(t)$ dies fast enough as l increases, for a reason to be explained later. This extension would allow for another representation of $A_{\pm}(s, t)$ known as the Sommerfeld-Watson representation [17],

$$A_{\pm}(s, t) = \frac{-1}{4i} \int_{C_1} dl (2l + 1) A_{\pm l}(t) \frac{P_l(z_t) + P_l(-z_t)}{\sin \pi l}. \quad (4.1.4)$$

As shown in Fig.(4.2.a) the contour C_1 encompasses all positive integers. The factor $\sin \pi l$ has simple poles for integer values of l with a residue $-2i(-1)^l$. With this residue one can directly see that (4.1.2) and (4.1.4) are identical. The next step is to open up the contour to a straight line as in the Fig.(4.2.b). The contribution of the big semicircular part of the contour closing to the right side (not shown in the figure) vanishes because of the assumption we made earlier. As opening the contour entails inclusion of the poles of A_l which were previously outside the contour, the contribution of these poles must be subtracted off. Let us suppose that $A_l(t)$ has poles at $l = \alpha_i(t)$ with residue $\beta_i(t)/(2\alpha_i(t) + 1)$. So we will have

$$A_{\pm}(s, t) = \frac{-1}{2i} \int_{L-i\infty}^{L+i\infty} dl (2l + 1) A_{\pm l}(t) \frac{P_l(z_t) + P_l(-z_t)}{\sin \pi l} \quad (4.1.5)$$

$$- \sum_i \frac{\pi \beta_i(t)}{\sin \pi \alpha_i(t)} [P_{\alpha_i(t)}(z_t) \pm P_{\alpha_i(t)}(-z_t)] .$$

In the above equation L must be smaller than the real part of all the $\alpha_i(t)$ in order to have all the poles of $A_l(t)$ included. We now move back to the s -channel physical region with $s \rightarrow \infty$ by allowing $z_t \rightarrow \infty$. From (4.1.3) we will have

$$z_t \rightarrow \infty \quad \Rightarrow \quad z_t \sim \frac{2s}{-t} . \quad (4.1.6)$$

Moreover, in this limit we have

$$P_l(z_t) \rightarrow \frac{\Gamma(l + \frac{1}{2})}{\sqrt{\pi} \Gamma(l + 1)} (2z_t)^l \quad (4.1.7)$$

Now from (4.1.5) the high energy behavior of $A_{\pm}(s, t)$ is dominated by the rightmost Regge pole. The integral part in (4.1.5) vanishes at least as fast as $s^{-1/2}$, so we will have from equations (4.1.5)-(4.1.7),

$$\begin{aligned} A_{\pm}(s, t) &\rightarrow - \frac{\pi \beta_j(t)}{\sin \pi \alpha_j(t)} \frac{\Gamma(\alpha_j(t) + \frac{1}{2})}{\sqrt{\pi} \Gamma(\alpha_j(t) + 1)} [(2z_t)^{\alpha_j(t)} \pm (-2z_t)^{\alpha_j(t)}] \\ &\rightarrow - \frac{\pi \beta_j(t)}{\sin \pi \alpha_j(t)} \frac{\Gamma(\alpha_j(t) + \frac{1}{2})}{\sqrt{\pi} \Gamma(\alpha_j(t) + 1)} \left(\frac{4s}{-t} \right)^{\alpha_j(t)} [1 \pm e^{i\pi \alpha_j(t)}] . \end{aligned} \quad (4.1.8)$$

As can be seen from this result, any simple pole of the partial wave amplitude results in an amplitude which grows as a power s . The partial wave amplitude may in general have cuts. These in general require more elaborate considerations and produce factors of $\ln(s)$ in the amplitude.

4.2 Dispersion relations

Before we go on to the BFKL equation it is necessary to give a quick review of the dispersion relation technique. We will also use the partial wave expansion that was used in the Regge theory. It should be mention that all of the gluon vertices in the BFKL ladder are effective vertices and are derived perturbatively by summing up diagrams with standard three and four gluon

vertices at tree level. Also, in the context of the BFKL equation we are considering solely parton production from a reggeized gluon exchanged in the t -channel. The kinematical region for this production process is the so called *multiregge* kinematical region [29]. More specifically in $g_a g_b \rightarrow g_{a'} g_{b'} g_1 \cdots g_n$ this region is characterized by $y_{b'} \ll y_1 \ll \cdots \ll y_n \ll y_a$ where y_i is the rapidity of the i th gluon defined by $y_i = \frac{1}{2} \ln \frac{E_i + p_{i||}}{E_i - p_{i||}}$.

Consider the elastic $g_a g_b \rightarrow g_{a'} g_{b'}$ amplitude in multiregge region. For two gluon exchange in the t -channel, the color dependence may be decomposed in terms of irreducible color elements of the tensor product of two adjoint representations $(\mathbf{8} \otimes \mathbf{8})$ of $SU(3)$ [30]

$$iM_{\mu_a \mu_b \mu_{a'} \mu_{b'}}^{aba'b'}(s, t, u) = ig_{\mu_a \mu_{a'}} g_{\mu_b \mu_{b'}} \sum_T P_{bb'}^{aa'}(T) A^T(s, t) \quad (4.2.9)$$

where the extraction of polarization factors indicate that at high energies helicity is conserved. $A^T(s, t)$ are the corresponding scalar amplitudes and $P_{bb'}^{aa'}(T)$ are the color projectors satisfying the orthogonality relation

$$P_{bb'}^{aa'}(T) P_{cc'}^{bb'}(T') = P_{cc'}^{aa'}(T) \delta_{TT'} . \quad (4.2.10)$$

These color projectors split into two groups, the symmetric projectors $(\mathbf{8} \otimes \mathbf{8})_S = \mathbf{1} \oplus \mathbf{8}_S \oplus \mathbf{27}$, and the antisymmetric ones $(\mathbf{8} \otimes \mathbf{8})_A = \mathbf{8}_A \oplus \mathbf{10} \oplus \overline{\mathbf{10}}$. Under $s \leftrightarrow u$ crossing we have

$$P_{b'b}^{aa'}(T) = (-1)^T P_{bb'}^{aa'}(T) \\ (-1)^T = \begin{cases} -1 & \text{for } (\mathbf{8} \otimes \mathbf{8})_A \\ +1 & \text{for } (\mathbf{8} \otimes \mathbf{8})_S \end{cases} . \quad (4.2.11)$$

The goal here is to express $A^T(s, t)$ in terms of a dispersion relation of its discontinuity $\text{Disc}A(s, t)$. To this end we first decompose the scalar amplitude $A^T(s, t)$ in terms of t -channel partial waves

$$A^T(s, t) = \sum_{l=0}^{\infty} (2l+1) A_l^T(t) P_l(z_t) , \quad (4.2.12)$$

where $P_l(z_t)$ are Legendre polynomials and $z_t = -\cos(\theta_t)$ with θ_t the scattering angle in t -channel physical region. The Mandelstam invariants are related according to

$$\begin{aligned} s &= -\frac{t}{2}(1+z_t), \\ u &= -\frac{t}{2}(1-z_t). \end{aligned} \quad (4.2.13)$$

The invariance of the amplitude $M(s, t, u)$ in (4.2.9) under $s \leftrightarrow u$ crossing, along with the parity of the projectors determines the parity of the scalar amplitude,

$$A(-z_t, t) = (-1)^T A^T(z_t, t), \quad (4.2.14)$$

where from (4.2.13) under $s \leftrightarrow u$ crossing $z_t \leftrightarrow -z_t$. The next step is to write the scalar amplitude in terms of its singularities. If we take t to have some fixed negative value then from $s+t+u=0$ we see that in the s -channel physical region $-\infty < u \leq 0$ and $-t \leq s < \infty$. Similarly, with the same assumption in the u -channel physical region we will have $-\infty < s \leq 0$ and $-t \leq u < \infty$. Using (4.2.13) the two ranges of values for s can be expressed in terms of z_t . So in the s -channel physical region $1 \leq z_t < \infty$ and in the u -channel physical region $-\infty < z_t \leq -1$. Therefore the dispersion relation for the scalar amplitude is

$$\begin{aligned} A^T(s, t) &= \oint_{\Omega} \frac{ds'}{2\pi i} \frac{A^T(s', t)}{s-s'} = \oint_{\Omega'} \frac{dz'_t}{2\pi i} \frac{A^T(z'_t, t)}{z'_t - z_t} \\ &= \int_{-\infty}^{-1} \frac{dz'_t}{2\pi i} \frac{\text{Disc}A^T(z'_t, t)}{z'_t - z_t} + \int_1^{\infty} \frac{dz'_t}{2\pi i} \frac{\text{Disc}A^T(z'_t, t)}{z'_t - z_t}, \end{aligned} \quad (4.2.15)$$

where

$$\text{Disc}A^T(s', t) = A^T(s' + i\epsilon, t) - A^T(s' - i\epsilon, t). \quad (4.2.16)$$

The contour of integration is shown in Fig.(4.3). Using the orthogonality of $P_l(z_t)$ we can invert (4.2.12) to obtain

$$A_l^T(t) = \frac{1}{2} \int_{-1}^1 dz_t P_l(z_t) A^T(z_t, t). \quad (4.2.17)$$

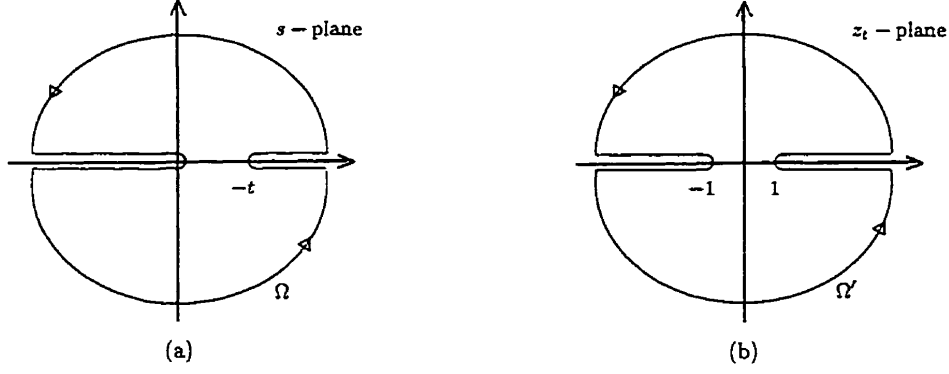


Figure 4.3: Integration contour in (a) s -plane (b) z_t -plane.

Replacing for $A^T(z_t, t)$ in (4.2.17) from (4.2.15) we will get

$$A_l^T(t) = \int_{-\infty}^{-1} \frac{dz'_t}{2\pi i} Q_l(z'_t) \text{Disc} A^T(z'_t, t) + \int_1^{\infty} \frac{dz'_t}{2\pi i} Q_l(z'_t) \text{Disc} A^T(z'_t, t), \quad (4.2.18)$$

where $Q_l(z_t)$ is the Legendre function defined by

$$Q_l(z') = \frac{1}{2} \int_{-1}^1 dz \frac{P_l(z)}{z' - z}. \quad (4.2.19)$$

Now using the following properties of the Legendre function and the discontinuity of the amplitude

$$\begin{aligned} \text{Disc} A^T(-z_t, t) &= (-1)^{T+1} \text{Disc} A^T(z_t, t), \\ Q_l(z_t) &= (-1)^{l+1} Q_l(z_t), \end{aligned} \quad (4.2.20)$$

we will get

$$A_l^T(t) = [1 + (-1)^{l+T}] \int_1^{\infty} \frac{dz'_t}{2\pi i} Q_l(z'_t) \text{Disc} A^T(z'_t, t). \quad (4.2.21)$$

We are now almost at the end of the road. The last step before we get the desired expression is to express the partial wave expansion in (4.2.12) using the Sommerfeld-Watson transformation. This gives

$$A^T(s, t) = \frac{1}{2i} \int_C (2l+1) \frac{A_l^T(t)}{\sin(\pi l)} P_l(-z_t), \quad (4.2.22)$$

where the contour C surrounds the positive real l axis in the complex l plane. Replacing for $A_l^T(t)$ in the above equation from (4.2.21) we get,

$$A^T(s, t) = -\frac{1}{4\pi} [1 + (-1)^{l+T}] \int_C (2l+1) \frac{P_l(-z_t)}{\sin(\pi l)} \int_1^\infty dz'_t Q_l(z'_t) \text{Disc} A^T(z'_t, t) . \quad (4.2.23)$$

We are interested in the asymptotic form of (4.1.1) in the limit as $z_t \sim -(2s/t) \rightarrow \infty$. The asymptotic form of the Legendre function and Legendre polynomial are [31],

$$\begin{aligned} P_l(z) &\rightarrow \frac{1}{\sqrt{s}} \frac{\Gamma(l+1/2)}{\Gamma(l+1)} (2z)^l \\ Q_l(z) &\rightarrow \sqrt{s} \frac{\Gamma(l+1)}{\Gamma(l+3/2)} (2z)^{-(l+1)} . \end{aligned} \quad (4.2.24)$$

Replacing these back in (4.2.23) we will get,

$$A^T(s, t) \simeq -\frac{1}{4\pi} \int_C [(-1)^l + (-1)^T] \frac{e^{y'l}}{\sin(\pi l)} \int_0^\infty dy' e^{-y'l} \text{Disc} A^T(y', t) , \quad (4.2.25)$$

where we have introduced the rapidity variable y by $z'_t = e^{y'}$. Using this equation it will be sufficient to calculate the discontinuity of the scalar amplitude. Plugging it into this equation will get us the whole amplitude.

4.3 The BFKL equation

The expression developed in (4.2.25) will now be used to derive the BFKL equation. As is seen from this equation one can construct the asymptotic form of the entire amplitude from a knowledge of its discontinuity.

It was briefly mentioned in the introduction that the hard or BFKL pomeron is the color-singlet part of the resummation of an infinite number of ladder diagrams of the type shown in Fig.(4.4). The incoming gluons with momenta p_a and p_b collide head on in the center of mass frame with total energy s assumed to be much larger the momentum transfer $(-t) \ll s$.

In this diagram the coupling between each horizontal gluon rung and the two sides is through an effective 3g vertex called the Lipatov vertex [32] which is expressed as

$$C^\mu(q_i, q_{i+1}) \simeq (q_i + q_{i+1})_\perp^\mu - \left(\frac{s_{ai}}{s} + 2 \frac{t}{s_{bi}} \right) p_b^\mu + \left(\frac{s_{bi}}{s} + 2 \frac{t}{s_{ai}} \right) p_a^\mu, \quad (4.3.26)$$

where

$$\begin{aligned} s_{ai} &= -2p_a \cdot k_i = - \sum_{j=0}^{n+1} k_{i\perp} \cdot k_{j\perp} e^{-(y_i - y_j)}, \\ s_{bi} &= -2p_b \cdot k_i = - \sum_{j=0}^{n+1} k_{i\perp} \cdot k_{j\perp} e^{y_i - y_j}. \end{aligned} \quad (4.3.27)$$

The vertex factor $C^\mu(q_i, q_{i+1})$ can be obtained, in the Regge kinematical region, by summing the five $g_a g_b \rightarrow g_a' g_b' g$ diagrams at tree level. An interesting property of this vertex is that it is gauge invariant, i.e.,

$$C(q_i, q_{i+1})^\mu k_\mu = 0. \quad (4.3.28)$$

In the ladder model the gluons exchanged in t -channel are reggeized gluons. This is based on the ansatz [32] that the leading logarithmic approximation of the virtual radiative corrections, to all orders in $\alpha_s = g^2/(4\pi)$, is obtained by replacing the propagator for the i th gluon with momentum q_i by

$$\frac{1}{q_i^2} \rightarrow \frac{1}{q_i^2} e^{\alpha(t_i)(y_{i-1} - y_i)} \quad (4.3.29)$$

with $\alpha(t_i)$ given by

$$\alpha(q_{i\perp}) = -\alpha_s N_c q_{i\perp} \int \frac{d^2 k_\perp}{(2\pi)^2} \frac{1}{k_\perp^2 (q_i - k)_\perp^2}. \quad (4.3.30)$$

In order to evaluate the discontinuity of the amplitude it is sufficient to implement Cutkosky rules, i.e., the propagators of the horizontal gluons must be replaced by [33]

$$\frac{i}{k_i^2} \rightarrow 2\pi \theta(k^0) \delta(k_i^2). \quad (4.3.31)$$

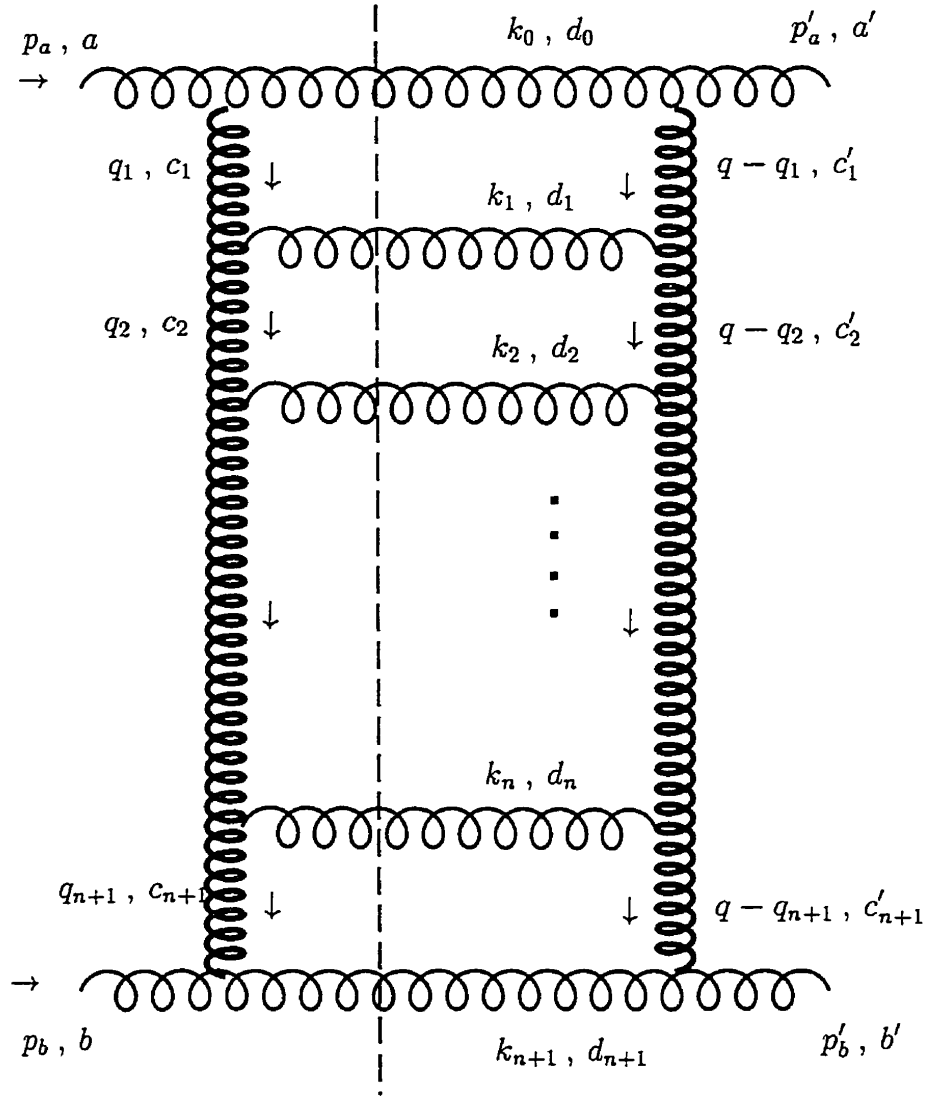


Figure 4.4: The BFKL ladder. Thin lines and thick lines represent elementary and reggeized gluons respectively.

Therefore the $n + 1$ loop integration measure will become,

$$\begin{aligned}
d\Phi_{n+1} &= \int \left(\prod_{i=0}^{n+1} \frac{d^4 k_i}{(2\pi)^4} (2\pi)^4 \right) \delta^4(p_a + p_b - \sum_{l=0}^{n+1} k_l) \prod_{j=0}^{n+1} 2\pi\theta(k_j^0) \delta(k_j^2) \\
&= \int \left(\prod_{i=0}^{n+1} \frac{dy_i d^2 k_{i\perp}}{4\pi(2\pi)^2} \right) (2\pi)^4 \delta^4(p_a + p_b - \sum_{l=0}^{n+1} k_l), \tag{4.332}
\end{aligned}$$

where use has been made of,

$$\begin{aligned}
\int \frac{d^4 k_i}{(2\pi)^4} [2\pi\theta(k_i^0) \delta(k_i^2)] &= \frac{d^3 k_i}{2\vec{k}_i^2 (2\pi)^3} = \frac{dy_i d^2 k_{i\perp}}{4\pi(2\pi)^2}, \\
k_{\parallel} &= k_{i\perp} \sinh(y_i) \quad ; \quad \vec{k}_i^2 = k_{i\perp}^2 + k_{\parallel}^2 = k_{i\perp} \cosh(y_i). \tag{4.333}
\end{aligned}$$

In the multiregge region, using the two-dimensional longitudinal components of δ^4 function, one can perform dy_0 and dy_{n+1} integrations, giving

$$d\Phi_{n+1} = \int \frac{1}{2s} \frac{d^2 k_{0\perp}}{(2\pi)^2} \frac{d^2 k_{n+1\perp}}{(2\pi)^2} \left(\prod_{i=1}^n \frac{dy_i d^2 k_{i\perp}}{4\pi(2\pi)^2} \right) (2\pi)^2 \delta^2 \left(\sum_{i=0}^{n+1} k_{i\perp} \right). \tag{4.334}$$

Now the ground is prepared and we can write the expression for the discontinuity of the amplitude of Fig.(4.4),

$$\begin{aligned}
\text{Disc} \left[iM_{\mu_a \mu_b \mu_{a'} \mu_{b'}}^{aba'b'} \right] &\simeq \sum_{n=0}^{\infty} \int \frac{1}{2s} \frac{d^2 k_{0\perp}}{(2\pi)^2} \frac{d^2 k_{n+1\perp}}{(2\pi)^2} \left(\prod_{i=1}^n \frac{dy_i d^2 k_{i\perp}}{4\pi(2\pi)^2} \right) (2\pi)^2 \delta^2 \left(\sum_{i=0}^{n+1} k_{i\perp} \right) \\
&\quad \times (2is)^2 \delta_{\mu_a \mu_{a'}} \delta_{\mu_b \mu_{b'}} (igf^{ad_0 c_1}) (igf^{c'_1 d_0 a'}) \\
&\quad \times \prod_{l=0}^n \frac{e^{[\alpha(t_{l+1}) + \alpha(t'_{l+1})](y_l - y_{l+1})}}{t_{l+1} t'_{l+1}} \\
&\quad \times \prod_{j=1}^n (igf^{c_j d_j c_{j+1}}) (igf^{c'_j d'_j c'_{j+1}}) \prod_{i=1}^n C(q_i, q_{i+1}) \cdot C(q - q_i, q - q_{i+1}) \\
&\quad \times (igf^{bd_{n+1} c_{n+1}}) (igf^{c'_{n+1} d_{n+1} b'}) \tag{4.335}
\end{aligned}$$

where $t'_i = (q - q_i)^2$ and q is the overall momentum transfer in the elastic scattering. For the contraction of two Lipatov vertices we have,

$$\begin{aligned}
C(q_i, q_{i+1}) \cdot C(q - q_i, q - q_{i+1}) &= -2 \left[q_{\perp}^2 - \frac{(q - q_i)_{\perp}^2 q_{i+1\perp}^2 + (q - q_{i+1})_{\perp}^2 q_i^2}{(q_i - q_{i+1})_{\perp}^2} \right] \\
&\equiv -2\mathcal{K}(q_i, q_{i+1}). \tag{4.336}
\end{aligned}$$

Now using (4.2.10), the discontinuity of the scalar amplitude, $\text{Disc}A^T(s, t)$, can be extracted via multiplying (4.2.9) by the desired projection operator,

$$\begin{aligned} \text{Disc}A^T(s, t) &= \sum_{n=0}^{\infty} (-g^2 C_T)^{n+2} \int \prod_{i=1}^n \frac{dy_i}{4\pi} \prod_{j=1}^{n+1} \frac{d^2 q_{j\perp}}{(2\pi)^2} \\ &\quad \times 2is \prod_{l=0}^n \frac{e^{[\alpha(t_{l+1}) + \alpha(t'_{l+1})](y_l - y_{l+1})}}{t_{l+1} t'_{l+1}} \prod_{m=1}^n 2\mathcal{K}(q_m, q_{m+1}), \end{aligned} \quad (4.3.37)$$

where the constant C_T comes from projecting the combination of color factors of the diagram out using the color projectors which are in turn given by

$$C_T = N_c \quad \text{for singlet} \quad ; \quad C_T = N_c/2 \quad \text{for octet.} \quad (4.3.38)$$

Note that the $d^2 k_{0\perp}$ integration has been carried out using the δ^2 function. Also, we have transformed the integration variables from the transverse momenta of the produced gluons to that of the gluons exchanged in t -channel.

With reference to (4.2.25), the next step is taking the Laplace transform of (4.3.37), as in

$$\begin{aligned} \mathcal{A}_i^T(t) &= \int_0^{\infty} dy e^{-ly} \text{Disc}A^T(s, t) \\ &= \sum_{n=0}^{\infty} (-g^2 C_T)^{n+2} \int_0^{\infty} dy e^{-yl} \int \prod_{i=1}^n \frac{dy_i}{4\pi} \prod_{j=1}^{n+1} \frac{d^2 q_{j\perp}}{(2\pi)^2} \\ &\quad \times 2is \prod_{k=0}^n \frac{e^{[\alpha(t_{k+1}) + \alpha(t'_{k+1})](y_k - y_{k+1})}}{t_{k+1} t'_{k+1}} \prod_{m=1}^n 2\mathcal{K}(q_m, q_{m+1}) \cdot (4.3.39) \end{aligned}$$

Now the y_i 's and y are a total of $n + 1$ variables. In the integrand, however, these are entangled as $n + 1$ differences $u_i = y_i - y_{i+1}$. Transforming from the original variables to u_i 's and keeping in mind that $y = y_0 - y_{n+1} = \ln(-s/t)$ is the overall rapidity, and $s = -t \exp(y_0 - y_{n+1}) = -t \exp[\sum_{i=0}^n (y_i - y_{i+1})]$, then the integration over u_i 's can easily be carried out and we will end up with

$$\begin{aligned} \mathcal{A}_l^T(t) &= -2it(4\pi\alpha_s)^2 C_T^2 \sum_0^\infty \int \frac{d^2 q_{j\perp}}{(2\pi)^2} \\ &\times \frac{1}{t_1 t'_1} \frac{1}{l-1-\alpha(t_1)-\alpha(t'_1)} \prod_{m=1}^n \frac{-2\alpha_s C_T \mathcal{K}(q_m, q_{m+1})}{t_{i+1} t'_{i+1} [l-1-\alpha(t_{i+1})-\alpha(t'_{i+1})]} . \end{aligned} \quad (4.3.40)$$

This result can be written as a recursive relation

$$\mathcal{A}_l^T(t) = -2it(4\pi\alpha_s)^2 C_T^2 \int \frac{d^2 q_{1\perp}}{(2\pi)^2} \frac{1}{q_{1\perp}^2 (q - q_1)_\perp^2} f_l^T(q_1, t) , \quad (4.3.41)$$

with the function $f_l^T(q, t)$ satisfying the equation

$$[l-1-\alpha(t_1)-\alpha(t'_1)] f_l^T(q_i, t) = 1 - 2\alpha_s C_T \int \frac{d^2 q_{2\perp}}{(2\pi)^2} \frac{\mathcal{K}(q_1, q_2)}{q_{2\perp} (q - q_2)_\perp^2} f_l(q_2, t) . \quad (4.3.42)$$

In the last step we have made the replacements $t_i \simeq -q_{i\perp}^2$ and $t'_{i\perp} \simeq -(q - q_i)_\perp^2$. The result in (4.3.42) is the BFKL integral equation [34]. It describes the evolution of a gluon ladder in LLA. The left side of the equation reflects the contribution of the virtual corrections in the t -channel and the function $\mathcal{K}(q_1 - q_2)$ on the right side reflects the effect of radiative corrections.

Solving this equation for the octet solution one obtains [30],

$$f_l^{oct}(q, t) = \frac{1}{l-1-\alpha(t)} , \quad (4.3.43)$$

with the corresponding amplitude,

$$A^{oct}(s, t) = -4\pi N_c \alpha_s \frac{\pi\alpha(t)}{\sin \pi\alpha(t)} \left(1 + e^{i\pi\alpha(t)}\right) \left(\frac{s}{-t}\right)^{1+\alpha(t)} . \quad (4.3.44)$$

The singlet solution is more involved. We define the new function $\bar{f}_l(q_1, q_2, t)$ [30] through

$$f_l^{sing}(q_1, t) = \int \frac{d^2 q_{2\perp}}{(2\pi)^2} \bar{f}_l(q_1, q_2, t) . \quad (4.3.45)$$

Then in forward scattering $t = 0$ we can further define $f_l(q_1, q_2)$ as

$$f_l(q_1, q_2) = \frac{1}{8\pi^2} \frac{q_{2\perp}^2}{q_{1\perp}^2} \bar{f}_l(q_1, q_2, t=0) , \quad (4.3.46)$$

and replacing for f_l^{sing} in terms of this new function, the BFKL equation will yield

$$f_l(q_1, q_2) \simeq \frac{1}{(2\pi)^2} \frac{1}{(q_{1\perp}^2 q_{2\perp}^2)^2} \frac{\pi}{[B(l-1-A)]^{1/2}} e^{-\nu_0 |\ln(q_{1\perp}^2/q_{2\perp}^2)|} \quad (4.3.47)$$

with

$$A = 4 \frac{\alpha_s N_c}{\pi} \ln 2 \quad ; \quad B = 14\zeta(3) \frac{\alpha_s N_c}{\pi} \quad ; \quad \nu_0 = \left(\frac{l-1-A}{B} \right)^{1/2} . \quad (4.3.48)$$

Using this function, the total scattering cross section turns out to be

$$\sigma_{tot} = s^A , \quad (4.3.49)$$

which obviously violates the Froiassart bound $\sigma_{tot} \leq \ln^2(s)$.

Chapter 5

Calculating high energy scattering amplitude using non-abelian cut diagrams

In this chapter we will present an introduction to the non-abelian cut diagram [22] technique as well as demonstrate its application to a 6th-order calculation [35]. This calculation has been done [19, 20, 21, 34] using standard Feynman rules. A notable but not so positive feature of using standard Feynman rules is the prevalent cancellation of leading powers of $\ln(s)$ which takes place among the diagrams of a certain order. This could be viewed as a down side for such an approach because much of the effort that is put into the calculation eventually disappears through cancellations. Here is where the merits of non-abelian cut diagram technique lie. The cancellations are prebuilt into the non-abelian cut rules so what one calculates is directly the sum with the cancellation already built in. This feature makes higher order calculations more feasible.

The outline of this chapter is as follows. In the next section high energy kinematics is reviewed. In section 2 abelian cut diagrams and in section 3 non-abelian cut diagrams will be discussed. A review of the lightcone integration method will be presented in section 4. Section 5 is devoted to a

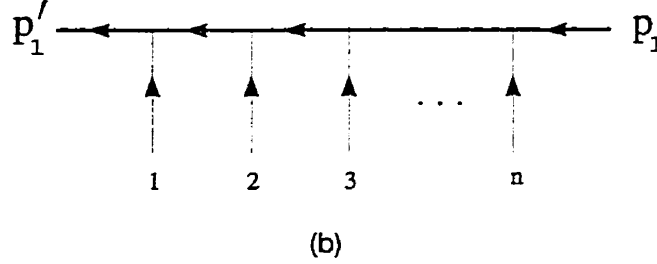
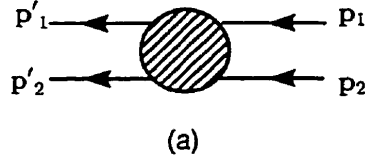


Figure 5.1: (a) External momenta (b) An electron (quark) \rightarrow electron (quark) + n photon (gluon) tree diagram

brief summary of the 6th-order calculation results. Sixth order cut diagram calculations are the subject of section 6. Finally, in section 7, a discussion of the results will be presented.

5.1 High energy kinematics

We will assume the colliding beams in their c.m. system to be directed along the z direction. In lightcone coordinates, $p^\pm = p^0 \pm p^3$, the components of a four-vector are labeled in the order $p^\mu = (p^+, p^-, \vec{p}_\perp)$, with the two-dimensional vector \vec{p}_\perp lying in the transverse x - y plane. For brevity, from now on we will suppress the vector sign over transverse vectors. In this notation, the incoming fermion momenta are $p_1 = (\sqrt{s}, 0; 0)$ and $p_2 = (0, \sqrt{s}; 0)$, in which their mass m has been neglected. The outgoing fermion momenta are approximately given by $p'_1 = (\sqrt{s}, 0; \Delta)$ and $p'_2 = (0, \sqrt{s}; -\Delta)$. See Fig.(5.1.a). Suppose n photons are connected to the upper fermion line as shown in Fig.(5.1.b). The initial and final fermions are on-shell but the pho-

tions can be off-shell, though with an amount of energy far less than \sqrt{s} . At high energy, the numerator of the propagator can be approximated by

$$(\gamma \cdot p + m) \simeq \gamma \cdot p = 2m \sum_{\lambda} u_{\lambda}(p_1) \bar{u}_{\lambda}(p_1), \quad (5.1.1)$$

provided the Dirac spinors are normalized to $\bar{u}_{\lambda}(p) u_{\lambda'}(p) = \delta_{\lambda\lambda'}$. With that, the dominant current $\bar{u}_{\lambda}(p_1) \gamma^{\alpha} u_{\lambda'}(p_1)$ at high energy is just its translational part $\delta_{\lambda\lambda'} p_1^{\alpha}/m$. This shows that the spin content at high energy is unimportant. All that it does is to enforce helicity conservation of the fermion and to produce a factor $2p_1$ at each vertex together with an overall normalization factor of $1/2m$. The denominator of the i th inverse propagator is

$$(p_1 + \sum_{j=1}^i q_j)^2 - m^2 + i\epsilon \simeq s(\sum_{j=1}^i x_j + i\epsilon) \quad (5.1.2)$$

where $x_i = q_{i-}/\sqrt{s}$. For a diagram of the form of Fig.(5.1) with the electron replaced by a scalar particle (making all the vertices scalar-scalar type), the scalar amplitude is given by

$$a[12 \cdots n] \equiv -2\pi i \delta \left(s \sum_{j=1}^n x_j \right) \cdot \prod_{i=1}^{n-1} \frac{1}{s \sum_{j=1}^i x_j + i\epsilon}. \quad (5.1.3)$$

Note that a momentum conservation δ -function for the negative components (together with an explicit factor $-2\pi i$) has been incorporated. In (5.1.3) the ordering of the vertical scalar lines from left to right is $[123 \cdots n]$. If they are ordered differently, say $[v_1 v_2 \cdots v_n] \equiv V$, then the corresponding amplitude is

$$a[v_1 v_2 \cdots v_n] \equiv a[V] \equiv -2\pi i \delta \left(s \sum_{j=1}^n x_{v_j} \right) \cdot \prod_{i=1}^{n-1} \frac{1}{s \sum_{j=1}^i x_{v_j} + i\epsilon}. \quad (5.1.4)$$

5.2 Abelian cut diagrams

The high energy limiting form of the propagator, (5.1.2), leads to some interesting results. It allows computing sums of Feynman diagrams with many

delicate cancellations in a simple way through special rules. This can be achieved by using the *cut diagrams* which we shall describe in this section and the next. The derivation of cut diagrams relies on two exact combinatorial formulas for the quantity $a[V]$ in (5.1.4), the *factorization formula* and the *multiple commutator formula*, derived in [22]. The latter will be used in QCD calculations. We shall discuss the former in this section, and the latter in the next section.

Consider a total of M photon (scalar particle) lines grouped in an arbitrary way into the form $\{n_1, n_2, \dots, n_j\}$ such that $M \equiv \sum_{i=1}^j n_i$. Suppose further that in each group, n_i , the photons have certain ordering, $[v_{i1} v_{i2} \dots v_{in_i}] \equiv V_i$. We shall use the notation $\{V_1; V_2; \dots; V_j\}$ to denote the set of *all* orderings of the M photon lines formed by merging photons from different groups together, *provided* the relative orderings of lines within each V_i are maintained. The number of orderings in this set is given by the multinomial coefficient $M! / \prod_{i=1}^j n_i!$. For example, if $V_1 = [135]$, $V_2 = [24]$, then $\{V_1; V_2\} \equiv \{135; 24\}$ consists of the $5!/3!2! = 10$ orderings $[13524]$, $[13254]$, $[13245]$, $[12354]$, $[12345]$, $[12435]$, $[21354]$, $[21345]$, $[21435]$, and $[24135]$.

We shall use the notation

$$a\{V_1; V_2; \dots; V_j\} \equiv \sum_{V \in \{V_1; V_2; \dots; V_j\}} a[V] \quad (5.2.5)$$

to denote the sum of all amplitudes for the gluon orderings in the set. The factorization formula [22] then states that

$$a\{V_1; V_2; \dots; V_j\} = \prod_{i=1}^m a[V_i]. \quad (5.2.6)$$

In particular, if each set $V_i = [v_i]$ consists of only one photon line labeled by v_i , then $\{V_1; V_2; \dots; V_m\}$ is the set of *all* orderings of the m photon lines. In that case the factorization formula reduces to the well-known *eikonal formula*

[19, 36]. Other special cases of this formula have also been discovered before [21, 37]. Since in (5.2.6) the ordering of the factors on the right side is immaterial we will call (5.2.6) an *abelian cut rule* and the corresponding diagrams *abelian cut diagrams*.

It is useful to adopt an alternative notation for the right hand side of (5.2.6) to denote $\prod_{i=1}^m a[V_i]$ simply as $a[V_1|V_2|\cdots|V_n]$. This notation is suggestive because the vertical bar can be interpreted graphically as a cut in the fermion propagator between the last photon line of V_i and the first photon line of V_{i+1} . For a cut propagator, instead of the usual factor $(s \sum_{j=1}^i x_{v_j} + i\epsilon)^{-1}$, we have $-2\pi i \delta(s \sum_{j=1}^i x_{v_j})$. This notation is also convenient because it makes (5.2.6) deceptively simple. It now reads $a\{V_1; V_2; \cdots; V_m\} = a[V_1|V_2|\cdots|V_m]$; we simply have to change the semicolons to vertical bars.

Cut propagators are not limited to tree diagrams like Fig.(5.1.b). The off-shell photons can be connected to other diagrams to form a composite diagram that inherits the original cuts. The cut diagrams so formed are similar to, but different from, the Cutkosky cut diagrams. Similar because we have the same factors for the cut propagators, different because the cuts here occur only on fermion lines whereas in a Cutkosky diagram they can occur on any line. Moreover, via (5.2.6), our cut diagram represents a sum of $M!/\prod_{j=1}^m n_j!$ (uncut) Feynman diagrams, with their real and imaginary parts fully included, which is unlike the Cutkosky diagrams in which only the imaginary part or the discontinuity is represented.

It is clear from (5.2.6) that the factorization formula can be thought of as a sum rule, to represent sums of Feynman diagrams as cut diagrams. As will be discussed in section 6, a cut diagram is easier to compute than an uncut diagram. In this way not only it is unnecessary to compute the individual diagrams first, the cut diagram representing the sum is actually easier to

compute than just one single Feynman diagram.

5.3 Non-abelian cut diagrams

The method of abelian cut diagrams introduced in the last section can be directly applied to QED diagrams as was illustrated. It can also be applied to similar QCD diagrams but with some extra considerations due to the color matrix t_a at each gluon-quark vertex. One can, however, use an extension of the factorization formula, (5.2.6), known as the *multiple commutator formula* to be discussed below.

In order to incorporate the color matrices we have to extend our previous notation of (5.1.4). With reference to Fig.(5.1.b), for n gluons attached to a quark line we adopt the following notation,

$$A[v_1 v_2 \cdots v_n] = a[v_1 v_2 \cdots v_n] t[v_1 v_2 \cdots v_n] \equiv a[V] t[V] \equiv A[V] \quad (5.3.7)$$

where $t[V] = t_{v_1} t_{v_2} \cdots t_{v_n}$. What we want is a formula for the sum of the $n!$ permuted gluon orderings, $\mathcal{A} = \sum_{V \in S_n} A[V]$. The generalization of the factorization formula, the multiple commutator formula is [22],

$$\mathcal{A} \equiv \sum_{V \in S_n} a[V] t[V] = \sum_{V \in S_n} a[V_c] t[V_c]. \quad (5.3.8)$$

It expresses the sum of $a[V] t[V]$ in terms of sums over the corresponding cut amplitude $a[V_c] t[V_c]$. Compared to the eikonal formula this looks complicated; instead of a single term on the right hand side we have now a sum over $n!$ terms. The complication is inevitable because we are attempting to sum up amplitudes for *every* color. However, we shall see that many of these terms are actually zero, and moreover, the cut diagrams on the right are considerably simpler to evaluate than the uncut diagrams on the left. Again delicate cancellations will largely be incorporated automatically as before.

It remains to say what each factor on the right side of (5.3.8) means. Given a $V = [v_1 v_2 \cdots v_n]$, start from the rightmost number v_n and proceed leftward until one comes to the first number less than v_n . Put a cut just to the right of this number. Then start from this number and proceed leftward again until one comes to the first number that is less than this number, and another cut is put just to the right of this new minimum number. Continue this way until the end and we have constructed the cut diagram V_c . For example, for $n = 2$, the 2 cut diagrams are $[12]_c = [1|2]$ and $[21]_c = [2|1]$. For $n = 3$, the six cut diagrams are $[123]_c = [1|2|3]$, $[213]_c = [2|1|3]$, $[312]_c = [3|1|2]$, $[132]_c = [1|3|2]$, $[231]_c = [2|3|1]$, and $[321]_c = [3|2|1]$.

To each cut diagram we associate a spacetime cut amplitude $a[V_c]$ as described in the last section. Namely, it is given by (5.1.4) except the propagator at a cut is replaced by $-2\pi i \delta(s \sum_j x_{v_j})$.

The complementary diagram V'_c of a cut diagram V_c is obtained as follows. If a cut appears between two numbers in V_c , then there will be no cut between the same two numbers in V'_c , and vice versa. For $n = 2$, the complementary cut diagrams are $[1|2]' = [12]$ and $[2|1]' = [21]$. For $n = 3$, the complementary cut diagrams are $[1|2|3]' = [123]$, $[2|1|3]' = [213]$, $[3|1|2]' = [312]$, $[1|3|2]' = [132]$, $[2|3|1]' = [231]$, and $[3|2|1]' = [321]$.

When no cut appears in V'_c the color factor $t[V'_c]$ is simply $t[v_1 v_2 \cdots v_n] = t_{v_1} t_{v_2} \cdots t_{v_n}$. If a cut appears between v_i and v_{i+1} , then the product $t_{v_i} t_{v_{i+1}}$ is replaced by their commutators $[t_{v_i}, t_{v_{i+1}}]$. If two or more consecutive cuts appears, then the corresponding product of t 's is replaced by multiple commutators. For example, $t[2|1|3] = [t_2, t_1] t_3$, $t[2|3|1] = [t_2, [t_3, t_1]]$, and $t[4|3|2|1] = [t_4, [t_3, [t_2, t_1]]] t_5$.

5.4 Lightcone integration

In this section we will review the technique of lightcone integration [19, 28]. As was mentioned in section 5.1 we adopt the lightcone coordinates for the external as well as loop momenta. In terms of lightcone coordinates we have for each loop,

$$\begin{aligned} \frac{i}{(2\pi)^4} d^4 q &= \frac{dq^+ dq^-}{2(2\pi)^2} \frac{d^2 q_\perp}{(2\pi)^2} = \frac{1}{4\pi} \left[\frac{\sqrt{s} dq^+}{-2\pi i} \right] dx \left[\frac{d^2 q_\perp}{(2\pi)^2} \right] \\ &\equiv \frac{1}{4\pi} [\mathcal{D}q^+] dx [\mathcal{D}q_\perp]. \end{aligned} \quad (5.4.9)$$

To find the asymptotic behavior of diagram we will need to take the following steps,

1. Performing the ‘+’ integrations using residue technique and flow diagrams.
2. Performing the ‘-’ integrations. This will lead to the appearance of powers of $\ln(s)$.
3. The q_\perp integration will be left undone.

5.4.1 The ‘+’ integration

Aside from being suitable for describing external colliding particles, lightcone coordinates make the implementation of the residue technique more straightforward. Since $a \cdot b = (1/2)(a^+ b^- + a^- b^+) - a_\perp \cdot b_\perp$ each denominator of a propagator is a linear function of q_i^+ . This means that each propagator provides a simple pole for each ‘+’ integration. The integration contour has a part along the real q_i^+ axis and a semicircle part that we always choose to lie in the lower plane. The result of integration is therefore $-2\pi i$ times the

residue of the pole summed over all the poles in the lower plane. The question now is which poles will be in the lower plane in a diagram with many propagators. The answer clearly depends on the sign and relative magnitude of ‘-’ momenta which are components of loop momenta themselves. The *flow diagrams* will provide the answer pictorially [19].

In a flow diagram the arrow on each line indicates the flow of the negative component of the momentum, i.e., p_- , a quantity which we always choose to be positive. Because of this latter specification there may be more than one flow diagram associated with each Feynman diagram. The reason is that in a standard Feynman diagram an arrow would indicate a momentum irrespective of its sign but in a flow diagram, by our convention, we are required to reverse the direction of the arrow and multiply the momentum by a minus sign when the momentum is negative. Conservation of ‘-’ momentum at each vertex would prevent all arrows pointing toward or away from a vertex, i.e., such diagrams are zero. Also in any loop of a flow diagram, one would generally have some of the arrows pointing in one direction and some in the opposite direction. The two groups will have their poles on opposite sides in the complex momentum plane. By choosing q_i^+ (or $-q_i^+$) as loop variable, which can always be done, we can make the group with fewer members to have poles in the lower plane. A corollary of this latter property is that a flow diagram whose one loop has all its arrows pointing in the same direction will be zero.

To illustrate the above explanations consider the following two examples. Figures (5.2.a) and (5.3.a) are Feynman diagrams and (5.2.b), (5.3.b,c) are flow diagrams. Since the lower line is always the source of negative current, at p_2 the arrow points inward and at p'_2 the arrow points outward. In Fig.(5.2.b) this will leave no freedom for the other flow lines but to be the way they

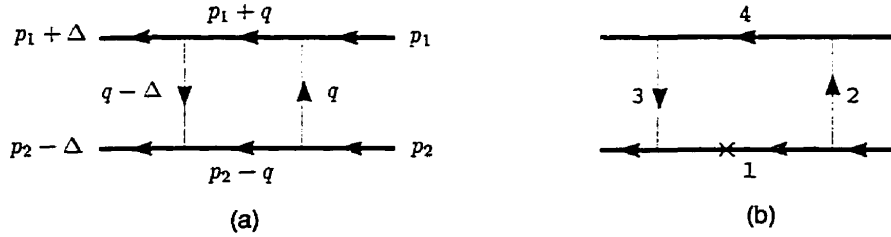


Figure 5.2: (a) A one loop Feynman diagram (b) its flow diagram

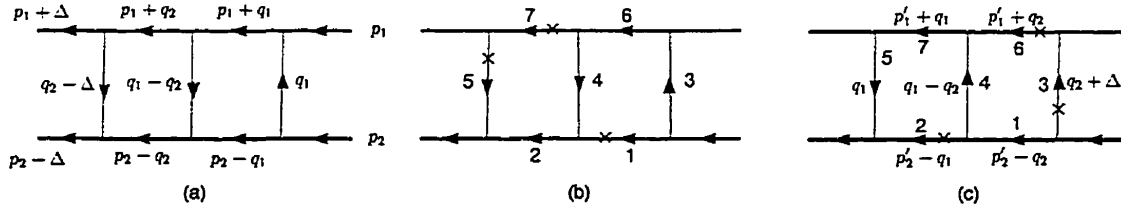


Figure 5.3: (a) A two-loop Feynman diagram, (b) and (c) its flow diagrams

are drawn. In Fig.(5.3.a), however, since the direction of the arrow on the boundary of the two loops can be changed there are two flow diagrams. Following the above discussion we choose the pole of line 1 (marked with an \times) to be in the lower plane which would require $-p_2^+$ to be the '+' loop momentum in (5.2.b). In (5.3.b) for the right loop we choose the pole of line 1. For the left loop there seem to be two choices (2, 4) and (5, 7). We have chosen (5, 7). The reason is that with the approximation of (5.1.2), q_i^+ never appears on the propagator along the top line, so apparent poles there are actually absent. So for the choice indicated one essentially has only one pole per loop.

5.4.2 The '-' integration

Having completed the '+' integrations, all positive momenta are now fixed by their values at the poles. In the propagators not taken as poles, we have the product of positive and negative momenta (some linear combination of

x_i times s) plus the transverse part. As a short hand notation let $a_m = k_{m\perp}^2$ when k_m^μ is the four momentum of the line. Since all x_i are positive, by our earlier convention, the lower limit of x_i integrations is zero, but in order for the approximation in (5.1.2) to be valid the lower limit cannot be zero but rather of the order of Δ^2/s which is a lower cutoff and is consistent with the leading-log approximation. In leading-log approximation, factors of $\ln(s)$ appear when x_i are close to the lower cutoff. Therefore we can safely ignore x_i compared to 1.

Following the '+' momentum integration of Fig.(5.2.b) with the pole as indicated we will have

$$q^+ = \frac{a_1 - i\epsilon}{\sqrt{s}(1-x)} \simeq 0, \quad (5.4.10)$$

so the denominator D and the numerator N are approximately

$$D = r_1 d_2 d_3 d_4 \simeq (1-x)a_2 a_3 (sx - a_4) ; \quad N \simeq g^4 \frac{[(2p_1) \cdot (2p_2)]^2}{(2m)^2} = \frac{g^4 s^2}{m^2}, \quad (5.4.11)$$

where r_1 is the coefficient of q^+ divided by \sqrt{s} . Using (5.4.9) the amplitude is,

$$\begin{aligned} M &= - \left(\frac{1}{4\pi} \right) \frac{g^4 s}{m^2} \int \mathcal{D}q_\perp \frac{1}{a_2 a_3} \int_{\frac{\Delta^2}{s}}^1 \frac{dx}{x} \\ &= - \frac{s \ln(se^{-i\pi})}{4\pi m^2} g^4 I_2(\Delta), \end{aligned} \quad (5.4.12)$$

where $I_2(\Delta)$ is defined as

$$I_n(\Delta) = \int \left(\prod_{i=1}^n \frac{d^2 q_{i\perp}}{(2\pi)^2} \right) \frac{1}{q_{i\perp}^2} (2\pi)^2 \delta^2 \left(\sum_{i=1}^n q_{i\perp} - \Delta \right). \quad (5.4.13)$$

In (5.4.12), for small values of x the denominator $(sx - a_4)$ is negative and therefore the logarithm picks up a factor of $e^{-i\pi}$.

In the second example of Figs.(5.3.b) the poles are at,

$$q_1^+ = \frac{a_3}{\sqrt{s}x_1} ; \quad -q_2^+ = \frac{a_2}{\sqrt{s}(1-x_2)} \simeq 0. \quad (5.4.14)$$

Therefore the denominator is

$$\begin{aligned}
D &= r_1 \cdot d_2 \cdot d_3 \cdot d_4 \cdot r_5 \cdot d_6 \cdot d_7 \\
&\simeq [(1-x_1)] \left[-\frac{a_5(1-x_2)}{x_2} - a_2 \right] [a_3] \left[-\frac{a_5(x_1-x_2)}{x_2} - a_4 \right] [x_2] [sx_1] [sx_2] \\
&\simeq s^2 a_3 a_5 x_1 [x_2(a_4 - a_5) + x_1 a_5], \tag{5.4.15}
\end{aligned}$$

and the numerator is $N = (2g^6 s^3)/m^2$. So the contribution of Fig.(5.3.b) is,

$$\begin{aligned}
M_b &= - \left(\frac{1}{4\pi} \right)^2 \frac{2g^6 s^3}{m^2} \int \mathcal{D}q_{1\perp} \mathcal{D}q_{2\perp} \frac{1}{a_3 a_5} \int \frac{dx_1 dx_2}{x_1 [x_1 a_5 + x_2 (a_4 - a_5)]} \\
&= - \frac{g^6 s \ln(s)}{8\pi m^2} \int \mathcal{D}q_{1\perp} \mathcal{D}q_{2\perp} \frac{\ln(a_5/a_4)}{a_3 a_5 (a_5 - a_4)}, \tag{5.4.16}
\end{aligned}$$

where the minus sign is an overall factor. Also, each loop has an i factor and the factor of $1/(4\pi)$ is due to (5.4.9).

In Fig.(5.3.c) we have used a slightly different momentum labeling for the lines which can be deduced from Fig.(5.3.a) by $q_1 \rightleftharpoons q_2$ followed by a shift $q_i \rightarrow q_i + \Delta$. Now if we let $q_{i\perp} \rightarrow -q_{i\perp}$, we can see that the Fig.(5.3.c) and (5.3.b) are in fact equal. Therefore the total result will be

$$M_a = M_b + M_c = 2M_b \simeq - \frac{g^6 s \ln(s)}{4\pi m^2} \int \mathcal{D}q_{1\perp} \mathcal{D}q_{2\perp} \frac{\ln(a_5/a_4)}{a_3 a_5 (a_5 - a_4)}. \tag{5.4.17}$$

The above two examples illustrate the the main features of lightcone integration technique. In the next section, we will use this method to calculate the $O(6)$ cut diagrams.

5.5 Review of the sixth-order calculations

With an overview of the lightcone integration method completed, we will now consider the leading-log calculations related to the scattering of two quarks up to 6th-order. The energy regime of interest is $-t \ll s$ where s is the square of c.m. energy and $t = \Delta^2$ is the square of momentum transfer.

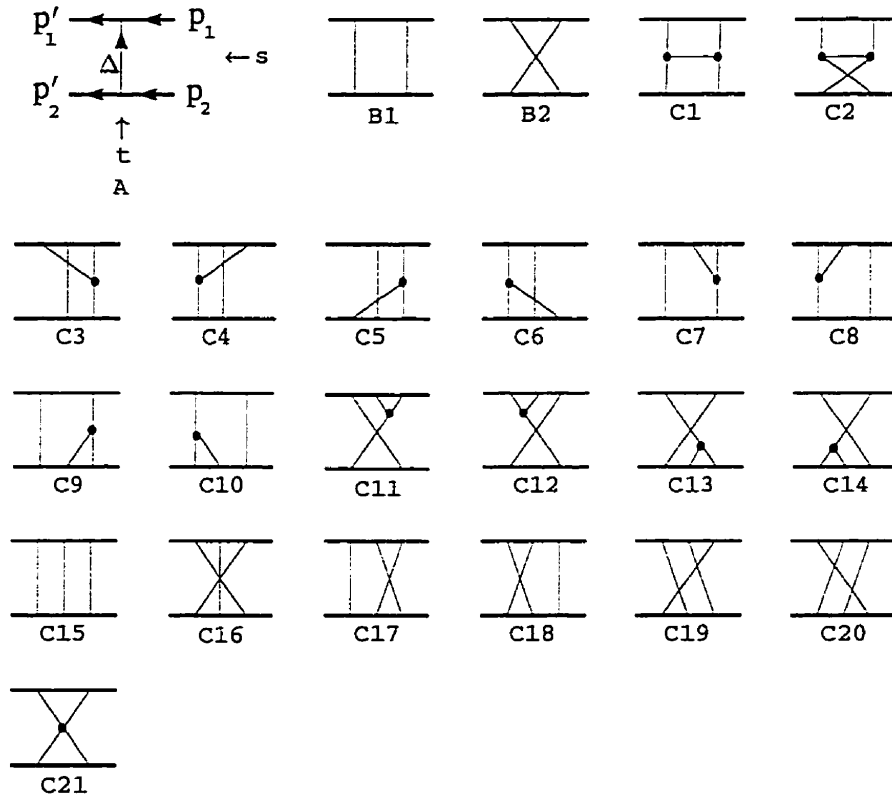


Figure 5.4: Quark-quark scattering in QCD up to 6th order. The thick lines at the top and bottom of each diagram are the q-lines, and the thin lines are gluon lines

As was mentioned earlier in the introduction, this calculation can be done using the standard Feynman diagrams [19, 20, 21]. We will first review the established results. The relevant topologically distinct diagrams up to 6th-order are shown in Fig.(5.4). The 2nd order diagram is labeled A, the 4th order diagrams labeled B1 and B2, and the 6th order diagrams C1 to C21. This last labeling¹ is identical to the ones used in Fig.(12.7) of Ref.[19].

Under the interchange of the Mandelstam variables $s = (p_1 + p_2)^2$ and

¹Note however that for later convenience the fermion arrows in Fig.(5.4) and all subsequent figures are drawn from right to left, reflecting the order one writes matrices as well as initial and final states on a piece of paper, whereas in Ref [19] they are drawn in a more conventional way from left to right.

$u = (p_1 - p'_2)^2$, the space-time part of each of these diagrams will either remain unchanged, or will become identical to the space-time part of another diagram in the set. For example, $A \leftrightarrow A$, $B_2 \leftrightarrow B_1$, $C_2 \leftrightarrow C_1$, $C_{15} \leftrightarrow C_{16}$, $C_{17} \leftrightarrow C_{19}$, and $C_{18} \leftrightarrow C_{20}$, under $s \leftrightarrow u$. There exist other symmetries as well, $(p_1 \rightleftharpoons p_2 \text{ and } p'_1 \rightleftharpoons p'_2) \Rightarrow (s \rightarrow s, u \rightarrow u)$ and $(p_1 \rightleftharpoons p'_1 \text{ and } p_2 \rightleftharpoons p'_2) \Rightarrow (s \rightarrow s, u \rightarrow u)$. Because of these symmetries many of these diagrams are equal. With the normalization of Dirac spinors as $\bar{u}u = 1$ the results are

$$\begin{aligned}
A &= -\frac{g^2 s}{2m^2} I_1 \cdot \mathbf{G}_1, \\
B_1 &= -\frac{g^4 s}{4\pi m^2} I_2 \cdot \mathbf{G}_2, \\
B_2 &= +\frac{g^4 s}{4\pi m^2} I_2 \cdot (\mathbf{G}_2 + c \mathbf{G}_1), \\
\overline{C_1} &= +\frac{g^6 s}{8\pi m^2} \ln^2(se^{-i\pi}) \left[\frac{1}{2} \Delta^2 I_2^2 - J_2 I_2 \right] \cdot \mathbf{G}_3, \\
\overline{C_2} &= -\frac{g^6 s}{8\pi m^2} \ln^2(s) \left[\frac{1}{2} \Delta^2 I_2^2 - J_2 I_2 \right] \cdot (\mathbf{G}_3 + c^2 \mathbf{G}_1), \\
C_3 &= C_4 = C_5 = C_6, \\
&= +\frac{g^6 s}{32\pi^2 m^2} \{ \ln^2(se^{-i\pi}) - \ln^2(s) \} J_2 I_2 \cdot (\mathbf{G}_3 - c \mathbf{G}_2), \\
C_7 &= C_8 = C_9 = C_{10}, \\
&= -\frac{g^6 s}{32\pi^2 m^2} \ln^2(se^{-i\pi}) J_2 I_2 \cdot (-c \mathbf{G}_2) \\
C_{11} &= C_{12} = C_{13} = C_{14} \\
&= +\frac{g^6 s}{32\pi^2 m^2} \ln^2(s) J_2 I_2 (-c \mathbf{G}_2 - c^2 \mathbf{G}_1), \\
C_{15} &= -\frac{g^6 s}{4\pi^2 m^2} J_3 \cdot \mathbf{G}_4, \\
C_{16} &= -\frac{g^6 s}{4\pi^2 m^2} \ln(s) J_3 \cdot (\mathbf{G}_4 - \mathbf{G}_3 + 3c \mathbf{G}_2 + c^2 \mathbf{G}_1), \\
C_{17} &= C_{18} = +\frac{g^6 s}{8\pi^2 m^2} (J_3 + i\pi I_3) \cdot (\mathbf{G}_4 + c \mathbf{G}_2), \\
C_{19} &= C_{20} = +\frac{g^6 s}{8\pi^2 m^2} (J_3 - i\pi I_3) \cdot (\mathbf{G}_4 - \mathbf{G}_3 + 2c \mathbf{G}_2). \quad (5.5.18)
\end{aligned}$$

In these expressions I_n is given by (5.4.13) and I_1 , $J_2(\Delta)$ and $J_3(\Delta)$ are

defined by

$$\begin{aligned}
I_1 &= \frac{1}{\Delta}, \\
J_2 &= \int \frac{d^2 q_\perp}{(2\pi)^2} \frac{1}{q_\perp^2}, \\
J_3 &= \int \left(\prod_{i=1}^3 \frac{dq_{i\perp}^2}{(2\pi)^2} \right) (2\pi)^2 \delta^2 \left(\sum_{i=1}^3 q_{i\perp} - \Delta \right) \frac{\ln \left(\frac{q_{2\perp}^2}{q_{3\perp}^2} \right)}{q_{1\perp}^2 q_{3\perp}^2 (q_{2\perp}^2 - q_{3\perp}^2)} \quad (5.5.19)
\end{aligned}$$

The functions I_2, I_3, J_2, J_3 are denoted respectively by I, I_1, K, I_2 in [19]. The infrared divergence of these integrals can be regulated by a mass, either put in by hand or via the Higgs mechanism. This regulation, discussed in the literature [19, 20, 21, 34], does not affect the following discussion so we shall ignore it. There is, however, an ultraviolet divergence in the integral defining $J_2(\Delta)$, but it turns out that this function disappears in the sum of the sixth order diagrams so it will cause no trouble.

The factors \mathbf{G}_i are the basis color factors depicted in Fig.(5.5) with $c = N/2$ for $SU(N)$ colors. Although these are not independent it turns out that they will lead to Reggeon resummation. Color decomposition of diagrams A – C21 can be easily carried out, see App.C, in a complete graphical manner [19] using the pictorial equivalent of the color commutation relations and the identities

$$[t_a, t_b] = if_{abc} t_c \quad ; \quad f_{abc} f_{abd} = 2c \delta_{cd} \quad ; \quad i^3 f_{adg} f_{bed} f_{cge} = ic f_{abc} \quad (5.5.20)$$

The color decomposition of each diagram in (5.5.18) remains valid irrespective of the color content of the quark, although the \mathbf{G}_i themselves would be different for different color of the quark.

The sum of all the terms in (5.5.18), from A to C20, is

$$\begin{aligned}
\mathcal{T} &= \frac{g^2 s}{2m^2} \left\{ -\frac{1}{\Delta^2} \left[1 - \bar{\alpha} \ln(s) + \frac{1}{2} \bar{\alpha}^2 \ln^2(s) \right] \cdot \mathbf{G}_1 + \frac{1}{2} i g^2 (I_2 - \frac{g^2 c}{\pi} I_3 \ln(s)) \cdot \mathbf{G}_2 \right. \\
&\quad \left. + i \frac{g^4}{2\pi} \ln(s) \left[I_3 - \frac{1}{2} \Delta^2 I_2^2 \right] \cdot \mathbf{G}_3 + \frac{g^4}{6} I_3 \cdot \mathbf{G}_4 \right\} \quad (5.5.21)
\end{aligned}$$

with

$$\bar{\alpha}(\Delta) \equiv \frac{g^2}{2\pi} c \Delta^2 I_2(\Delta). \quad (5.5.22)$$

The coefficient of \mathbf{G}_1 suggests the t -channel reggeized gluon to sixth-order. It is important to note the various cancellations that takes place to make the sum (5.5.21) vastly simpler than the individual terms appearing in (5.5.18). For example,

1. In the fourth order, the leading term proportional to $\ln(s)$ is cancelled out between B1 and B2 in the color amplitude proportional to \mathbf{G}_2 , though not in \mathbf{G}_1 .
2. In the sixth order, the leading $\ln(s)$ contributions to \mathbf{G}_4 from C15 to C20 also add up to zero. The expressions given in (5.5.18) are not accurate enough to deal with the subleading terms. The term in (5.5.21) proportional to \mathbf{G}_4 is obtained separately from the eikonal formula.
3. As a result of these cancellations, the energy dependence and the $SU(N)$ (or c) dependence of the \mathbf{G}_1 amplitude is $[g^2 c \ln(s)]^m$, and those of \mathbf{G}_2 , \mathbf{G}_3 and \mathbf{G}_4 are respectively $g^2 [g^2 c \ln(s)]^m$, $g^2 [g^2 \ln(s)]^m$, $g^4 [g^2 c \ln(s)]^m$. These dependences can be summarized all at once by introducing a different notation for the color factors. We shall use the notation $\mathbf{F}_{i,j}$ to denote a color factor with i parallel vertical lines connecting the two fermions, and j parallel horizontal lines joining any two of the vertical gluon lines. We shall also write $\mathbf{F}_{i,0}$ simply as \mathbf{F}_i . The relations with the color factors \mathbf{G}_i are $\mathbf{G}_1 = \mathbf{F}_1$, $\mathbf{G}_2 = \mathbf{F}_2$, $\mathbf{G}_3 = \mathbf{F}_{2,1}$, and $\mathbf{G}_4 = \mathbf{F}_3$. The g, c and $\ln(s)$ dependences of $\mathbf{F}_{i,j}$ in (5.5.21) are then given by $g^{2(i-1)} [g^2 c \ln(s)]^m c^{-j}$ for a diagram of order $2(m+i)$. We

shall refer to such dependences as *Regge-like*, for the Reggeization of the scattering amplitude to be discussed later relies critically on this feature of the scattering amplitude. Note from (5.5.18) that contributions from individual diagrams are not Regge-like. Only the sum is.

4. Simplification in transverse-momentum dependences also occurs in the sum. The simple integrals I_n survive, but the complicated integral J_3 and the divergent integral J_2 do not appear in the sum. This cancellation is highly nontrivial because both of them contribute different amounts to different color amplitudes. More specifically,
5. The function $J_3(\Delta)$ appears in all the color amplitudes $\mathbf{G}_1, \mathbf{G}_2, \mathbf{G}_3$ and \mathbf{G}_4 in diagrams C15 to C20. Those in $\mathbf{G}_2, \mathbf{G}_3, \mathbf{G}_4$ actually get cancelled out in the sum, but its presence in the \mathbf{G}_1 amplitude survives. However, since this term is of order $g^6 \ln(s)$, it is negligible compared to terms of order $g^6 \ln(s)s$ appearing in the \mathbf{G}_1 amplitudes of $\overline{\mathcal{C}2}$ and C11 to C14, it can be ignored in the leading-log result displayed in (5.5.21).
6. $J_2(\Delta)$ appears in the color amplitudes $\mathbf{G}_1, \mathbf{G}_2$ and \mathbf{G}_3 in individual diagrams C1 to C14 and all these appearances get cancelled out.

As a result of these cancellations, \mathcal{T} acquires a very simple interpretation in terms of reggeized gluon exchanges. These exchanges are constructed in such a way to ensure s -channel unitarity [19, 21].

Let us denote the reggeon propagator by

$$R_1(\Delta, s) = \frac{1}{\Delta^2} \exp[-\bar{\alpha}(\Delta) \ln(s)] . \quad (5.5.23)$$

This reduces to the (transverse part of the) ordinary propagator $I_1(\Delta) = \Delta^{-2}$

for small $g^2 c \ln(s)$. Similarly, let us denote the reggeized version of $I_n(\Delta)$ by

$$R_n(\Delta, s) = \int \left(\prod_{i=1}^n \frac{d^2 q_{i\perp}}{(2\pi)^2} R_1(q_{i\perp}, s) \right) \cdot (2\pi)^2 \delta^2 \left(\sum_{i=1}^n q_{i\perp} - \Delta \right) \quad (5.5.24)$$

indicating the exchange of n reggeons. Then to order g^6 in \mathcal{T} , we can write

$$\mathcal{T} = \frac{g^2 s}{2m^2} \left\{ -R_1(\Delta, s) \cdot \mathbf{F}_1 + i \frac{g^2}{2!} [R_2(\Delta, s) \cdot \mathbf{F}_2 + R_{2,1}(\Delta, s) \cdot \mathbf{F}_{2,1}] + \frac{g^4}{3!} R_3(\Delta, s) \cdot \mathbf{F}_3 \right\}. \quad (5.5.25)$$

In other words, the $\mathbf{F}_1, \mathbf{F}_2, \mathbf{F}_{2,1}$, and \mathbf{F}_3 components looked precisely like diagrams A, B1, C1, and C15 respectively, but with the vertical gluons replaced by their reggeized version whose propagators are given in (5.5.23), *and* with all longitudinal-momentum integrations omitted. To interpret it this way for $R_{2,1}\mathbf{F}_{2,1}$ we need to know the Lipatov-Dickinson vertex [38, 39] describing how elementary gluons are produced and absorbed from the reggeized gluons.

This remarkable simplicity and regularity led to the conjecture [19, 38] that the reggeized formula (5.5.25), suitably generalized, is the correct high energy limit to all perturbative orders. This conjecture is very difficult to verify on account of the sheer complexity in higher order calculations. For QCD in the 8th order it is simply not manageable without simplifying assumptions. If one assumes all cancellations occurred up to $O(g^6)$ will also occur in higher orders, the final result can be extracted from a *relatively* small set of diagrams. It is reported that this reggeization conjecture is true to 8th and 10th orders [38]. Even so these heroic calculations are so lengthy and complicated that to our knowledge the full details have never been published.



Figure 5.5: Color basis.

5.6 Sixth-order cut diagram calculations

Cut diagram calculations would require that we redraw the diagrams of Fig.(5.4) following the prescription described in section 5.3. We would therefore generate two new sets of diagrams, one for the space-time part and one for the color part. Then straightforward calculation will be carried out on individual elements of each set. For the sake of cut diagram calculations the group C1-C21 will be split into four sets, $S1 \equiv C1+C2+C21 = \overline{C1} + \overline{C1}$, $S2 \equiv C3+C4+C7+C8+C11+C12$, $S3 \equiv C5+C6+C9+C10+C13+C14$ and $S4 \equiv C15+C16+C17+C18+C19+C20$.

Due to the symmetries described in section 5.5 $S2=S3$, so calculation of $S2$ will be sufficient. The reason for this grouping is that the multiple-commutator formula gives a resummation of a set whose members are elements of a permutation group.

To implement the cut technique the first step is the numbering of the gluon lines as is required by the cutting prescription. Following the rule explained in section 5.3 we get the space-time cut-diagrams shown in Fig.(5.6). The corresponding color cut-diagrams and their decomposition into the color basis is shown in Fig.(5.7). The color decomposition of the cut diagrams can be carried out in a completely pictorial way using graphical identities of App.(C). We now proceed to calculate the space-time cut diagrams. The method of calculation is similar to the uncut diagrams described in sec-

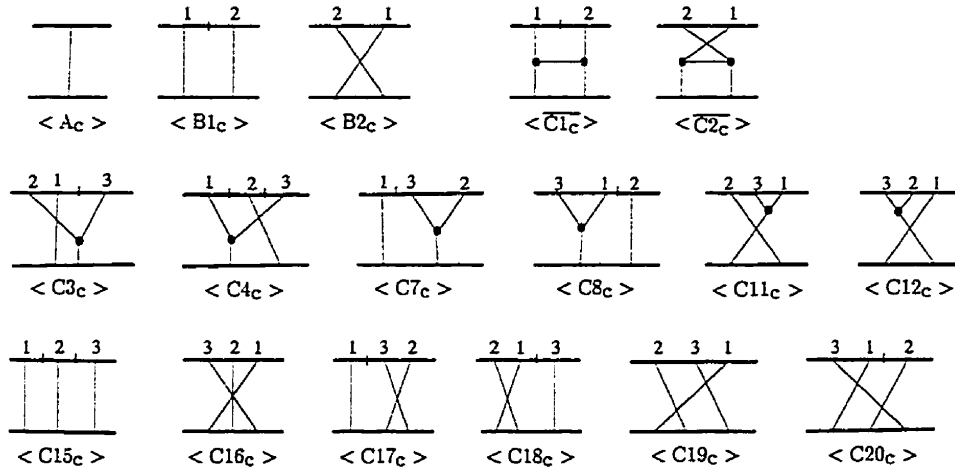


Figure 5.6: Space-time cut diagrams

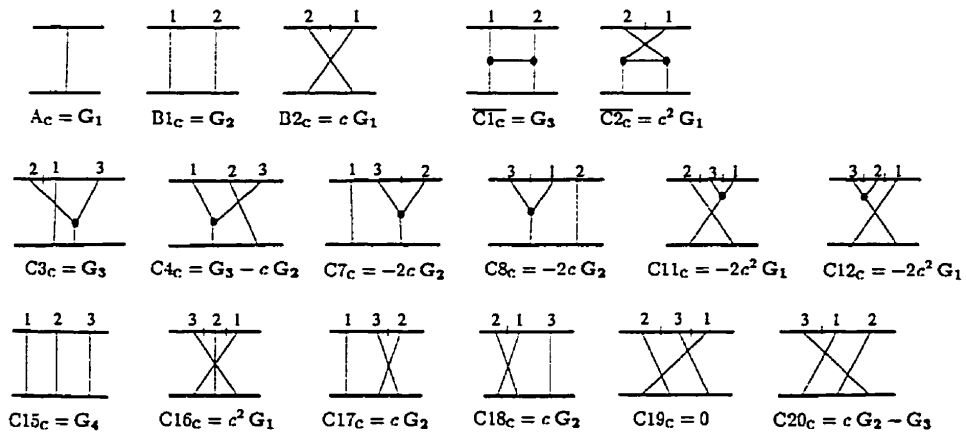


Figure 5.7: Color cut diagrams

tion 5.4 with the exception that each cut propagator has to be assigned $-2\pi i\delta(q^2 - m^2) \simeq -2\pi i\delta(sx)$ rather than $(q^2 - m^2 + i\epsilon)^{-1}$, where q is the four-momentum of the line and $q^- \equiv sx = s \sum_i x_i$.

5.6.1 Diagrams A_c , $B1_c$ and $B2_c$

The first diagram, A, is quite simple. It is equal to

$$\langle A \rangle = -\frac{2g^2s}{4m^2} \left(\frac{1}{\Delta^2} \right) = -\frac{g^2s}{2m^2} I_1(\Delta). \quad (5.6.26)$$

The flow diagrams for $B1_c$ and $B2_c$ are shown in Fig.(5.8.a,b). For $B1_c$ we have,

$$-q^+ = \frac{a_1}{\sqrt{s(1-x)}} \sim 0 \quad (5.6.27)$$

therefore

$$\begin{aligned} \langle B1_c \rangle &\simeq -\frac{g^4}{4\pi} \left(\frac{(2s)^2}{4m^2} \right) \int \mathcal{D}q_\perp \int_0^1 dx \frac{-2\pi i\delta(sx)}{a_2 a_4} \\ &= \frac{ig^4s}{4m^2} \int \mathcal{D}q_\perp \frac{1}{a_2 a_3} = \frac{ig^4s}{4m^2} I_2. \end{aligned} \quad (5.6.28)$$

Note that integrating $\delta(x)$ from zero to 1 has produced a factor of (1/2) because only half of delta function is integrated.

Next is diagram $B2_c$. The flow path is shown in Fig.(5.8.b). From the figure we see that again

$$-q^+ = \frac{a_1}{\sqrt{s(1-x)}} \sim 0, \quad (5.6.29)$$

and therefore

$$\begin{aligned} \langle B2_c \rangle &\simeq -\frac{g^4}{4\pi} \left(\frac{(2s)^2}{4m^2} \right) \int \mathcal{D}q_\perp \int_{1/s}^1 dx \frac{1}{a_2 a_4(-sx)} \\ &= \frac{g^4s \ln(s)}{4\pi m^2} \int \mathcal{D}q_\perp \frac{1}{a_2 a_4} = \frac{g^4s \ln(s)}{4\pi m^2} I_2(\Delta). \end{aligned} \quad (5.6.30)$$

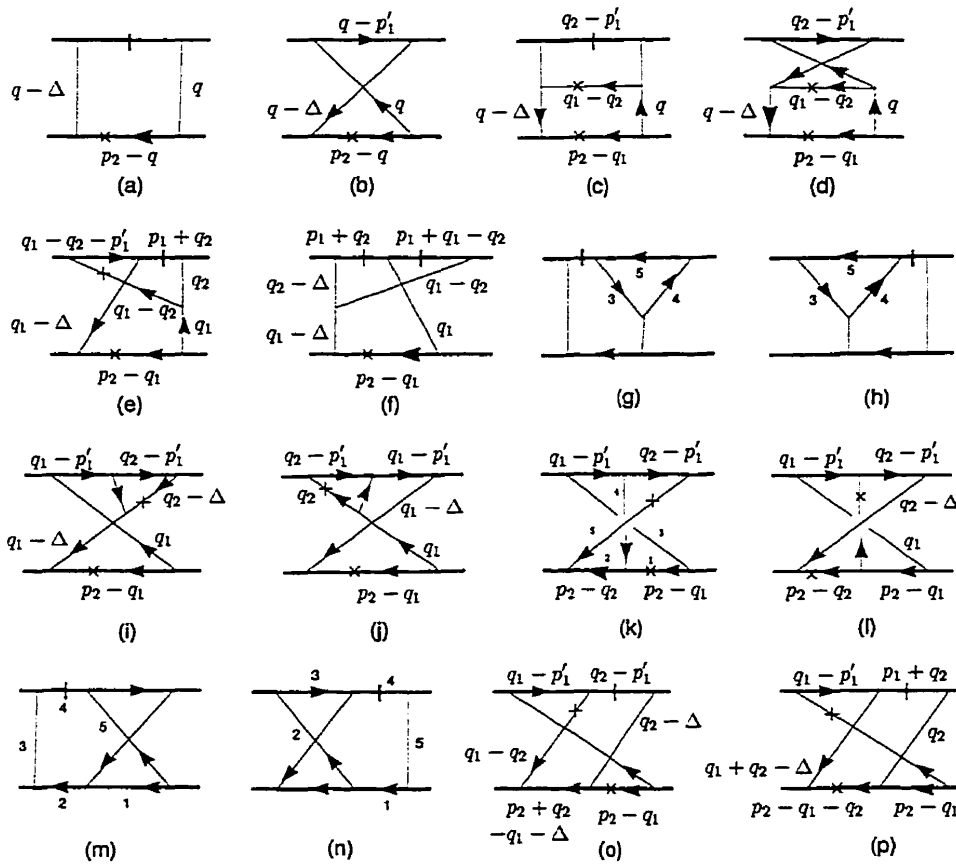


Figure 5.8: Flow diagrams

5.6.2 Diagrams $\overline{\text{C1}}_c$ and $\overline{\text{C2}}_c$

In diagrams C1 and C2 it is advantageous to first combine them with C21. In so doing one achieves a cancellation of longitudinal terms before any integration is performed. Consider Fig.(5.8.c). The numerator of this diagram is

$$\begin{aligned}
N1 &\simeq \mathbf{G}_3 \frac{g^6 s^2}{4m^2} [g^{\mu-}(q_1 - 2q_2)^+ + g^{\mu+}(q_2 - 2q_1)^- + g^{+-}(q_1 + q_2 - 2\Delta)^\mu] \\
&\quad \times g^{\mu\nu} [g^{\nu+}(q_2 - 2q_1)^- + g^{\nu-}(q_1 - 2q_2)^+ + g^{+-}(q_2 + q_1)^\nu] \\
&\simeq \mathbf{G}_3 \frac{g^6 s^2}{m^2} [q_1^- q_2^+ - (q_1 + q_2)_\perp \cdot (q_1 + q_2 - 2\Delta)_\perp], \tag{5.6.31}
\end{aligned}$$

where we have implemented $q_1^+ \simeq q_2^- \simeq 0$, since the dominant contribution comes from this region. Next consider Fig.(5.8.d), the numerator is

$$\begin{aligned}
N2 &\simeq [\mathbf{G}_3 + 2c \mathbf{G}_1] \frac{g^6 s^2}{4m^2} [g^{\mu-}(q_1 - 2q_2)^+ + g_{\mu+}(q_2 - 2q_1)^- + g_{+-}(q_1 + q_2 - 2\Delta)^\mu] \\
&\quad \times g^{\mu\nu} [g^{\nu+}(q_2 - 2q_1)^- + g^{\nu-}(q_1 - 2q_2)^+ + g^{+-}(q_2 + q_1)^\nu] \\
&\simeq [\mathbf{G}_3 + 2c \mathbf{G}_1] \frac{g^6 s^2}{m^2} [q_1^- q_2^+ - (q_1 + q_2)_\perp \cdot (q_1 + q_2 - 2\Delta)_\perp]. \tag{5.6.32}
\end{aligned}$$

Lastly, consider the C21 diagram. The numerator of this diagram is

$$\begin{aligned}
N21 &= \frac{g^6 s^2}{4m^2} (q_1 - q_2)^2 [\mathbf{G}_3 g^{+-} g^{+-} + (\mathbf{G}_3 + 2c^2 \mathbf{G}_1) g^{+-} g^{+-}] \\
&\simeq \frac{g^6 s^2}{m^2} [-q_1^- q_2^+ - (q_1 - q_2)_\perp^2] [\mathbf{G}_3 + (\mathbf{G}_3 + 2c \mathbf{G}_1)]. \tag{5.6.33}
\end{aligned}$$

Combining color factors of $N21$ with their counterparts from $N1$ and $N2$ we will get

$$\begin{aligned}
\overline{N1} &= \mathbf{G}_3 \frac{-g^6 s^2}{m^2} [(q_1 - q_2)_\perp^2 + (q_1 + q_2)_\perp \cdot (q_1 + q_2 - 2\Delta)_\perp] \\
&= \mathbf{G}_3 \frac{-2g^6 s^2}{m^2} [q_{1\perp}^2 + q_{2\perp}^2 - \Delta_\perp \cdot (q_1 + q_2)_\perp] \\
&= \mathbf{G}_3 \frac{-2g^6 s^2}{m^2} [q_{1\perp}^2 + q_{2\perp}^2 - \Delta_\perp^2], \tag{5.6.34}
\end{aligned}$$

$$\begin{aligned}
\overline{N2} &= [\mathbf{G3} + 2c \mathbf{G1}] \frac{-g^6 s^2}{m^2} [(q_1 - q_2)_\perp^2 + (q_1 + q_2)_\perp \cdot (q_1 + q_2 - 2\Delta)_\perp] \\
&= [\mathbf{G3} + 2c \mathbf{G1}] \frac{-2g^6 s^2}{m^2} [q_{1\perp}^2 + q_{2\perp}^2 - \Delta_\perp^2]. \tag{5.6.35}
\end{aligned}$$

In the last step of (5.6.34) we have rewritten $q_{1\perp} \cdot \Delta_\perp$ as

$$\Delta \cdot q_{i\perp} = \frac{1}{2} \Delta \cdot q_{i\perp} + \frac{1}{2} \Delta \cdot q_{i\perp} = \frac{1}{2} \Delta_\perp \cdot (\Delta - q_i)_\perp + \frac{1}{2} \Delta_\perp \cdot q_{i\perp} = \frac{1}{2} \Delta_\perp^2.$$

As was previously mentioned, the longitudinal terms are cancelled out. Now we can implement the cutting prescription and obtain the diagrams which were shown earlier in Fig.(5.8.c,d). In this figure we have

$$-q_1^+ = \frac{a_1}{\sqrt{s}(1-x_1)} \sim 0 \quad ; \quad q_1^+ - q_2^+ = \frac{a_4}{\sqrt{s}(x_1-x_2)},$$

$$D = (1-x_1)[a_2][a_3](x_1-x_2) \left[\frac{x_2 a_4}{x_1-x_2} + a_5 \right] \left[\frac{x_2 a_4}{x_1-x_2} + a_6 \right],$$

and the dominant contribution comes from the region $x_2 \ll x_1$. Therefore we will have

$$\begin{aligned}
\overline{C1_c} &\simeq - \left(\frac{1}{4\pi} \right)^2 \left(\frac{2g^6 s^2}{m^2} \right) \int \mathcal{D}q_{1\perp} \mathcal{D}q_{2\perp} \\
&\quad \times \int_{1/s}^1 dx_1 \int_0^{x_1} dx_2 \frac{[-2\pi i \delta(sx)] [q_{1\perp}^2 + q_{2\perp}^2 - \Delta_\perp^2]}{a_2 a_3 a_5 a_6 x_1} \\
&\simeq \frac{ig^6 s \ln(s)}{8\pi} \left[2 \int \mathcal{D}q_{1\perp} \frac{1}{(q_1 - \Delta)_\perp^2} \int \mathcal{D}q_{2\perp} \frac{1}{q_{2\perp}^2 (q_2 - \Delta)_\perp^2} \right. \\
&\quad \left. - \Delta_\perp^2 \left[\int \mathcal{D}q_{1\perp} \frac{1}{q_{1\perp}^2 (q_1 - \Delta)_\perp^2} \right]^2 \right] \\
&\simeq - \frac{ig^6 s \ln(s)}{4\pi} \left[\frac{1}{2} \Delta_\perp^2 I_2^2 - J_2 I_2 \right]. \tag{5.6.36}
\end{aligned}$$

The calculation of $\overline{C2_c}$ is similar except for the upper fermion line which is uncut and therefore there will be a $(x_1 x_2)$ factor in the denominator resulting in a factor of $\ln^2(s)$, giving

$$\overline{C2_c} \simeq - \frac{g^6 s \ln(s)^2}{8\pi m^2} \left[\frac{1}{2} \Delta_\perp^2 I_2^2 - J_2 I_2 \right]. \tag{5.6.37}$$

5.6.3 Diagrams C3_c, C4_c, C7_c, C8_c, C11_c and C12_c

The flow paths relevant to these diagrams are shown in Fig.(5.8.e-j). Consider, for example, C3_c. With the poles taken as indicated in the figure we will have

$$-q_1^+ = \frac{a_1}{\sqrt{s}(1-x_1)} \sim 0 \quad ; \quad q_1^+ - q_2^+ = \frac{a_6}{\sqrt{s}(x_1-x_2)} \quad , \quad (5.6.38)$$

for which the numerator D and the denominator N are

$$D \simeq (x_1 - x_2)a_2 \left[\frac{-x_2 a_6}{x_1 - x_2} - a_3 \right] [-s(x_1 - x_2)]a_7 \quad , \quad (5.6.39)$$

$$\begin{aligned} N &\simeq \frac{g^6[-2\pi i \delta(sx_2)](2s)^2}{4m^2} s [(x_2 - 2x_1)^- + (x_2 + x_1)] \\ &\simeq -\frac{2\pi i g^6 s^2}{m^2} \delta(x_2)[2x_2 - x_1] \quad . \end{aligned} \quad (5.6.40)$$

With the dominant contributing region being $x_2 \ll x_1$ we will have,

$$\begin{aligned} C3_c &\simeq -\left(\frac{1}{4\pi}\right) \left(\frac{-2\pi i g^6 s^2}{m^2}\right) \int \mathcal{D}q_{1\perp} \mathcal{D}q_{2\perp} \\ &\quad \times \int_{1/s}^1 dx_1 \int_0^{x_1} dx_2 \frac{-x_1 \delta(x_2)}{(-a_3)a_2 a_7 x_1 (-sx_1)} \\ &\simeq -\frac{2ig^6 s \ln(s)}{16\pi m^2} \frac{1}{2} \int \mathcal{D}q_{1\perp} \frac{1}{a_2 a_7} \int \mathcal{D}q_{2\perp} \frac{1}{a_3} \\ &\simeq -\frac{ig^6 s \ln(s)}{16\pi m^2} I_2 J_2 \quad . \end{aligned} \quad (5.6.41)$$

Next consider diagram (5.8.f). Choosing the poles as shown, the '+' momenta are fixed as in (5.6.38), then the denominator D and the numerator N will be

$$D \simeq (x_1 - x_2)a_2 a_7 \left[-\frac{x_2 a_6}{x_1 - x_2} - a_3 \right] \quad , \quad (5.6.42)$$

$$\begin{aligned} N &\simeq \frac{g^6(-2\pi i)^2 \delta(sx_2) \delta[s(x_1 - x_2)]}{4m^2} (2s)^2 s [(q_1 + q_2)^- + (q_2 - 2q_1)^-] \\ &\simeq -\frac{4g^6 \pi^2 \delta(x_2) \delta(x_1 - x_2) s}{m^2} (2x_2 - x_1) \quad . \end{aligned} \quad (5.6.43)$$

The dominant contribution comes from $x_2 \ll x_1$ and we will have in this case

$$\begin{aligned} C4_c &\simeq -\left(\frac{1}{4\pi}\right)^2 \frac{s}{m^2} \int \mathcal{D}q_{1\perp} \int \mathcal{D}q_{2\perp} \int_0^1 dx_1 \int_0^{x_1} dx_2 \frac{-4\pi^2 \delta(x_2) \delta(x_1) (-x_1)}{x_1 a_2 a_7 (-a_3)} \\ &= \frac{g^6 s}{16m^2} I_2 J_2 . \end{aligned} \quad (5.6.44)$$

Next consider $C7_c$ and $C8_c$. As one can see, because of the cut, the negative current flow is forced to go round in the (3,4,5) loop and therefore both these diagrams will vanish

$$C7_c = C8_c = 0 . \quad (5.6.45)$$

Diagrams $C11_c$ and $C12_c$ can likewise be calculated with the result

$$C11_c = C12_c = \frac{g^6 s \ln^2(s)}{32\pi^2 m^2} I_2 J_2 . \quad (5.6.46)$$

5.6.4 Diagrams $C15_c - C20_c$

We now come to the last six diagrams. The first in this set is $C15_c$. This diagram is a bit tricky to calculate using the method employed so far. The reason is a combination of the following facts. There are two cut lines, the relative magnitude of the small ‘-’ flows matter and this produces two flow diagrams without poles on the lower fermion line. To calculate this diagram, one can use the factorization formula explained in section 5.2. Because of the cuts on the top line, one can interchange the location of the lines in any of the six possible configurations. This will now allow the application of the factorization formula to the lower fermion line. This is shown pictorially in Fig.(5.9). We then will have

$$\begin{aligned} C15_c &\simeq -\frac{1}{6} \left(\frac{1}{4\pi}\right)^2 \frac{g^6 (2s)^3}{4m^2} \int \mathcal{D}q_{1\perp} \mathcal{D}q_{2\perp} \int \frac{\sqrt{s} dq_1^+}{-2\pi i} \int \frac{\sqrt{s} dq_2^+}{-2\pi i} \int dx_1 \int dx_2 \\ &\quad \times \frac{(-2\pi i)^4 \delta(sx_1) \delta(sx_2) \delta(-\sqrt{s} q_1^+) \delta(-\sqrt{s} x_2)}{q_{1\perp}^2 (q_1 - q_2)_\perp^2 (q_2 - \Delta)_\perp^2} \\ &= \frac{g^6}{12m^2} I_3 . \end{aligned} \quad (5.6.47)$$

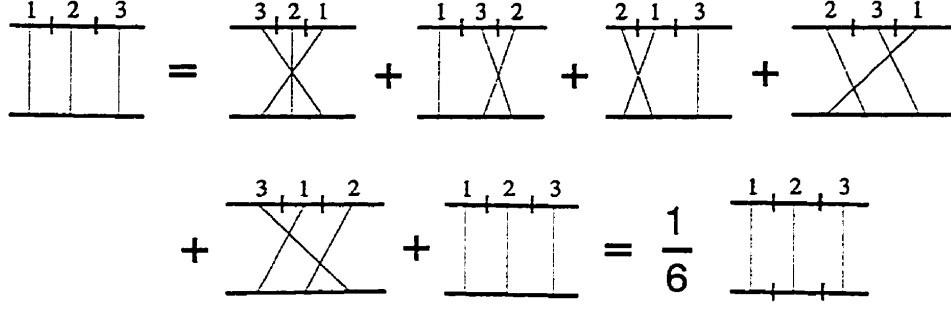


Figure 5.9: Factorization formula applied to $C15_c$

Next is $C16_c$. There are two flow diagrams as shown in Fig.(5.8.k,l). For the flow diagram (5.8.k) we have

$$-q_1^+ = \frac{a_1}{\sqrt{s}(1-x_1)} \sim 0 \quad ; \quad q_2^+ = \frac{a_5}{\sqrt{s}x_2}, \quad (5.6.48)$$

and accordingly the denominator D is

$$D = (1-x_1)x_2 \left[-\frac{a_5(1-x_2)}{x_2} - a_2 \right] [a_3] \left[-\frac{a_5(x_1-x_2)}{x_2} - a_4 \right] (-sx_2)(-sx_1). \quad (5.6.49)$$

The dominant contributing region is $x_1 \ll 1$ and $x_2 \ll 1$. So we will have,

$$\begin{aligned} C16_c^a &\simeq -\left(\frac{1}{4\pi}\right)^2 \frac{g^6(2s)^3}{4m^2} \int \mathcal{D}q_{1\perp} \mathcal{D}q_{2\perp} \\ &\quad \times \int_{1/s}^1 dx_1 \int_0^{x_1} dx_2 \frac{1}{a_5 a_3 [a_5(x_1-x_2) + a_4 x_2]} \\ &= -\frac{g^6 s \ln(s)}{8\pi^2 m^2} \int \mathcal{D}q_{1\perp} \mathcal{D}q_{2\perp} \frac{\ln\left(\frac{a_5}{a_4}\right)}{a_5 a_3 (a_5 - a_4)} \\ &= -\frac{g^6 s \ln(s)}{8\pi^2 m^2} J_3. \end{aligned} \quad (5.6.50)$$

The contribution of $C16_c^b$ is identical to that of $C16_c^a$ and therefore their sum is equal to

$$C16_c = C16_c^a + C16_c^b = 2C16_c^a \simeq -\frac{g^6 s \ln(s)}{4\pi^2 m^2} J_3. \quad (5.6.51)$$

We continue with diagrams C17_c and C18_c. In these diagrams, because of the cut the negative current is forced to flow round the loop (12345) and consequently the diagrams will vanish. Therefore we have

$$C17_c = C18_c = 0 . \quad (5.6.52)$$

Lastly, we have C19_c and C20_c. Diagram C20_c is basically the same as the uncut diagram and straightforward calculation gives

$$C20_c = -\frac{ig^6 s \ln(s)}{8\pi^2 m^2} I_3 . \quad (5.6.53)$$

we do not need to calculate diagram C19_c since its corresponding cut color diagram vanishes.

5.6.5 A recap of the final results

Before we conclude this section it would be worthwhile to summarize the results of the previous three subsections. The quark-quark scattering calculations using cut diagrams of Fig.(5.6) and (5.7) led to the following results,

$$\begin{aligned} A_c &= -\frac{g^2 s}{2m^2} I_1(\Delta) \cdot \mathbf{G}_1 , \\ B1_c &= \frac{ig^4 s}{4m^2} I_2 \cdot (c \mathbf{G}_2) , \\ B2_c &= \frac{g^4 s \ln(s)}{4\pi m^2} I_2(\Delta) \cdot (c \mathbf{G}_1) , \\ \overline{C1}_c &= -\frac{ig^6 s \ln(s)}{4\pi} \left[\frac{1}{2} \Delta_{\perp}^2 I_2^2 - J_2 I_2 \right] \cdot \mathbf{G}_3 , \\ \overline{C2}_c &= -\frac{g^6 s \ln(s)^2}{8\pi m^2} \left[\frac{1}{2} \Delta_{\perp}^2 I_2^2 - J_2 I_2 \right] \cdot (c^2 \mathbf{G}_1) , \\ C3_c &= -\frac{ig^6 s \ln(s)}{16\pi m^2} I_2 J_2 \cdot \mathbf{G}_3 , \\ C4_c &= \frac{g^6 s}{16m^2} I_2 J_2 \cdot (\mathbf{G}_3 - c \mathbf{G}_2) , \\ C11_c &= C12_c = \frac{g^6 s \ln^2(s)}{32\pi^2 m^2} I_2 J_2 \cdot (-2c^2 \mathbf{G}_1) , \end{aligned}$$

$$\begin{aligned}
C15_c &= \frac{g^6}{12m^2} I_3 \cdot \mathbf{G}_4 , \\
C16_c &= -\frac{g^6 s \ln(s)}{4\pi^2 m^2} J_3 \cdot (c^2 \mathbf{G}_1) , \\
C20_c &= -\frac{ig^6 s \ln(s)}{8\pi^2 m^2} I_3 \cdot (c \mathbf{G}_2 - \mathbf{G}_3) , \\
C7_c &= C8_c = C17_c = C18_c = C19_c = 0 .
\end{aligned} \tag{5.6.54}$$

5.7 Discussion

Having demonstrated the cut diagram calculations at some length we notice the following:

1. $\ln(s)$ factors that get cancelled in the sum of the Feynman amplitude (see points (1) to (3) in Sec.5.5) never even appear in (5.6.54). Cancellations of this kind are automatically built into the cut diagram formalism.
2. The transverse function J_3 appears only in $C16_c$ in (5.6.54). This expression survives the sum but can be ignored compared to the contribution from $\overline{C2}_c$. In other words, as opposed to the Feynman amplitude (5.5.18) where J_3 appears in many places, most of them being cancelled out at the end (see points (4) and (5) in Sec.5.5), in the cut amplitude J_3 do not appear except when it survives the sum.
3. The cut amplitude is not as successful in cancelling the transverse function J_2 (point (6) of Sec.5.5), although there is still an improvement here over (5.5.18) in that J_2 appears in fewer places. In fact, it appears in $C3_c$ to $C20_c$ only when absolutely needed to cancel its previous appearance in $\overline{C1}_c$ and $\overline{C2}_c$. In order for J_2 to disappear completely it is necessary to combine diagrams with triple and four gluon vertices together using the Lipatov-Dickinson vertex [34]. The technique of cut

diagrams by itself, which deals mainly with the fermion lines, is not sufficient for that purpose.

4. Other than the J_2 complication mentioned above, the summands of the final answer (5.5.21) appear directly in the cut amplitudes. In that sense the cut amplitudes are as economical and as simple as they can ever be. In particular, the Regge-like feature mentioned in point (3) of Sec.5.5 is present already in individual cut diagrams.

Chapter 6

Eighth-Order Diagrams with 4-point fermion loops

Leading log calculations, as were previously discussed, does not lead to the correct asymptotic amplitude of parton scattering since the total cross section following such calculations violate the Froissart bound. This fact is a hint at the relative importance of non-leading contributions since the sum of non-leading terms can in principle be comparable or even higher than the sum of leading terms. Such contributions come from different sources. One such source is the same class of diagrams that has already been considered only to leading log approximation. Systematic improvement to subleading contributions is very difficult to conduct for such diagrams and so progress along this direction faces serious problems. Another source of subleading contributions has a more subtle nature. Current finite order calculations seem to support the picture that t -channel exchanged gluons fuse into a composite, color-octet object dubbed a 'reggeized gluon' or 'reggeon'. The exchange of a single reggeon, therefore, will occur in the color-octet channel. The exchange of two reggeons, however, will occur in both the octet and singlet color channels. The color-octet contribution of two reggeon exchange is subleading to that of a single reggeon exchange since it carries an extra

factor of α_s . So, as can be seen, leading log calculations of Feynman diagrams will lead to a multi-reggeon exchange resummed structure (verified explicitly to sixth-order) within which one can identify leading as well as subleading contributions in certain color channels. There are recent studies along this direction[23, 24].

Another source of subleading contributions whose study is not as extensive as pure gluon exchange diagrams are diagrams with fermion loops. The study of such diagrams goes back to the work of Cheng and Wu [19, 26] in the context of QED. In electron-electron scattering experiments, the exchanged photons can produce electron-positron pairs. The fact that photon-photon scattering in QED is UV finite enables one to carry out the calculations without need to regularize the diagrams. Performing similar calculations in QCD, however, requires one to regularize the diagrams first. The purpose of this chapter is to take this step and find the high energy behavior of three eight-order diagrams that have been considered by Cheng and Wu in the context of QED.

6.1 Fermion loop subdiagrams

The diagrams of interest are shown in Fig.(6.1). In order to calculate the high energy behavior of such diagrams it will be helpful to look at the similar QED situation first. This has been extensively discussed by Cheng and Wu [19, 26]. In their treatment, in the leading log approximation, each of the three diagrams, similar to Fig.(6.1), turn out to carry quadratically divergent factors of transverse momenta. These factors cancel out in the sum of the three diagrams as one would naturally expect since the four photon subamplitude is finite without any need for a counter term.

The presence of quadratically divergent factors in their calculation for

each diagram is a point that makes these results not suitable for the corresponding QCD situation. In fact the quadratic divergence is something unexpected to begin with. By power counting the expected divergence is just logarithmic. The reason for this inconsistency is the imposition of high energy approximations, implemented without having dealt with the divergence of the fermion loop subamplitude.

In QCD however, one is obliged to deal with the UV divergence of the loop first. So before any high energy calculation can be achieved it is necessary to regulate the fermion loop subdiagram. Then after removing the divergence using a 4g counter-term one can move on to the asymptotic calculation. This is basically what we intend to do in this chapter.

In this section we will present the details of the regularization and removal of the divergences of the fermion loops. Then, in the next section, these results will be used in the calculation of the high energy behavior of the 8th-order diagrams. We will then see that as a result of regularization the 8th-order diagrams demonstrate $\ln^3(s)$ behavior.

First, we briefly write down the the expression of the 8th-order diagrams. Referring to Figs.(6.1.a,b,c) we have the following three amplitudes respectively,

$$(\mathcal{M}^1)_{lk}^{ji} \simeq (ig^4) \frac{s}{2^2} (W_{egcd})_{lk}^{ji} N_{\mu\sigma\nu\rho} \int \prod_{i=1}^2 \mathcal{D}p_i \frac{(\mathcal{A}_1)^{\mu\nu\rho\sigma}}{D}, \quad (6.1.1)$$

$$(\mathcal{M}^2)_{lk}^{ji} \simeq (ig^4) \frac{s}{2^2} (W_{egcd})_{lk}^{ji} N_{\mu\sigma\nu\rho} \int \prod_{i=1}^2 \mathcal{D}p_i \frac{(\mathcal{A}_2)^{\mu\nu\rho\sigma}}{D'}, \quad (6.1.2)$$

$$(\mathcal{M}^3)_{lk}^{ji} \simeq (ig^4) \frac{s}{2^2} (W_{egcd})_{lk}^{ji} N_{\mu\sigma\nu\rho} \int \prod_{i=1}^2 \mathcal{D}p_i \frac{(\mathcal{A}_3)^{\mu\nu\rho\sigma}}{D}, \quad (6.1.3)$$

$$\mathcal{D}p_i = \frac{d^2 p_{i\perp}}{(2\pi)^2} \frac{dx_i}{2\pi} \frac{dp_i^+}{2\pi} \quad (6.1.4)$$

$$D = [\sqrt{s}x_2p_2^+ - a_1][\sqrt{s}x_2p_2^+ - a_2][\sqrt{s}x_1p_1^+ - a_5][\sqrt{s}x_1p_1^+ - a_6]$$

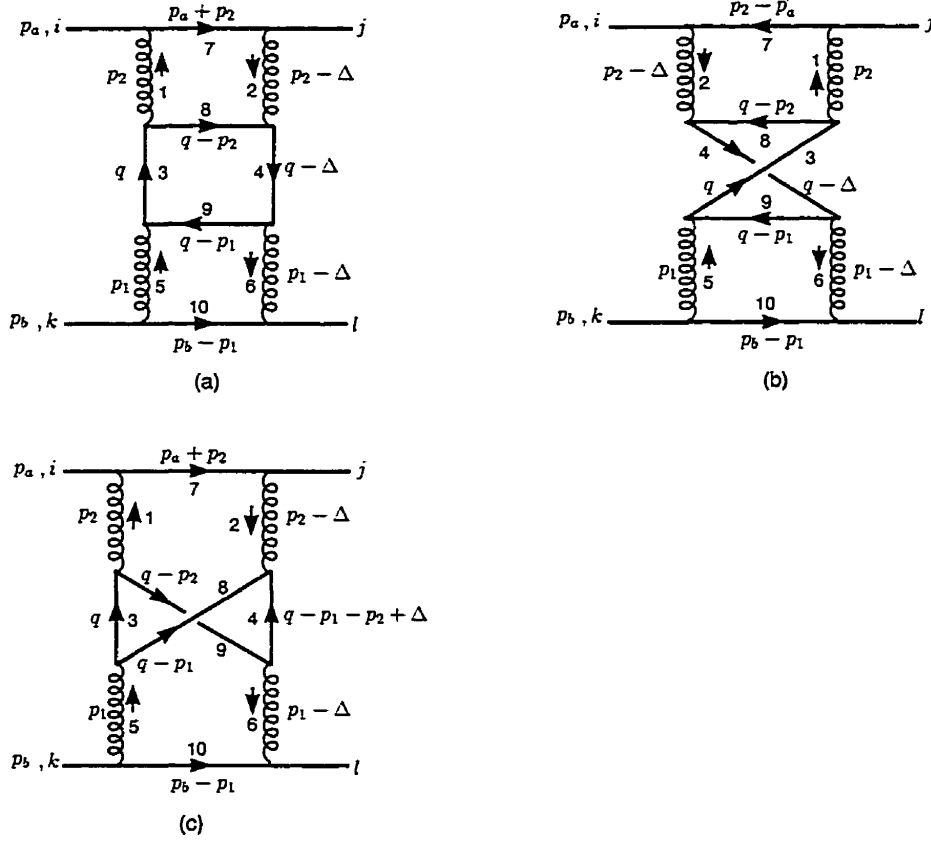


Figure 6.1: 8th-order diagrams.

$$\times [sx_2 - a_7] [\sqrt{s}(1-x_1)p_1^+ - a_{10}] , \quad (6.1.5)$$

$$D' = [\sqrt{s}x_2p_2^+ - a_1] [\sqrt{s}x_2p_2^+ - a_2] [\sqrt{s}x_1p_1^+ - a_5] [\sqrt{s}x_1p_1^+ - a_6] \\ \times [-sx_2 - a_7] [\sqrt{s}(1-x_1)p_1^+ - a_{10}] , \quad (6.1.6)$$

$$(W_{egcd})^{ji} = (T_d T_e)^{ji} (T_c T_g)_{lk} \quad ; \quad N^{\mu\nu\rho\sigma} = \frac{(2p_a^\mu)(2p_a^\nu)(2p_b^\rho)(2p_b^\sigma)}{(2m)^2} , \\ p_a^\mu = (\sqrt{s}, 0; \mathbf{0}) \quad ; \quad p_b^\mu = (0, \sqrt{s}; \mathbf{0}) . \quad (6.1.7)$$

In the above expressions \mathcal{A}_1 , \mathcal{A}_2 and \mathcal{A}_3 represent the fermion loop subamplitudes of Figs.(6.2.a,b,c), respectively. As was mentioned at the outset we will calculate these subamplitudes first. Starting with the amplitude of the

diagram of Fig.(6.2.a) we have

$$(\mathcal{A}_1)_{egcd}^{-++-} = \Gamma_{egcd}^1 A_1^{-++-} , \quad (6.1.8)$$

$$\Gamma_{egcd}^1 = Tr(T_e T_g T_c T_d) + Tr(T_e T_d T_c T_g) , \quad (6.1.9)$$

$$A_1^{-++-} = g^4 \sum_f^{N_f} \int \frac{d^4 q}{(2\pi)^4} \dots \quad (6.1.10)$$

$$\times \frac{-Tr[\gamma^-(\not{q} + m_f)\gamma^+(\not{q} - \not{p}_1 + m_f)\gamma^+(\not{q} - \not{p}_2 + m_f)\gamma^-(\not{q} - \not{p}_2 + m_f)]}{[q^2 - m_f^2][(q - \Delta)^2 - m_f^2][(q - p_1)^2 - m_f^2][(q - p_2)^2 - m_f^2]} .$$

The reason for having only one index configuration in (6.1.8) is due to the fact that p_a and p_b in (6.1.7) have only one nonvanishing lightcone component. Introducing Feynman parameters z_1, z_2 and z_3 and moving to $n = 4 - 2\epsilon$ dimensions will cast the above expression into the form

$$A_1 = \Gamma(4) g^4 \mu^{4(2-n/2)} \sum_f^{N_f} \int \mathcal{D}z \int \frac{d^n q}{(2\pi)^n} \quad (6.1.11)$$

$$\times \frac{-32(q - p_2)^-(q - p_1)^+(q_\perp^2 - q_\perp \cdot \Delta_\perp + m_f^2)}{[q^2 - 2q \cdot (z_1 p_1 + z_2 p_2 + z_0 \Delta) + z_1 p_1^2 + z_2 p_2^2 + z_0 \Delta^2 - m_f^2 + i\epsilon]^4} ,$$

$$\int \mathcal{D}z_a \equiv \int_0^1 dz_1 \int_0^{1-z_1} dz_2 \int_0^{1-z_1-z_2} dz_0 , \quad (6.1.12)$$

where we have suppressed the upper indices of A_1 for brevity and we have used

$$(\gamma^+)^2 = (\gamma^-)^2 = 0 ; \quad \gamma^\mp \not{q} \gamma^\pm = \not{q}_\perp \gamma^\mp \gamma^\pm ; \quad \gamma^\pm \not{q} \gamma^\mp = 2q^\pm \gamma^\pm ; \quad \not{q}_\perp \equiv -\vec{q}_\perp \cdot \vec{\gamma}_\perp \quad (6.1.13)$$

to simplify the numerator. Using the standard integrals, listed in App.(D) for reference, and after some algebra the above expression becomes

$$A_1 = \frac{-32i\pi^2 g^4 \mu^{2\epsilon}}{(2\pi)^4} \sum_f^{N_f} \int \mathcal{D}z_a \left[\frac{-\pi^{-\epsilon} \Gamma(\epsilon) \mu^{2\epsilon}}{(2\pi)^{-2\epsilon} D_1^\epsilon} + \frac{-(k_1 + p_1)^+(k_1 + p_2)^- + m_f^2}{D_1} \right. \\ \left. + \frac{(k_{1\perp}^2 + k_\perp \cdot \Delta_\perp + m_f^2)(k_1 + p_1)^+(k_1 + p_2)^-}{D_1^2} \right] \quad (6.1.14)$$

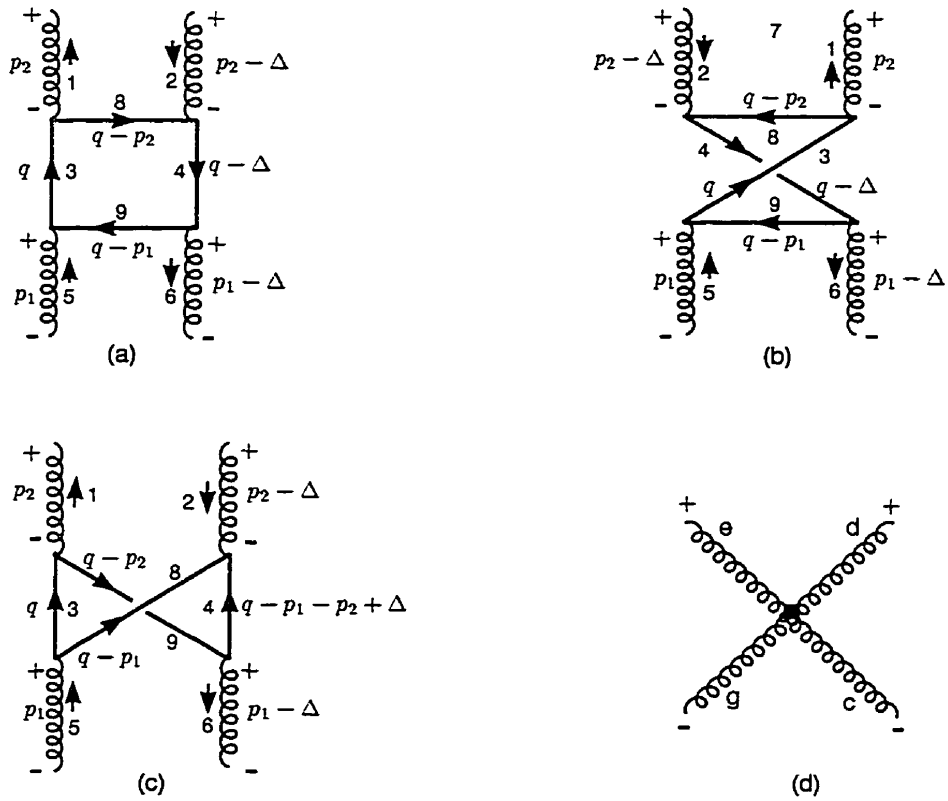


Figure 6.2: Fourth-order subdiagrams

where k_1^μ , M_1^2 and D_1 are defined by

$$k_1^\mu = -z_1 p_1^\mu - z_2 p_2^\mu - z_0 \Delta^\mu , \quad (6.1.15)$$

$$M_1^2 = -z_1 p_1^2 - z_2 p_2^2 - z_0 \Delta^2 + m_f^2 , \quad (6.1.16)$$

$$D_1 = -k_1^2 - M_1^2 + i\epsilon . \quad (6.1.17)$$

Now using

$$\Gamma(\epsilon) = \frac{1}{\epsilon} - \gamma - O(\epsilon) \quad ; \quad a^{-\epsilon} = e^{-\epsilon \ln(a)} \simeq 1 - \epsilon \ln(a) \quad (6.1.18)$$

we will get

$$\begin{aligned} A_1 = & \frac{-32i\pi^2 g^4 \mu^{2\epsilon}}{(2\pi)^4} \sum_f^{N_f} \int \mathcal{D}z_a \left[\frac{-1}{\epsilon} + \gamma - 1 + \ln\left[\frac{-m_f^2}{4\pi\mu^2}\right] + \ln\left[\frac{k_1^2 + M_1^2}{m_f^2}\right] \right. \\ & + \frac{-(k_1 + p_1)^+(k_1 + p_2)^- + m_f^2}{D_1} + 1 \\ & \left. + \frac{(k_{1\perp}^2 + k_{1\perp} \cdot \Delta_\perp + m_f^2)(k_1 + p_1)^+(k_1 + p_2)^-}{D_1^2} \right] \end{aligned} \quad (6.1.19)$$

where we have added and subtracted 1 and $\ln[-m_f^2/(4\pi\mu^2)]$ so as to make the subtraction at zero-momentum point easier.

Next we take the diagram of Fig.(6.2.b). The propagator structure of this diagram is similar to that of the previous diagram. So without any further work we can write

$$(\mathcal{A}_2)_{ecgd}^{-++-} = \Gamma_{ecgd}^2 A_2^{-++-} \quad ; \quad A_2^{-++-} = A_1^{-++-} , \quad (6.1.20)$$

$$\Gamma_{ecgd}^2 = Tr(T_e T_c T_g T_d) + Tr(T_e T_d T_g T_c) . \quad (6.1.21)$$

Next is the diagram of Fig.(6.2.c). By straightforward use of Feynman rules we get

$$(\mathcal{A}_3)_{ecdg}^{-++-} = \Gamma_{ecdg}^3 A_3^{-++-} , \quad (6.1.22)$$

$$\Gamma_{ecdg}^3 = Tr(T_e T_c T_d T_g) + Tr(T_e T_g T_d T_c) , \quad (6.1.23)$$

$$A_3^{-++-} = g^4 \sum_f^{N_f} \int \frac{d^4 q}{(2\pi)^4} \quad (6.1.24)$$

$$\times \frac{-\text{Tr}[\gamma^-(\not{q} + m_f)\gamma^+(\not{q} - \not{p}_1 + m_f)\gamma^-(\not{q} - \not{p}_1 - \not{p}_2 + \not{\Delta} + m_f)\gamma^+(\not{q} - \not{p}_2 + m_f)]}{[q^2 - m_f^2][(q - p_1)^2 - m_f^2][(q - p_2)^2 - m_f^2][(q - p_1 - p_2 + \Delta)^2 - m_f^2]}.$$

Introducing Feynman parameters and moving to $n = 4 - 2\varepsilon$ dimensions the above expression will take on the form

$$A_3 = \Gamma(4) g^4 \mu^{4(2-n/2)} \sum_f^{N_f} \int \mathcal{D}z_b \int \frac{d^n q}{(2\pi)^n} \frac{N}{D_c^4}, \quad (6.1.25)$$

where

$$\begin{aligned} N = & -32 \left[(q_\perp^2 + m_f^2)^2 + 2(q_\perp \cdot p_{1\perp})(q_\perp \cdot p_{2\perp}) - p_{2\perp}^2(q_\perp \cdot p_{1\perp}) \right. \\ & - p_{1\perp}^2(q_\perp \cdot p_{2\perp})(q_\perp^2 + m_f^2) [p_{1\perp}^2 + p_{2\perp}^2 + p_{1\perp} \cdot p_{2\perp} - 2q_\perp \cdot (p_1 + p_2)_\perp \\ & - \Delta_\perp \cdot (p_1 + p_2 - q)_\perp] + (q_\perp \cdot p_{1\perp})(p_{2\perp} \cdot \Delta_\perp) \\ & \left. + (q_\perp \cdot p_{2\perp})(p_{1\perp} \cdot \Delta_\perp) - (p_{1\perp} \cdot p_{2\perp})(q_\perp \cdot \Delta_\perp) \right], \end{aligned} \quad (6.1.26)$$

$$\begin{aligned} D_c = & q^2 - 2q \cdot [(1 - z_0 - z_2)p_1 + (1 - z_0 - z_1)p_2 - (1 - z_0 - z_1 - z_2)\Delta] \\ & + z_1 p_1^2 + z_2 p_2^2 + (1 - z_0 - z_1 - z_2)(p_1 + p_2 - \Delta)^2 - m_f^2 + i\varepsilon, \end{aligned} \quad (6.1.27)$$

$$\int \mathcal{D}z_b \equiv \int_0^1 dz_0 \int_0^{1-z_0} dz_1 \int_0^{1-z_0-z_1} dz_2. \quad (6.1.28)$$

Here we have used the identities in (6.1.13) and have carried out the gamma algebra in the numerator N . Note that the upper indices of A_3 have been suppressed for conciseness. Now performing the q integration using integral relations of App.(D) and simplifying the result we obtain

$$A_3 = \frac{-32i\pi^2 g^4 \mu^{2\varepsilon}}{(2\pi)^4} \sum_f^{N_f} \int \mathcal{D}z_b \left[\frac{2\pi^{-\varepsilon} \Gamma(\varepsilon) \mu^{2\varepsilon}}{(2\pi)^{-2\varepsilon} D_3^\varepsilon} + \frac{N_3''}{D_3^2} + \frac{N_3'}{D_3} \right], \quad (6.1.29)$$

where

$$\begin{aligned} N_3'' = & (k_{3\perp}^2 + m_f^2)^2 - (p_{1\perp} \cdot \Delta_\perp)(p_{2\perp} \cdot k_{3\perp}) + (p_{1\perp} \cdot p_{2\perp})(k_{3\perp} \cdot \Delta_\perp) - (p_{2\perp} \cdot \Delta_\perp)(p_{1\perp} \cdot k_{3\perp}) \\ & + (k_{3\perp}^2 + m_f^2) [p_{1\perp}^2 + p_{2\perp}^2 + p_{1\perp} \cdot p_{2\perp} + 2k_{3\perp} \cdot (p_1 + p_2)_\perp - \Delta_\perp \cdot (k_3 + p_1 + p_2)_\perp] \\ & + 2(p_{1\perp} \cdot k_{3\perp})(p_{2\perp} \cdot k_{3\perp}) + p_{2\perp}^2(p_{1\perp} \cdot k_{3\perp}) + p_{1\perp}^2(p_{2\perp} \cdot k_{3\perp}), \end{aligned} \quad (6.1.30)$$

$$N'_3 = -2k_{3\perp}^2 - [(p_1 + p_2)_\perp^2 - \Delta_\perp \cdot (p_1 + p_2)_\perp + 2m_f^2] - 2k_{3\perp} \cdot [2(p_1 + p_2) - \Delta]_\perp, \quad (6.1.31)$$

where in turn

$$k_3^\mu = (1 - z_0 - z_2)p_1^\mu + (1 - z_0 - z_1)p_2^\mu - (1 - z_0 - z_1 - z_2)\Delta^\mu \quad (6.1.32)$$

$$M_3^2 = -z_1 p_1^2 - z_2 p_2^2 - (1 - z_0 - z_1 - z_2)(p_1 + p_2 - \Delta)^2 + m_f^2, \quad (6.1.33)$$

$$D_3 = -k_3^2 - M_3^2 + i\epsilon. \quad (6.1.34)$$

Using (6.1.18), the first term in (6.1.29) can be simplified to

$$A_3 = \frac{-32i\pi^2 g^4 \mu^{2\epsilon}}{(2\pi)^4} \sum_f^{N_f} \int \mathcal{D}z_b \quad (6.1.35)$$

$$\times \left[\frac{2}{\epsilon} - 2\gamma + 2 - \ln\left[\frac{-m_f^2}{4\pi\mu^2}\right] - 2 \ln\left[\frac{k_3^2 + M_3^2}{m_f^2}\right] + \frac{N_3''}{D_3^2} - 1 + \frac{N_3'}{D_3} - 2 \right].$$

Each of the results in equations (6.1.19),(6.1.20) and (6.1.29) carry the UV divergent part $1/\epsilon$. The last diagram is the 4g counter term which will cancel these UV divergent terms by a suitable adjustment of the constant Z_4 . The amplitude of the diagram of Fig.(6.2.d) is,

$$\mathcal{A}_4 = 4 g^2 \mu^{2\epsilon} (Z_4 - 1) [\Gamma_{egcd}^1 + \Gamma_{ecgd}^2 - 2\Gamma_{ecdg}^3]. \quad (6.1.36)$$

Now by equating the sum of the divergent parts (plus constant terms) of $\mathcal{A}_1, \mathcal{A}_2$ and \mathcal{A}_3 with \mathcal{A}_4 we find Z_4 to be

$$Z_4 = 1 + \frac{ig^2}{12\pi^2} \left[N_f \left(\frac{1}{\epsilon} - \gamma - 1 \right) + \sum_f^{N_f} \ln\left[\frac{-m_f^2}{4\pi\mu^2}\right] \right], \quad (6.1.37)$$

which means we have subtracted the constant at $p_1^\mu = p_2^\mu = \Delta^\mu = 0$ from each of the three diagrams. The regularized results for the three fermion loop subdiagrams are then

$$A_{1reg} = \frac{-32i\pi^2 g^4}{(2\pi)^4} \sum_f^{N_f} \int \mathcal{D}z_a \left[\ln\left[\frac{k_1^2 + M_1^2}{m_f^2}\right] + \frac{N_1}{D_1} + \frac{N_1^{+-}}{D_1} + \frac{N_1'^{+-}}{D_1^2} \right] \quad (6.1.38)$$

$$A_{2reg} = A_{1reg} \quad (6.1.39)$$

$$N_1 = k_{1\perp}^2 - z_1 p_{1\perp}^2 - z_2 p_{2\perp}^2 - z_0 \Delta_{\perp}^2, \quad (6.1.40)$$

$$N_1^{+-} = -(k_1 + p_1)^+ (k_1 + p_2)^- - k_1^+ k_1^- + z_1 p_1^+ p_1^- + z_2 p_2^+ p_2^- + z_0 \Delta^+ \Delta^-,$$

$$N_1'^{+-} = (k_1 + p_1)^+ (k_1 + p_2)^- \left[k_{1\perp}^2 + k_{1\perp} \cdot \Delta_{\perp} + m_f^2 \right],$$

$$A_{3reg} = \frac{-32i\pi^2 g^4}{(2\pi)^4} \sum_f^{N_f} \int \mathcal{D}z_b \left[-2 \ln \left[\frac{k_3^2 + M_3^2}{m_f^2} \right] + \frac{N_3''}{D_3^2} - 1 + \frac{N_3}{D_3} + \frac{N_3^{+-}}{D_3} \right] \quad (6.1.41)$$

where

$$\begin{aligned} N_3 = & -4k_{3\perp}^2 + [1 - 2(z_0 + z_1 + z_2)](p_1 + p_2)_{\perp}^2 - 4k_{3\perp} \cdot (p_1 + p_2)_{\perp} \\ & + 2z_1 p_{1\perp}^2 + 2z_2 p_{2\perp}^2 + 2k_{3\perp} \cdot \Delta_{\perp} - [3 - 4(z_0 + z_1 + z_2)]\Delta_{\perp} \cdot (p_1 + p_2)_{\perp} \\ & + 2(1 - z_0 - z_1 - z_2)\Delta_{\perp}^2, \end{aligned} \quad (6.1.42)$$

$$\begin{aligned} N_3^{+-} = & 2k_3^+ k_3^- - 2z_1 p_1^+ p_1^- - 2z_2 p_2^+ p_2^- \\ & - 2(1 - z_0 - z_1 - z_2)(p_1 + p_2 - \Delta)^+ (p_1 + p_2 - \Delta)^-. \end{aligned} \quad (6.1.43)$$

In A_{1reg} and A_{2reg} only N_1/D_1 and in A_{3reg} only N_3/D_3 will produce leading asymptotic terms. This is because in the other terms one either has or will produce ‘ \pm ’ momentum components in the numerator (as a result of having a second degree pole). These will subsequently produce x_i factors in the numerator which have dampening effects, i.e., they will reduce the power of $\ln(s)$. Using the result of (6.1.38), (6.1.39) and (6.1.41) in the next section we will carry out the calculation of the asymptotic behavior of 8th-order diagrams.

6.2 8th-order Calculations

In order to determine the high energy behavior of the 8th-order diagrams it is necessary to carry out the integration over the ‘+’ and ‘-’ components of

momenta p_1 and p_2 .

Starting from (6.1.1) with \mathcal{A}_1 given by the N_1/D_1 term of (6.1.38) (D_1 is given by(6.1.17) we have,

$$(\mathcal{M}_1)_{ik}^{ji} = (W_{egcd})_{ik}^{ji} \Gamma_{egcd}^1 M_1 \quad (6.2.44)$$

where

$$M_1 = ig^4 \frac{s}{2^2} \frac{s^2}{(2m)^2} \frac{-32i\pi^2 g^4}{(2\pi)^4} \sum_f^{N_f} \int \prod_{i=1}^2 \mathcal{D}p_i \int \mathcal{D}z_\alpha \frac{N_1}{D_1 D} \quad (6.2.45)$$

where in turn

$$\begin{aligned} D &= [\sqrt{s}x_2 p_2^+ - a_1] [\sqrt{s}x_2 p_2^+ - a_2] [\sqrt{s}x_1 p_1^+ - a_5] [\sqrt{s}x_1 p_1^+ - a_6] \\ &\quad \times [sx_1 - a_7] [\sqrt{s}(1-x_1)p_1^+ - a_{10}] \end{aligned} \quad (6.2.46)$$

$$D_1 = \sqrt{s}p_1^+ F_1 - \sqrt{s}p_2^+ F_2 - T_1 + i\epsilon, \quad (6.2.47)$$

$$F_1 = f_1 x_1 - h x_2 ; \quad F_2 = h x_1 - f_2 x_2 ; \quad f_i = z_i(1-z_i) ; \quad h = z_1 z_2, \quad (6.2.48)$$

$$T_1 = f_1 p_{1\perp}^2 + f_2 p_{2\perp}^2 + f_0 \Delta_\perp^2 - 2Z_{12} p_{1\perp} \cdot p_{2\perp} - 2Z_{01} p_{1\perp} \cdot \Delta_\perp - 2Z_{02} p_{2\perp} \cdot \Delta_\perp + m_f^2,$$

$$Z_{ij} = z_i z_j. \quad (6.2.49)$$

Now we begin by carrying out the p_1^+ integration using the residue technique.

The denominator has poles for certain value of p_1^+ . These are

$$p_{1a}^+ = \frac{a_{5,6} - i\epsilon}{\sqrt{s}x_1} ; \quad p_{1b}^+ = \frac{a_{10} - i\epsilon}{\sqrt{s}(x_1 - 1)} ; \quad p_{1c}^+ = \frac{T_1 - i\epsilon}{\sqrt{s}F_1} + p_2^+ \frac{F_2}{F_1}. \quad (6.2.50)$$

The location of the poles in (6.2.50) depends on the sign and magnitude of x_1 and x_2 . Throughout this section our convention for closing the contour is as follows. For x_1 (or x_2) < 0 we close the contour of p_1^+ (p_2^+) integration from below and for $0 < x_1$ (or x_2) from above. Table 1. summarizes the pole locations.

$x_1 < 0$	$p_{1a}^+ \uparrow, p_{1b}^+ \uparrow$	$x_2 < \beta_1$	$p_{1c}^+ \downarrow$
		$\beta_1 < x_2$	$p_{1c}^+ \uparrow$
$0 < x_1 < 1$	$p_{1a}^+ \downarrow, p_{1b}^+ \uparrow$	$x_2 < \beta_1$	$p_{1c}^+ \downarrow$
		$\beta_1 < x_2$	$p_{1c}^+ \uparrow$
$1 < x_1$	$p_{1a}^+ \downarrow, p_{1b}^+ \downarrow$	$x_2 < \beta_1$	$p_{1c}^+ \downarrow$
		$\beta_1 < x_2$	$p_{1c}^+ \uparrow$

Table 1.

Here β_1 is defined by,

$$F_1 = 0 \quad \Rightarrow \quad \beta_1 = x_2 = \frac{f_1 x_1}{h}. \quad (6.2.51)$$

In this table and later such ones \uparrow (\downarrow) specify a pole residing in the upper (lower) half plane. Also \uparrow (\downarrow) indicates that the pole is being enclosed by a contour closing from above (below). Using this information the result of p_1^+ integration is

$$M_1 = \frac{g^8 s^3}{8\pi^2 m^2} \frac{2\pi i}{(2\pi)^4} \sum_f \int \prod_{i=1}^2 \mathcal{D}p_{i\perp} \int dp_2^+ \int \mathcal{D}z_a$$

$$\left[\int_{-\infty}^{\infty} dx_2 \int_0^1 dx_1 \frac{N_1}{D_{1b}} + \left\{ \int_0^{\infty} dx_1 \int_{\beta}^{\infty} dx_2 - \int_{-\infty}^0 dx_1 \int_{-\infty}^{\beta} dx_2 \right\} \frac{N_1}{D_{1c}} \right] \quad (6.2.52)$$

where

$$D_{1b} = \sqrt{s}(x_1 - 1) \left[\frac{x_1 a_{10}}{1 - x_1} + a_5 \right] \left[\frac{x_1 a_{10}}{1 - x_1} + a_6 \right] [\sqrt{s}x_2 p_2^+ - a_1][\sqrt{s}x_2 p_2^+ - a_2]$$

$$\times [sx_2 - a_7] \left[\frac{a_{10} F_1}{x_1 - 1} - \sqrt{s}F_2 p_2^+ - T_1 \right], \quad (6.2.53)$$

$$D_{1c} = \sqrt{s}F_1 [\sqrt{s}x_2 p_2^+ - a_1][\sqrt{s}x_2 p_2^+ - a_2][sx_2 - a_7]$$

$$\times \left[x_1 \left(\frac{T_1}{F_1} + \sqrt{s}p_2^+ \frac{F_2}{F_1} \right) - a_5 \right] \left[x_1 \left(\frac{T_1}{F_1} + \sqrt{s}p_2^+ \frac{F_2}{F_1} \right) - a_6 \right]$$

$$\times \left[(x_1 - 1) \left(\frac{T_1}{F_1} + \sqrt{s}p_2^+ \frac{F_2}{F_1} \right) - a_{10} \right]. \quad (6.2.54)$$

So we see that the p_1^+ integration has generated three terms. Next is the p_2^+ integration. The first integral has poles for the following values of p_2^+ ,

$$p_{2d}^+ = \frac{a_{1,2} - i\epsilon}{\sqrt{s}x_2} \quad ; \quad p_{2e}^+ = \frac{T_1 - i\epsilon}{-\sqrt{s}F_2} + \frac{a_{10}F_1}{(x_1 - 1)F_2}, \quad (6.2.55)$$

where pole locations are given in table 2.

$x_2 < 0$	$p_{2d}^+ \uparrow$		$p_{2e}^+ \uparrow$
$0 < x_2$	$p_{2d}^+ \downarrow$	$x_2 < \chi_1$	$p_{2e}^+ \uparrow$
		$\chi_1 < x_2$	$p_{2e}^+ \downarrow$

Table 2.

Here we have

$$F_2 = 0 \quad \Rightarrow \quad \chi_1 = x_2 = \frac{hx_1}{f_2}. \quad (6.2.56)$$

As for the poles in p_2^+ of the second and third integrals, they occur at,

$$\begin{aligned} p_{2f}^+ &= \frac{a_{1,2} - i\epsilon}{\sqrt{sx_2}} \quad ; \quad p_{2g}^+ = \frac{a_{5,6} - i\epsilon}{\sqrt{sx_1}} \left(\frac{F_1}{F_2} \right) - \frac{T_1}{\sqrt{sF_2}}, \\ p_{2h}^+ &= \frac{a_{10} - i\epsilon}{-\sqrt{s(1-x_1)}} \left(\frac{F_1}{F_2} \right) - \frac{T_1}{\sqrt{sF_2}}, \end{aligned} \quad (6.2.57)$$

with pole locations in Table 3.

$x_1 < 0$	$x_2 < \beta < 0$	$p_{2f}^+ \uparrow, p_{2g}^+ \uparrow, p_{2h}^+ \uparrow$
$0 < x_1 < 1$	$0 < \beta < x_2$	$p_{2f}^+ \downarrow, p_{2g}^+ \downarrow, p_{2h}^+ \uparrow$
$1 < x_1$	$0 < \beta < x_2$	$p_{2f}^+ \downarrow, p_{2g}^+ \downarrow, p_{2h}^+ \downarrow$

Table 3.

There is only one non-zero pole contribution, that of p_{2h}^+ . Thus p_2^+ integration in (6.2.52) will give

$$\begin{aligned} M_1 &= \frac{ig^8 s^3}{16\pi^3 m^2} \frac{2\pi i}{(2\pi)^2} \sum_f^{N_f} \int \prod_{i=1}^2 \mathcal{D}p_{i\perp} \int \mathcal{D}z_a \\ &\times \left[\int_0^1 dx_1 \int_0^{x_1} dx_2 \frac{N_1}{D_{1be}} + \int_0^1 dx_1 \int_\beta^\infty dx_2 \frac{N_1}{D_{1ch}} \right] \end{aligned} \quad (6.2.58)$$

where

$$\begin{aligned} D_{1be} &= -D_{1ch} = \\ &s(1-x_1)F_2(sx_2 - a_7) \left[\frac{x_1 a_{10}}{1-x_1} + a_5 \right] \left[\frac{x_1 a_{10}}{1-x_1} + a_6 \right] \\ &\times \left[x_2 \left(\frac{T_1}{F_2} + \frac{a_{10} F_1}{(1-x_1)F_2} \right) + a_1 \right] \left[x_2 \left(\frac{T_1}{F_2} + \frac{a_{10} F_1}{(1-x_1)F_2} \right) + a_2 \right]. \end{aligned} \quad (6.2.59)$$

Having completed the ‘+’ momentum integrations we still have the x_i and z_i integrations to do. As one can see M_1 receives contributions from different regions of the x_i (and z_i) integrations but enhancements come from certain regions only. So, for the asymptotic behavior of M_1 , it would be sufficient to determine those regions as $s \rightarrow \infty$. Let’s consider the first integral in (6.2.58). Inspecting the denominator D_{1be} , we see that at $F_2 = 0$ and $x_1 = 1$ it equals infinity causing the integrand to vanish. This situation occurs at the upper bound of x_1 and x_2 integrations. We do not, therefore, expect a major contribution from those points. To avoid those points let us demand that

$$0 < F_2 \quad \Rightarrow \quad x_2 < \frac{hx_1 - 1/s}{f_2}, \quad (6.2.60)$$

which places restrictions on x_1 and $z_{1,2}$ as well,

$$\begin{aligned} 0 < hx_1 - \frac{1}{s} &\Rightarrow \frac{1}{sh} < x_1 < 1 \quad \Rightarrow \quad \frac{1}{sz_1} < z_2 < 1 - z_1 \quad (6.2.61) \\ &\Rightarrow \frac{1}{s} < z_1 - z_1^2 \Rightarrow z_1^- < z_1 < z_1^+ ; \{z_1^- \simeq \frac{1}{s}, z_1^+ \simeq 1 - \frac{1}{s}\}. \end{aligned}$$

Also by introducing a cutoff ρ we can avoid $x_1 = 1$. Now consider values of x_2 sufficiently small such that,

$$x_2 \ll F_2 \quad \text{and} \quad x_2 \ll \frac{F_2}{F_1} \quad \Rightarrow \quad x_2 \ll \frac{hx_1}{1 + f_2} = \Lambda x_1 \quad (6.2.62)$$

Also x_1 could be sufficiently small such that $\frac{1}{sh} < x_1 \ll 1$. This is the region of main contribution to M_1 . Because of the smallness of x_1 and x_2 one can actually ignore the terms proportional to x_1 and x_2 in the factors of the denominator in D_{1be} . In F_2 , the x_2 term can now be ignored compared to x_1 . Now consider the second integral in (6.2.58). The major difference in this integral is that x_2 is bounded from below and therefore this integral will not make a leading contribution. One can then write

$$M_1 \simeq \frac{-g^8 s^2}{32\pi^4 m^2} \sum_f^{N_f} \quad (6.2.63)$$

$$\times \int \prod_{i=1}^2 \mathcal{D}p_{i\perp} \int_{1/s}^{1-1/s} dz_1 \int_{1/(sz_1)}^{1-z_1} dz_2 \int_0^{1-z_1-z_2} dz_0 \int_{\frac{1}{hs}}^{\rho} dx_1 \int_{\frac{1}{s}}^{\xi\Lambda x_1} dx_2 \frac{N_1}{D_{1be}}$$

$$D_{1be} \simeq a_1 a_2 a_5 a_6 h x_1 (s x_2 - a_7 + i\epsilon), \quad (6.2.64)$$

where ξ is a small constant introduced to meet the requirement of (6.2.62).

Before performing the integrations let us define a new variable, $x'_1 = \xi\Lambda x_1$ in terms of which

$$M_1 \simeq \frac{-g^8 s^2}{32\pi^4 m^2} \sum_f^{N_f}$$

$$\times \int \prod_{i=1}^2 \mathcal{D}p_{i\perp} \int_{1/s}^{1-1/s} dz_1 \int_{1/(sz_1)}^{1-z_1} dz_2 \int_0^{1-z_1-z_2} dz_0 \int_{\frac{\xi\Lambda}{sh}}^{\rho\xi\Lambda} dx'_1 \int_{\frac{1}{s}}^{x'_1} dx_2 \frac{N_1}{D_{1be}}$$

$$D_{1be} \simeq a_1 a_2 a_5 a_6 h x'_1 (s x_2 - a_7 + i\epsilon) \quad (6.2.65)$$

Now integration over x_2 yields

$$M_1 \simeq \frac{-g^8 s^2}{32\pi^4 m^2} \sum_f^{N_f} \int \prod_{i=1}^2 \mathcal{D}p_{i\perp} \int_{1/s}^{1-1/s} dz_1 \int_{1/(sz_1)}^{1-z_1} dz_2 \int_0^{1-z_1-z_2} dz_0 \int_{\frac{\xi\Lambda}{sh}}^{\rho\xi\Lambda} dx'_1$$

$$\times \frac{N_1}{s a_1 a_2 a_5 a_6 h x'_1} [\ln(s x'_1) - i\pi] \quad (6.2.66)$$

All that is left is the x'_1 and z_i integrations. This is a long and tedious calculation and we will spare the reader the details and simply state the final result which is

$$M_1 \simeq \frac{-g^8 s}{32\pi^4 m^2} \sum_f^{N_f}$$

$$\int \prod_{i=1}^2 \frac{\mathcal{D}p_{i\perp}}{a_1 a_2 a_5 a_6} \left\{ \frac{\ln^3(s)}{6} \left[-p_{1\perp}^2 - p_{2\perp}^2 + (p_1 + p_2)_\perp \cdot \Delta_\perp + \frac{5}{6} \Delta_\perp^2 \right] \right.$$

$$\left. + i\pi \left[\frac{\ln^3(s)}{6} \Delta_\perp^2 + \frac{\ln^2(s)}{3} \left\{ p_{1\perp}^2 + p_{2\perp}^2 - (p_1 - p_2)_\perp \cdot \Delta_\perp - \frac{5}{6} \Delta_\perp^2 \right\} \right] \right\} . \quad (6.2.67)$$

We now proceed to calculate the next amplitude, M_2 . As one can see from Fig.(6.1a,b) the only difference between M_2 and M_1 is in the propagator of the upper fermion line. The calculation is then similar to (6.2.65). We can thus write,

$$\begin{aligned}
(\mathcal{M}_2)_{ik}^{ji} &\simeq (W_{egcd})_{ik}^{ji} \Gamma_{ecgd}^2, \\
M_2 &\simeq \frac{-g^8 s^2}{32\pi^4 m^2} \sum_f^{N_f} \\
&\times \int \prod_{i=1}^2 \mathcal{D}p_{i\perp} \int_{1/s}^{1-1/s} dz_1 \int_{1/(sz_1)}^{1-z_1} dz_2 \int_0^{1-z_1-z_2} dz_0 \\
&\times \int_{\frac{1}{s}}^h dx'_1 \int_{\frac{1}{s}}^{x'_1} dx_2 \frac{N_1}{D_{1de}}, \\
D_{1de} &\simeq a_1 a_2 a_5 a_6 h x'_1 (-s x_2 - a_7 + i\epsilon).
\end{aligned} \tag{6.2.68}$$

This integral will not develop an imaginary part. Carrying out the x_2 integration gives,

$$\begin{aligned}
M_2 &\simeq \frac{g^8 s^2}{32\pi^4 m^2} \sum_f^{N_f} \int \prod_{i=1}^2 \mathcal{D}p_{i\perp} \int_{1/s}^{1-1/s} dz_1 \int_{1/(sz_1)}^{1-z_1} dz_2 \int_0^{1-z_1-z_2} dz_0 \int_{\frac{1}{s}}^h dx'_1 \\
&\times \frac{1}{s} \frac{N_1 \ln(sx'_1)}{a_1 a_2 a_5 a_6}.
\end{aligned} \tag{6.2.69}$$

Now performing the long integrations over x_i and z_i 's we get,

$$\begin{aligned}
M_2 &\simeq \frac{g^8 s}{32\pi^4 m^2} \sum_f^{N_f} \\
&\times \int \prod_{i=1}^2 \frac{\mathcal{D}p_{i\perp}}{a_1 a_2 a_5 a_6} \frac{\ln^3(s)}{6} \left[-p_{1\perp}^2 - p_{2\perp}^2 + (p_1 - p_2)_\perp \cdot \Delta_\perp + \frac{5}{6} \Delta_\perp^2 \right].
\end{aligned} \tag{6.2.70}$$

The last amplitude is that of (6.1.3). As was mentioned earlier only the term N_3/D_3 of A_{3reg} in (6.1.41) will have the leading contribution. So taking that term we have from (6.1.3)

$$(\mathcal{M}_3)_{ik}^{ji} \simeq (W_{egcd})_{ik}^{ji} \Gamma_{ecdg}^3 M_3 \tag{6.2.71}$$

$$M_3 = ig^4 \frac{s}{2^2} \frac{s^2}{(2m)^2} \frac{-32i\pi^2 g^4}{(2\pi)^4} \sum_f^{N_f} \int \prod_{i=1}^2 \mathcal{D}p_i \int \mathcal{D}z_b \frac{N_3}{D_3 D}, \tag{6.2.72}$$

where N_3 and D are given by (6.1.42) and (6.1.5) respectively, D_3 is given by (6.1.34) which, in terms of lightcone components, is

$$D_3 = \sqrt{s}H_2p_1^+ + \sqrt{s}H_1p_2^+ - T_2 + i\epsilon, \quad (6.2.73)$$

$$H_1 = [n_1x_2 - wx_1] \quad ; \quad H_2 = [n_2x_1 - wx_2],$$

$$n_1 = (z_0 + z_1)(1 - z_0 - z_1) \quad ; \quad n_2 = (z_0 + z_2)(1 - z_0 - z_2) \quad ;$$

$$w = (z_0 + z_1)(z_0 + z_2) - z_0,$$

$$T_2 = n_2p_{1\perp}^2 + n_1p_{2\perp}^2 - 2wp_{1\perp} \cdot p_{2\perp} + Z(1 - Z)\Delta_{\perp}^2 - 2Z_{02}(1 - Z)p_{1\perp} \cdot \Delta_{\perp} - 2Z_{01}(1 - Z)p_{2\perp} \cdot \Delta_{\perp} + m_f^2$$

$$Z = z_0 + z_1 + z_2 \quad ; \quad Z_{01} = z_0 + z_1 \quad ; \quad Z_{02} = z_0 + z_2.$$

Like the previous case we begin by performing the p_1^+ integrations. Our choice for closing the contour is as before, i.e., closing the contour from above for $0 < x_1$ and from below for $x_1 < 0$. The denominator has poles at the following values of p_{1c}^+ ,

$$p_{1a}^+ = \frac{a_{5,6} - i\epsilon}{\sqrt{s}x_1} \quad ; \quad p_{1b}^+ = \frac{a_{10} - i\epsilon}{\sqrt{s}(x_1 - 1)} \quad ; \quad p_{1c}^+ = \frac{T_2 - i\epsilon}{\sqrt{s}H_2} - p_2^+ \frac{H_1}{H_2}. \quad (6.2.74)$$

Table 4 summarizes the location of the poles for different integration regions,

Table 4.

$x_1 < 0$.	$p_{1a}^+ \uparrow, p_{1b}^+ \uparrow$	$z_2 < V(z)$	$x_2 < \beta$.	$p_{1c}^+ \uparrow$
	.	$p_{1a}^+ \uparrow, p_{1b}^+ \uparrow$	$0 < \beta$	$\beta < x_2$	e	$p_{1c}^+ \downarrow$
	.	$p_{1a}^+ \uparrow, p_{1b}^+ \uparrow$	$V(z) < z_2$	$x_2 < \beta$	f	$p_{1c}^+ \downarrow$
	.	$p_{1a}^+ \uparrow, p_{1b}^+ \uparrow$	$\beta < 0$	$\beta < x_2$.	$p_{1c}^+ \uparrow$
$0 < x_1 < 1$	a	$p_{1a}^+ \downarrow, p_{1b}^+ \uparrow$	$z_2 < V(z)$	$x_2 < \beta$	g	$p_{1c}^+ \uparrow$
	b	$p_{1a}^+ \downarrow, p_{1b}^+ \uparrow$	$\beta < 0$	$\beta < x_2$.	$p_{1c}^+ \downarrow$
	c	$p_{1a}^+ \downarrow, p_{1b}^+ \uparrow$	$V(z) < z_2$	$x_2 < \beta$.	$p_{1c}^+ \downarrow$
	d	$p_{1a}^+ \downarrow, p_{1b}^+ \uparrow$	$0 < \beta$	$\beta < x_2$	h	$p_{1c}^+ \uparrow$
$1 < x_1$.	$p_{1a}^+ \downarrow, p_{1b}^+ \downarrow$	$z_2 < V(z)$	$x_2 < \beta$	i	$p_{1c}^+ \uparrow$
	.	$p_{1a}^+ \downarrow, p_{1b}^+ \downarrow$	$\beta < 0$	$\beta < x_2$.	$p_{1c}^+ \downarrow$
	.	$p_{1a}^+ \downarrow, p_{1b}^+ \downarrow$	$V(z) < z_2$	$x_2 < \beta$.	$p_{1c}^+ \downarrow$
	.	$p_{1a}^+ \downarrow, p_{1b}^+ \downarrow$	$0 < \beta$	$\beta < x_2$	j	$p_{1c}^+ \uparrow$

where β and $V(z)$ are defined by,

$$H_2 = 0 \quad \Rightarrow \quad \beta = x_2 = \frac{n_2 x_1}{w} \quad (6.2.75)$$

$$0 = w \quad \Rightarrow \quad z_2 = V(z) \quad ; \quad V(z) = \frac{z_0(1 - z_0 - z_1)}{z_0 + z_1} . \quad (6.2.76)$$

One can now readily write down the result of p_1^+ integration,

$$\begin{aligned} M_3 &= \frac{g^8 s^3}{8\pi^2 m^2} \frac{2\pi i}{(2\pi)^4} \sum_f \int \prod_{i=1}^2 \mathcal{D}p_{i\perp} \int_0^1 dz_0 \int_0^{1-z_0} dz_1 \int dp_2^+ \\ &\quad \left[\int_0^{1-z_0-z_1} dz_2 \int dx_2 \int_0^1 dx_1 \frac{N_3}{D_b} \right. \\ &\quad - \int_{-\infty}^0 dx_1 \left\{ \int_{V(z)}^{1-z_0-z_1} dz_2 \int_{-\infty}^{\beta} dx_2 + \int_0^{V(z)} dz_2 \int_{\beta}^{\infty} dx_2 \right\} \frac{N_3}{D_c} \\ &\quad \left. + \int_0^{\infty} dx_1 \left\{ \int_0^{V(z)} dz_2 \int_{-\infty}^{\beta} dx_2 + \int_{V(z)}^{1-z_0-z_1} dz_2 \int_{\beta}^{\infty} dx_2 \right\} \frac{N_3}{D_c} \right] , \\ D_b &= \sqrt{s}(x_1 - 1) \left[\frac{x_1 a_{10}}{1 - x_1} + a_5 \right] \left[\frac{x_1 a_{10}}{1 - x_1} + a_6 \right] [sx_2 - a_7] \\ &\quad \times [\sqrt{s}x_2 p_2^+ - a_1] [\sqrt{s}x_2 p_2^+ - a_2] \left[\frac{H_2 a_{10}}{x_1 - 1} + \sqrt{s}H_1 p_2^+ - T_2 \right] , \\ D_c &= \sqrt{s}H_2 \left[\frac{x_1 T_2}{H_2} - \sqrt{s}x_1 p_2^+ \frac{H_1}{H_2} - a_5 \right] \left[\frac{x_1 T_2}{H_2} - \sqrt{s}x_1 p_2^+ \frac{H_1}{H_2} - a_6 \right] \\ &\times \left[\frac{(x_1 - 1)T_2}{H_2} - \sqrt{s}(x_1 - 1)p_2^+ \frac{H_1}{H_2} - a_{10} \right] [\sqrt{s}x_2 p_2^+ - a_1] [\sqrt{s}x_2 p_2^+ - a_2] [sx_2 - a_7] . \end{aligned}$$

Next is the p_2^+ integration. The convention for closing the contour of integration is as before. For the integrand N_3/D_b related to (a) , (b) , (c) and (d) entries in table 4 the poles of p_2^+ occur at,

$$p_{2d}^+ = \frac{a_{1,2} - i\epsilon}{\sqrt{s}x_2} \quad ; \quad p_{2e}^+ = \frac{T_2 - i\epsilon}{\sqrt{s}H_1} - \frac{H_2 a_{10}}{\sqrt{s}(x_1 - 1)H_1} .$$

The location of the two poles in different integration regions are summarized in Table 5.

Table 5.

0 < x ₁ < 1	z ₂ < V(z)	x ₂ < χ < 0	p _{2d} ⁺ ↑ , p _{2e} ⁺ ↑
		χ < x ₂ < 0	p _{2d} ⁺ ↑ , p _{2e} ⁺ ↓
	V(z) < z ₂	x ₂ < 0	p _{2d} ⁺ ↑ , p _{2e} ⁺ ↑
		0 < x ₂ < χ	p _{2d} ⁺ ↓ , p _{2e} ⁺ ↑
	z ₂ < V(z)	0 < χ < x ₂	p _{2d} ⁺ ↓ , p _{2e} ⁺ ↓
		0 < x ₂	p _{2d} ⁺ ↓ , p _{2e} ⁺ ↓

In Thable 5 χ is defined by

$$H_1 = 0 \quad \Rightarrow \quad \chi = x_2 = \frac{wx_1}{n_1}. \quad (6.2.77)$$

For the second and third integrals with integrand N_3/D_c , the poles of p_2^+ occur at

$$p_{2f}^+ = \frac{a_{1,2} - i\epsilon}{\sqrt{s}x_2} \quad ; \quad p_{2g}^+ = \frac{a_{5,6} - i\epsilon}{-\sqrt{s}x_1} \left(\frac{H_2}{H_1} \right) + \frac{T_2}{\sqrt{s}H_1},$$

$$p_{2h}^+ = \frac{a_{10} - i\epsilon}{\sqrt{s}(1-x_1)} \left(\frac{H_2}{H_1} \right) + \frac{T_2}{\sqrt{s}H_1},$$

with the location of the poles summarized in table 6,

$x_1 < 0$	$z_2 < V(z), 0 < \beta < x_2$	e	$p_{2f}^+ \downarrow, p_{2g}^+ \downarrow, p_{2h}^+ \downarrow$	$0 < H_2, 0 < H_1$
	$V(z) < z_2, x_2 < \beta < 0$	f	$p_{2f}^+ \uparrow, p_{2g}^+ \uparrow, p_{2h}^+ \uparrow$	$0 < H_2, H_1 < 0$
$0 < x_1 < 1$	$z_2 < V(z), x_2 < \beta < 0$	g	$p_{2f}^+ \uparrow, p_{2g}^+ \uparrow, p_{2h}^+ \downarrow$	$H_2 < 0, H_1 < 0$
	$V(z) < z_2, 0 < \beta < x_2$	h	$p_{2f}^+ \downarrow, p_{2g}^+ \downarrow, p_{2h}^+ \uparrow$	$H_2 < 0, 0 < H_1$
$1 < x_1$	$z_2 < V(z), x_2 < \beta < 0$	i	$p_{2f}^+ \uparrow, p_{2g}^+ \uparrow, p_{2h}^+ \uparrow$	$H_2 < 0, H_1 < 0$
	$V(z) < z_2, 0 < \beta < x_2$	j	$p_{2f}^+ \downarrow, p_{2g}^+ \downarrow, p_{2h}^+ \downarrow$	$H_2 < 0, 0 < H_1$

Table 6.

Each entry in Table 6 refers to the same entry labels as in table 4. From the above table the only non-zero contributions are those of (g) and (h) due to a pole at $p_2^+ = p_{2h}^+$ and these two differ by a sign. Putting these pieces together the result of p_2^+ integration is

$$M_3 = \frac{g^8 s^3}{8\pi^2 m^2} \frac{(2\pi i)^2}{(2\pi)^4} \sum_f^{N_f} \int \prod_{i=1}^2 \mathcal{D}p_{i\perp} \int_0^1 dz_0 \int_0^{1-z_0} dz_1 \quad (6.2.78)$$

$$\times \left[\int_0^{V(z)} dz_2 \int_0^1 dx_1 \int_x^\infty dx_2 - \int_{V(z)}^{1-z_0-z_1} dz_2 \int_0^1 dx_1 \int_0^x dx_2 \right. \\ \left. + \int_{v(z)}^{1-z_0-z_1} dz_2 \int_0^1 dx_1 \int_\beta^\infty dx_2 - \int_0^{V(z)} dz_2 \int_0^1 dx_1 \int_{-\infty}^\beta dx_2 \right] \frac{N_3}{D_{be(ch)}},$$

$$D_{be(ch)} = sH_1(1-x_1)(sx_2 - a_7) \left[\frac{x_1 a_{10}}{1-x_1} + a_5 \right] \left[\frac{x_1 a_{10}}{1-x_1} + a_6 \right] \quad (6.2.79)$$

$$\times \left[x_2 \left(\frac{T_2}{H_1} + \frac{a_{10}H_2}{(1-x_1)H_1} \right) - a_1 \right] \left[x_2 \left(\frac{T_2}{H_1} + \frac{a_{10}H_2}{(1-x_1)H_1} \right) - a_2 \right].$$

In order to determine the high energy behavior of M_3 it is necessary to find the region of x_i (and z_i) integration that makes the highest contribution or produces an enhancement. This usually occurs for small values of x_i 's. In the first two integrals the integrand vanishes at the χ boundary of x_2 integration. The same occurs at $x_1 = 1$. We can cut off the region close to $x_2 = \chi$ and $x_1 = 1$ by replacing $\chi \rightarrow \alpha\chi$ and $1 \rightarrow \xi$ where $0 < \alpha < 1$, $0 < \xi < 1$. Then we can approximate

$$\begin{aligned} |x_2| < |\chi| &\Rightarrow H_1 \simeq -wx_1 \quad ; \quad H_2 \simeq n_2x_1, & (6.2.80) \\ \frac{x_2}{H_1} &\simeq -\frac{x_2}{wx_1} \quad ; \quad \frac{x_2H_2}{(1-x_1)H_1} \simeq -\frac{n_2x_2}{w}. \end{aligned}$$

Further, if we go to regions of smaller x_2 , i.e., $|x_2| < |wx_1|$, we can ignore these last two factors as well.

The above discussion on the magnitude of x_2 further requires us to write

$$\begin{aligned} \frac{1}{s} < |w|x_1 &\Rightarrow \frac{1}{s|w|} < x_1 < 1 \Rightarrow \frac{1}{s} < |w| \\ \Rightarrow W^+(z) < z_2, \quad z_2 < W^-(z) &; \quad W^\pm = V(z) \pm \frac{1}{s(z_0 + z_1)} \end{aligned} \quad (6.2.81)$$

which places further restrictions on z_0 and z_1 . For example $z_2 < W^-$ restricts z_0 and z_1 as follows

$$\begin{aligned} 0 < z_0 < \frac{z_0(1 - z_0 - z_1) - 1/s}{z_0 + z_1} &\Rightarrow 0 < z_1 < z_1^+ \quad ; \quad z_1^+ = 1 - z_0 - \frac{1}{sz_0} \\ \Rightarrow \frac{1}{sz_0} < 1 - z_0 &\Rightarrow z_0^- < z_0 < z_0^+ \quad ; \quad z_0^- = \frac{1}{s}, \quad z_0^+ = 1 - \frac{1}{s}. \end{aligned}$$

The requirement that $W^+ < z_2$ would place the same restriction on z_0 and z_1 . Now we go back to (6.2.79). The second and third integrals don't make leading contributions as $s \rightarrow \infty$ since $|x_2|$ is bounded from below. Therefore we will have,

$$M_3 = \frac{-g^8 s^2}{32\pi^4 m^2} \sum_f \int \prod_{i=1}^2 \mathcal{D}p_{i\perp} \int_{z_0^-}^{z_0^+} dz_0 \int_0^{z_1^+} dz_1 \quad . \quad (6.2.82)$$

$$\times \left[\int_{W^+}^{1-z_0-z_1} dz_2 \int_{\frac{1}{sw}}^1 dx_1 \int_{\frac{1}{s}}^{wx_1} dx_2 - \int_0^{W^-} dz_2 \int_{\frac{1}{-sw}}^1 dx_1 \int_{wx_1}^{-\frac{1}{s}} dx_2 \right]$$

$$\times \frac{N_3}{wx_1(sx_2 - a_7)a_1a_2a_5a_6}.$$

Then if we let $x_1 = (x'_1/w)$ in the first integral and $x_1 = -(x'_1/w)$ followed by $x_2 \rightarrow -x_2$ in the second integral we will have,

$$M_3 = \frac{-g^8 s^2}{32\pi^4 m^2} \sum_f^{N_f} \int \prod_{i=1}^2 \mathcal{D}p_{i\perp} \frac{1}{a_1 a_2 a_5 a_6} \int_{z_0^-}^{z_0^+} dz_0 \int_0^{z_1^+} dz_1 \quad (6.2.83)$$

$$\times \left[\int_{W^+}^{1-z_0-z_1} dz_2 \int_{\frac{1}{s}}^w dx'_1 \int_{\frac{1}{s}}^{x'_1} dx_2 \frac{N_3}{wx'_1(sx_2 - a_7)} \right. \\ \left. - \int_0^{W^-} dz_2 \int_{\frac{1}{s}}^{-w} dx'_1 \int_{\frac{1}{s}}^{x'_1} dx_2 \frac{N_3}{wx'_1(-sx_2 - a_7)} \right].$$

Carrying out the x_2 integration we get

$$M_3 = \frac{-g^8 s^2}{32\pi^4 m^2} \sum_f^{N_f} \int \prod_{i=1}^2 \mathcal{D}p_{i\perp} \frac{1}{a_1 a_2 a_5 a_6} \int_{z_0^-}^{z_0^+} dz_0 \int_0^{z_1^+} dz_1$$

$$\times \left[\int_{W^+}^{1-z_0-z_1} dz_2 \int_{\frac{1}{s}}^w dx'_1 \frac{N_3}{swx'_1} [\ln(sx'_1) - i\pi] \right. \\ \left. - \int_0^{W^-} dz_2 \int_{\frac{1}{s}}^{-w} dx'_1 \frac{N_3 \ln(sx'_1)}{-swx'_1} \right]. \quad (6.2.84)$$

Next carrying out the integration over x'_1 yields

$$M_3 = \frac{-g^8 s}{32\pi^4 m^2} \sum_f^{N_f} \int \prod_{i=1}^2 \mathcal{D}p_{i\perp} \frac{1}{a_1 a_2 a_5 a_6} \int_{z_0^-}^{z_0^+} dz_0 \int_0^{z_1^+} dz_1$$

$$\times \left[\int_{W^+}^{1-z_0-z_1} dz_2 \frac{N_3}{w} \left[\frac{1}{2} \ln^2(s) + \ln(s) \ln(w) \right. \right. \\ \left. \left. + \frac{1}{2} \ln(w)^2 - i\pi[\ln(w) + \ln(s)] \right] \right. \\ \left. + \int_0^{W^-} dz_2 \frac{N_3}{w} \left[\frac{1}{2} \ln^2(s) + \ln(s) \ln(-w) + \frac{1}{2} \ln(-w)^2 \right] \right] \quad (6.2.85)$$

The z_i integrations are long and tedious and here we simply give the final result

$$\begin{aligned}
M_3 = & \frac{-i\pi g^8 s \ln^2(s)}{32\pi^4 m^2} \sum_f^{N_f} \int \prod_{i=1}^2 \mathcal{D}p_{i\perp} \frac{1}{a_1 a_2 a_5 a_6} \\
& \times \left[\frac{5}{3} (p_{1\perp}^2 + p_{2\perp}^2 - \Delta_\perp (p_1 + p_2)_\perp) + \frac{7}{2} p_{1\perp} \cdot p_{2\perp} + \frac{2}{9} \Delta_\perp^2 \right] .
\end{aligned} \tag{6.2.86}$$

As one can see, the real leading part has canceled out between the two terms leaving behind only the imaginary part.

Equations (6.2.67), (6.2.70) and (6.2.86) are the final results for the space-time part of diagrams in Fig.(6.1).

In brief, in this chapter we have improved on the calculation of the so called abelian contributions to the eighth-order scattering of two quarks. We used dimensional regularization to isolate the UV divergence of the fermion loop which is then removed by the four-gluon vertex counter-term. The leading terms of the finite parts are then used to calculate the high energy behavior of eighth-order diagrams. This result constitutes part of the corrections due to fermion pair production to the BFKL equation.

We would like to mention two points. A quick comparison of our results (6.2.67), (6.2.70) and (6.2.86) and those of Cheng and Wu [19] regarding energy dependence of 8th-order e-e diagrams shows that our results are generally one power of $\ln(s)$ higher than theirs. Their results however carry an infinite quadratic multiplicative integral factor that has arisen due to the lack of regularization of the diagrams. For this reason it seems to us that the extra power has more to do with the renormalization than with the true high energy behavior of the diagrams. Therefore a definitive statement regarding the true non-leading behavior should involve other diagrams that play a role in the renormalization of 4g vertex.

The second point is that since the discussion so far has been in the context

of QCD, there are other contributions that need to be considered in order to obtain the final result concerning the contribution of fermion loops up to eighth-order. These are due to the so called non-abelian diagrams and involve a combination of 3g vertex and a triangular fermion loop. What we have calculated here are the so called abelian contributions which simply means that they are like QED diagrams multiplied by color factors. Given this fact, the $\ln(s)$ dependences of the above results cannot be taken as indicating the definitive behavior of diagrams containing fermion loops as they need to be supplemented by non-abelian contributions.

In summary, the role of diagrams with fermion loops cannot *a priori* be ignored in the discussion of high energy behavior of parton scattering amplitudes on grounds of their making only non-leading contributions. One reason for this is that leading order calculations such as those offered by BFKL equation violate the Froissart bound. So, to fix this, attention has to be directed toward non-leading contributions. Although there are pure non-leading gluonic contributions as was explained at the beginning of this chapter, one cannot be *a priori* assured that other non-leading contributions such as those originating from diagrams with fermion loops are of no importance.

One other reason for considering diagrams with fermion loops is that they are inevitably tied to and mixed with pure gluonic diagrams through renormalization process. Our calculations in this chapter have been an endeavor along these lines.

Appendix A

Conventions and some fine details

A.1 Spinor helicity technique

In chapter 3 we make extensive use of the spinor helicity formalism. For that to be well defined a review of the essentials of this formalism [40] will be given here.

When considering massless fermions it is convenient to adopt the chiral representation of Dirac matrices where γ_5 is diagonal. A massless Dirac spinor with momentum p is then given by,

$$\begin{aligned} u_+(p)|_{m=0} &\equiv |p+\rangle = \sqrt{2p^0} \begin{pmatrix} \chi_+(\mathbf{p}) \\ 0 \end{pmatrix}, \\ u_-(p)|_{m=0} &\equiv |p-\rangle = -\sqrt{2p^0} \begin{pmatrix} 0 \\ \chi_-(\mathbf{p}) \end{pmatrix}, \\ \bar{u}_+(p)|_{m=0} &\equiv \langle p+| = -\sqrt{2p^0} (0 \ \chi_+^*(\mathbf{p})), \\ \bar{u}_-(p)|_{m=0} &\equiv \langle p-| = \sqrt{2p^0} (\chi_-^*(\mathbf{p}) \ 0), \end{aligned} \tag{A.1.1}$$

where the two-component helicity eigenstate $\chi_\lambda(\mathbf{p})$ satisfies

$$\sigma \cdot p \chi_\lambda(\mathbf{p}) = \lambda |\mathbf{p}| \chi_\lambda(\mathbf{p}) ; \chi_{\lambda'}^*(\mathbf{p}) \chi_\lambda(\mathbf{p}) = \delta_{\lambda\lambda'}. \tag{A.1.2}$$

The normalization adopted in (A.1.1) gives

$$\langle p \pm | \lambda^\mu | p \pm \rangle = 2p^\mu \tag{A.1.3}$$

while chirality conservation implies

$$\langle p \pm | q \pm \rangle = 0 . \quad (\text{A.1.4})$$

We also adopt the notation,

$$\langle pq \rangle \equiv \langle p - | q + \rangle \quad ; \quad [pq] \equiv \langle p + | q - \rangle , \quad (\text{A.1.5})$$

and since $\sigma_2 \sigma \sigma_2 = -\sigma^*$, it is convenient to choose the phase of the helicity eigenstates to satisfy

$$\sigma_2 \chi_\lambda(\mathbf{p}) = i \lambda \chi_\lambda^*(\mathbf{p}) . \quad (\text{A.1.6})$$

This then implies

$$\langle pq \rangle = - \langle qp \rangle \quad ; \quad [pq] = -[qp] = \text{sign}(p \cdot q) \langle qp \rangle^* . \quad (\text{A.1.7})$$

Throughout our discussion we assume vectors to be in the forward lightcone so $p \cdot q \geq 0$. The choice of phase also gives rise to the relations

$$\begin{aligned} \langle p \pm | \gamma_{\mu_1} \cdots \gamma_{\mu_{2n+1}} | q \pm \rangle &= \langle q \pm | \gamma_{\mu_{2n+1}} \cdots \gamma_{\mu_1} | p \pm \rangle , \\ \langle p \pm | \gamma_{\mu_1} \cdots \gamma_{\mu_{2n}} | q \mp \rangle &= - \langle q \pm | \gamma_{\mu_{2n+1}} \cdots \gamma_{\mu_1} | p \mp \rangle . \end{aligned} \quad (\text{A.1.8})$$

Using (A.1.3) and

$$\gamma \cdot p = |p+ \rangle \langle p- | + |p- \rangle \langle p+ | \quad (\text{A.1.9})$$

it is easy to see that

$$\langle p+ | \gamma \cdot k | q+ \rangle = [pk] \langle kq \rangle \quad ; \quad \langle p- | \gamma \cdot k | q- \rangle = \langle pk \rangle [kq] . \quad (\text{A.1.10})$$

In particular using (A.1.3) one gets

$$\langle qp \rangle [pq] = 2p \cdot q \quad (\text{A.1.11})$$

Fierz identities can be expressed as

$$\langle AD \rangle \langle CB \rangle + \langle AC \rangle \langle BD \rangle = \langle AB \rangle \langle CD \rangle \quad (\text{A.1.12})$$

$$[AD][CB] + [AC][BD] = [AB][CD] , \quad (\text{A.1.13})$$

$$\langle A + |\gamma_\mu|B+ \rangle \langle C - |\gamma^\mu|D- \rangle = 2[AD] \langle CB \rangle , \quad (\text{A.1.14})$$

$$\langle A + |\gamma_\mu|B+ \rangle \langle C + |\gamma^\mu|D+ \rangle = 2[AC] \langle DB \rangle . \quad (\text{A.1.15})$$

The spinor-helicity representation of polarization vector for an outgoing photon or gluon with momentum p and helicity \pm is given by,

$$\epsilon_\pm^\mu(p, k) = \pm \frac{\langle p \pm | \gamma^\mu | k \pm \rangle}{\sqrt{2} \langle k \mp | p \pm \rangle} \quad (\text{A.1.16})$$

where the *reference momentum* k is massless but otherwise arbitrary. The choice of a different value of k corresponds to the choice of a different gauge, and these different choices are related by

$$\epsilon_+^\mu(p, k) \rightarrow \epsilon_+^\mu(p, k') - \sqrt{2} \frac{\langle k k' \rangle}{\langle k p \rangle \langle k' p \rangle} p^\mu . \quad (\text{A.1.17})$$

The polarization vectors satisfy the following identities:

$$\begin{aligned} \epsilon_\pm^\mu(p, k) &= (\epsilon_\mp^\mu(p, k))^* & ; & \quad p \cdot \epsilon_\pm(p, k) = k \cdot \epsilon(p, k) = 0 , \\ \epsilon_\pm(p, k) \cdot \epsilon_\pm(p, k') &= 0 & ; & \quad \epsilon_\pm(p, k) \cdot \epsilon_\mp(p, k') = -1 , \\ \epsilon_\pm(p, k) \cdot \epsilon_\pm(p', k) &= 0 & ; & \quad \epsilon_\pm(p, k) \cdot \epsilon_\pm(k, k') = 0 , \end{aligned} \quad (\text{A.1.18})$$

and also satisfy the following two relations

$$\epsilon_+^\mu(p, k) \epsilon_-^\nu(p, k) + \epsilon_-^\mu(p, k) \epsilon_+^\nu(p, k) = -g^{\mu\nu} + \frac{p^\mu k^\nu + p^\nu k^\mu}{p \cdot k} , \quad (\text{A.1.19})$$

$$\gamma \cdot \epsilon_\pm(p, k) = \pm \frac{\sqrt{2}}{\langle k \mp | p \pm \rangle} (|p \mp \rangle \langle k \mp | + |k \pm \rangle \langle p \pm |) , \quad (\text{A.1.20})$$

which completes our quick review of the spinor helicity formalism.

A.1.1 Off-shell Fierz identities

In section (3.1) we mentioned that the diagrammatic relations hold even when the momenta of the lines are off-shell. This fact relies on the off-shell versions of the Fierz identities in (A.1.13). Here we show how these off-shell relations could be derived from the on-shell ones. Our considerations in section (3.1) were restricted to tree-level diagrams, so an off-shell momentum can always be written as a sum of on-shell external momenta,

$$p_A^\mu = \sum_i c_{Ai} p_i^\mu, \quad (\text{A.1.21})$$

where p_i^μ are the external momenta and $c_{Ai} = \{-1, 0, 1\}$ depending on how one decomposes a given internal momentum. Now it follows from (A.1.9) that

$$\not{p}_A = \sum_i c_{Ai} \not{p}_i = \sum_i c_{Ai} (|p_{i+}\rangle\langle p_{i+}| + |p_{i-}\rangle\langle p_{i-}|). \quad (\text{A.1.22})$$

Notice that of the two terms in the above relation, which is the typical numerator of an interim fermion propagator, only one will eventually survive because at the end points one always multiplies by the definite helicity spinors of the external lines. So we can further define

$$|p_{A\pm}\rangle\langle p_{A\pm}| \equiv \sum_i c_{Ai} |p_{i\pm}\rangle\langle p_{i\pm}|. \quad (\text{A.1.23})$$

To see what the off-shell Fierz identity looks like consider the following expression,

$$I \equiv \langle p_a + | \not{p}_A \not{p}_B | p_b - \rangle \langle p_c + | \not{p}_C \not{p}_D | p_d - \rangle, \quad (\text{A.1.24})$$

where p_a, p_b, p_c and p_d are arbitrary on-shell momenta not necessarily those of the incoming ones. Now using (A.1.23) we can write the above expression as

$$I = [a p_A] \langle p_A p_B \rangle [p_B b] [c p_C] \langle p_C p_D \rangle [p_D d]. \quad (\text{A.1.25})$$

The on-shell Fierz relation for the angle brackets can now be used to expand the product of the two angle brackets in the above relation,

$$\begin{aligned}
I &= [ap_A] \langle p_{APD} \rangle [p_B b] [c p_C] \langle p_C p_B \rangle [p_D d] \\
&\quad + [ap_A] \langle p_{APC} \rangle [p_B b] [c p_C] \langle p_B p_D \rangle [p_D d] \\
&= \langle p_a + |\not{p}_A \not{p}_D | p_{d-} \rangle \langle p_c + |\not{p}_C \not{p}_B | p_{b-} \rangle \\
&\quad + \langle p_a + |\not{p}_A \not{p}_C | p_{c-} \rangle \langle p_b + |\not{p}_B \not{p}_D | p_{d-} \rangle \quad (A.1.26)
\end{aligned}$$

This last equality is the off-shell version of the Fierz relations for the angle brackets. The on-shell relation can be retrieved if we assume all the momenta with capital-letter lower index are on-shell momenta. In this case one can discard all the on-shell square bracket factors from both sides of the first equality as they are well defined on-shell spinor products and the remaining angle bracket factors will make the on-shell relation.

Similarly, one can work out the off-shell Fierz relation for the square brackets. It reads

$$\begin{aligned}
&\langle p_a - |\not{p}_A \not{p}_B | p_{b+} \rangle \langle p_c - |\not{p}_C \not{p}_D | p_{d+} \rangle \\
&\quad = \langle p_a - |\not{p}_A \not{p}_D | p_{d+} \rangle \langle p_c - |\not{p}_C \not{p}_B | p_{b+} \rangle \\
&\quad + \langle p_a - |\not{p}_A \not{p}_C | p_{c+} \rangle \langle p_b - |\not{p}_B \not{p}_D | p_{d+} \rangle \quad (A.1.27)
\end{aligned}$$

Two other useful relations which can be worked out following the above procedure are,

$$\begin{aligned}
&\langle p_a \pm |\not{p}_A | p_{b\pm} \rangle \langle p_c \pm |\not{p}_C \not{p}_D | p_{d\mp} \rangle \\
&\quad = \langle p_b \mp |\not{p}_C | p_{c\mp} \rangle \langle p_a \pm |\not{p}_A \not{p}_D | p_{d\mp} \rangle \\
&\quad - \langle p_b \mp |\not{p}_D | p_{d\mp} \rangle \langle p_a \pm |\not{p}_A \not{p}_C | p_{c\mp} \rangle, \quad (A.1.28) \\
&\langle p_a \mp |\not{p}_A | p_{b\mp} \rangle \langle p_c \pm |\not{p}_C \not{p}_D | p_{d\mp} \rangle
\end{aligned}$$

$$\begin{aligned}
&= \langle p_a \mp \not{p}_D | p_d \mp \rangle \langle p_c \pm \not{p}_C \not{p}_A | p_b \mp \rangle \\
&\quad + \langle p_a \mp \not{p}_C | p_c \mp \rangle \langle p_b \pm \not{p}_A \not{p}_D | p_d \mp \rangle . \tag{A.1.29}
\end{aligned}$$

A.2 Supersymmetry conventions

Our conventions follow those of Sohnius [41]. The Minkowski flat-space metric is taken to be,

$$g_{\mu\nu} = \text{diag}(+, -, -, -) , \tag{A.2.30}$$

Dirac matrices are taken in the Chiral representation as

$$\gamma^\nu = \begin{pmatrix} 0 & \sigma^\nu \\ \bar{\sigma}^\nu & 0 \end{pmatrix} , \tag{A.2.31}$$

where the the four matrices σ^ν and $\bar{\sigma}^\mu$ are defined in terms of Pauli-matrices σ and $\mathbf{1}$ as,

$$\sigma^\nu = (\mathbf{1}, \sigma) \quad ; \quad \bar{\sigma}^\mu = (\mathbf{1}, \sigma) . \tag{A.2.32}$$

The γ_5 and $\sigma^{\mu\nu}$ are defined as follows

$$\gamma_5 = \gamma_0 \gamma_1 \gamma_2 \gamma_3 = \begin{pmatrix} -i & 0 \\ 0 & i \end{pmatrix} \quad ; \quad \sigma^{\mu\nu} = \frac{i}{2} [\gamma^\mu, \gamma^\nu] . \tag{A.2.33}$$

A general spinor $\psi(x)$ satisfying the Dirac equation

$$(i\not{\partial} - m)\psi(x) = 0$$

has the following representation independent mode expansion,

$$\psi(x) = \int \frac{d^3 p}{(2\pi)^3 2p^0} \sum_{\lambda=\pm} [b_\lambda(p) e^{-ip \cdot x} u_\lambda(p) + d_\lambda^\dagger(p) e^{ip \cdot x} v_\lambda(p)] \tag{A.2.34}$$

where $u_\lambda(p)$ and $v_\lambda(p)$ are spinor wavefunctions of definite helicity λ and momentum p and satisfy,

$$\begin{aligned}
(\not{p} - m)u_\lambda(p) &= 0 \quad ; \quad (\not{p} + m)v_\lambda(p) = 0 , \\
C\bar{u}_\lambda^\dagger(p) &= v_\lambda(p) \quad ; \quad C\bar{v}_\lambda^\dagger(p) = u_\lambda(p) , \tag{A.2.35}
\end{aligned}$$

where \mathcal{C} is the charge conjugation operator and in the representation (A.2.31) is given by

$$\mathcal{C} = \begin{pmatrix} -i\sigma^2 & 0 \\ 0 & i\sigma^2 \end{pmatrix}. \quad (\text{A.2.36})$$

Equation (A.2.34) represents the expansion of an unconstrained spinor. If we impose the Majorana constraint

$$\psi^{\text{M}}(x) = \psi^{\text{c}}(x) \equiv \mathcal{C} (\overline{\psi}^\dagger)^\text{T},$$

then together with (A.2.35) we will have,

$$\psi^{\text{M}}(x) = \int \frac{d^3p}{(2\pi)^3 2p^0} \sum_{\lambda=\pm} [b_\lambda(p) e^{-ip \cdot x} u_\lambda(p) + b_\lambda^\dagger(p) e^{ip \cdot x} v_\lambda(p)] \quad (\text{A.2.37})$$

which represents a self-conjugate (Majorana) field where the anti-particle (second term) is identical to the particle (first term).

A.3 Some fine details

In equation (2.2.6) we gave the results for the SUSY transformations of on-shell particle creation and annihilation operators. Here we will show how these commutation relations are derived from the general off-shell SUSY transformations of (2.2.5).

Consider $|\Psi\rangle$ to be an arbitrary quantum state. Then we will have

$$0 = \langle 0 | \widehat{Q} \Phi | \Psi \rangle = \langle 0 | [\widehat{Q}, \Phi] | \Psi \rangle + \langle 0 | \Phi \widehat{Q} | \Psi \rangle, \quad (\text{A.3.38})$$

where $\widehat{Q} = \bar{\xi} Q$ and Φ stands for λ^a or A_μ^a . Here we have used the fact that the vacuum is invariant under SUSY transformations which would imply $\widehat{Q}|0\rangle = 0 = \langle 0|\widehat{Q}$. By appropriate choice of the state Ψ for each field we can find how the on-shell operators transform under SUSY transformations. Let us begin by choosing $|\Psi\rangle = |g_h^a(p)\rangle$ for $\Phi \equiv \lambda^a$ where $|g_h^a(p)\rangle$ represents

an incoming gluon with definite momentum p , helicity h and color a . Then we will have using (2.2.5)

$$0 = -\frac{1}{2}\sigma^{\mu\nu}\xi < 0 | (\partial_\mu A_\nu^a - \partial_\nu A_\mu^a) | g_h^a(p) > + < 0 | \lambda^a \widehat{Q} | g_h^a(p) > . \quad (\text{A.3.39})$$

Note that in $F^{(a)\mu\nu}$ we have dropped the term proportional to g because we are considering free on-shell states. The action of \widehat{Q} on a gluon state will produce, up to a constant, a fermion state

$$\widehat{Q} | g_h^a(p) > = n_h(p, k) | \Lambda_h^a(p) > , \quad (\text{A.3.40})$$

so we will have

$$n_h(p, k) | p, h > e^{-ip \cdot x} = i \frac{1}{2} \sigma^{\mu\nu} \xi e^{-ip \cdot x} (p_\mu \epsilon_{h,\nu}^{in}(p) - p_\nu \epsilon_{h,\mu}^{in}(p)) , \quad (\text{A.3.41})$$

where we have used¹

$$\begin{aligned} < 0 | \lambda^a | \Lambda_h^a(p) > &= e^{-ip \cdot x} u_h^a(p) \equiv e^{-ip \cdot x} \chi^a | p, h > , \\ < 0 | A_\mu^a | g_h^a(p) > &= e^{-ip \cdot x} \epsilon_{h,\mu}^{a,in}(p) , \end{aligned} \quad (\text{A.3.42})$$

and where χ^a is the color wave function and $| p, h >$ represents the spinor wave function. Note that the color index a in (A.3.41) has been dropped since the color wave function of the fermion and vector particle are the same and therefore can be dropped from all terms. In order to proceed we need an explicit representation for the polarization vector. Choosing this to be the spinor-helicity basis representation,

$$\epsilon_{h,\mu}^{out}(p, q) = h \frac{< p, h | \gamma_\mu | q, h >}{\sqrt{2} < q, -h | p, h >} \quad \text{For outgoing } p , \quad (\text{A.3.43})$$

with q the reference momentum, we will have upon multiplying (A.3.41) by $< q, -h |$,

$$n_h(p, k) < q, -h | p, h > = \dots$$

¹For a review of spinor-helicity basis see App. (A.1)

$$i < q, -h | \sigma^{\mu\nu} [|k+ \rangle \bar{\theta} + |k- \rangle \theta] p_\mu \epsilon_{-h,\nu}^{out}(p, q), \quad (\text{A.3.44})$$

where we have used

$$\xi \equiv |k+ \rangle \bar{\theta} + |k- \rangle \theta \quad (\text{A.3.45})$$

$$\epsilon_{h,\nu}^{in}(p, q) = [\epsilon_{h,\nu}^{out}(p, q)]^* = \epsilon_{-h,\nu}^{out}(p, q) = -h \frac{\langle p, h | \gamma_\nu | q, h \rangle}{\sqrt{2} \langle q, h | p, -h \rangle}, \quad (\text{A.3.46})$$

and where in (A.3.45) θ and $\bar{\theta}$ are two anti-commuting numbers introduced to represent the anticommuting nature of ξ . Now, fixing the helicity $h = +$ in (A.3.44) and using explicit form of $\sigma^{\mu\nu}$ together with (A.3.46) will give,

$$\begin{aligned} n_+ \langle qp \rangle &= -\frac{1}{2} \bar{\theta} \{ \langle q - \not{p} \not{\epsilon}_-^{out}(p, q) - \not{\epsilon}_-^{out}(p, q) \not{p} | k+ \rangle \} \\ &= -\frac{1}{2} \bar{\theta} \left\{ \frac{-\sqrt{2}}{[qp]} \langle qp \rangle [pq] \langle \bar{p} \not{\epsilon} \rangle + \frac{\sqrt{2}}{[qp]} \langle qp \rangle [qp] \langle pk \rangle \right\} \\ n_+ &= +\sqrt{2} \bar{\theta} \langle kp \rangle. \end{aligned} \quad (\text{A.3.47})$$

Similarly, we can work out the result for $h = -$, with the result

$$n_- = -\sqrt{2} \theta [kp]. \quad (\text{A.3.48})$$

The job is now half complete. Going back to (A.3.38) and choosing $\Phi \equiv A_\mu^a$ and $|\Psi \rangle = |\Lambda_h^a(p) \rangle$ and using (2.2.5) we obtain

$$0 = -i \langle 0 | i \bar{\xi} \gamma_\mu \lambda^a | \Lambda_h(p)^a \rangle + \langle 0 | A_\mu^a \hat{Q} | \Lambda_h(p)^a \rangle. \quad (\text{A.3.49})$$

Also since supersymmetry transforms fermionic states into gluonic ones we will have

$$\hat{Q} | \Lambda_h^a(p) \rangle = m_h(p, q) | g_h^a(p) \rangle, \quad (\text{A.3.50})$$

then (A.3.49) will take on the form,

$$\begin{aligned} -m_h(p, k) \langle 0 | A_\mu^a | g_h^a \rangle &= \bar{\xi} \gamma_\mu \langle 0 | \lambda^a | \Lambda_h^a \rangle \\ -m_h(p, k) \epsilon_{h,\mu}^{in}(p, k) &= \bar{\xi} \gamma_\mu | p, h \rangle \\ -m_h(p, k) \frac{-h \langle k, h | \gamma_\mu | p, h \rangle}{\sqrt{2} \langle k, h | p, -h \rangle} &= (\bar{\theta} \langle k- | + \theta \langle k+ |) \gamma_\mu | p, h \rangle \end{aligned} \quad (\text{A.3.51})$$

Now if we let $h = \pm$ we will get,

$$m_+(p, k) = +\sqrt{2} \theta [kp] \quad ; \quad m_-(p, k) = -\sqrt{2} \bar{\theta} \langle kp \rangle . \quad (\text{A.3.52})$$

Having found the constants resulting from the action of \widehat{Q} on gluon and fermion states we can now easily find the transformation of on-shell operators. To this end let us write (A.3.40) as follows,

$$\widehat{Q} \widehat{g}_h^\dagger(p)|0 \rangle = [\widehat{Q}, g_h^\dagger(p)]|0 \rangle = n_h(p, k) \widehat{\Lambda}_h^\dagger(p)|0 \rangle , \quad (\text{A.3.53})$$

so we will have

$$\begin{aligned} [\widehat{Q}, g_+^\dagger(p)] &= +\sqrt{2} \bar{\theta} \langle kp \rangle \widehat{\Lambda}_+^\dagger(p) \equiv +N_-(p, k) \widehat{\Lambda}_+^\dagger(p) , \\ [\widehat{Q}, g_-^\dagger(p)] &= -\sqrt{2} \theta [kp] \widehat{\Lambda}_+^\dagger(p) \equiv -N_+(p, k) \widehat{\Lambda}_+^\dagger(p) , \end{aligned} \quad (\text{A.3.54})$$

and similarly we can find the supersymmetric transformation of Λ^\dagger by writing (A.3.50) as

$$\widehat{Q} \widehat{\Lambda}_h^\dagger(p)|0 \rangle = [\widehat{Q}, \Lambda_h^\dagger(p)]|0 \rangle = m_h \widehat{g}_h^\dagger(p)|0 \rangle . \quad (\text{A.3.55})$$

Replacing for both values of h we will get

$$\begin{aligned} [\widehat{Q}, \Lambda_+^\dagger(p)] &= +\sqrt{2} \theta [kp] \widehat{g}_+^\dagger(p) \equiv +N_+(p, k) \widehat{g}_+^\dagger(p) , \\ [\widehat{Q}, \Lambda_-^\dagger(p)] &= -\sqrt{2} \bar{\theta} \langle kp \rangle \widehat{g}_+^\dagger(p) \equiv -N_-(p, k) \widehat{g}_+^\dagger(p) , \end{aligned} \quad (\text{A.3.56})$$

and finally taking hermitian conjugation of (A.3.54) and (A.3.56) we will get the commutation relations used in (2.2.6).

Appendix B

Color oriented vertices

Color oriented vertices can be derived from normal vertices in the following way. Begin with the 3g and 4g vertex factors, written

$$T_{\alpha\beta\gamma}^{abc} = igf^{abc}[g_{\alpha\beta}(p_1 - p_2)_\gamma + g_{\beta\gamma}(p_2 - p_3)_\alpha + g_{\gamma\alpha}(p_3 - p_1)_\beta], \quad (\text{B.0.1})$$

$$\begin{aligned} W_{\alpha\beta\gamma\delta}^{abcd} = & -g^2[f^{abe}f^{ecd}(g_{\alpha\gamma}g_{\beta\delta} - g_{\alpha\delta}g_{\beta\gamma}) + f^{ace}f^{ebd}(g_{\alpha\beta}g_{\gamma\delta} - g_{\alpha\delta}g_{\beta\gamma}) \\ & + f^{bce}f^{ead}(g_{\beta\alpha}g_{\gamma\delta} - g_{\beta\delta}g_{\alpha\gamma})]. \end{aligned} \quad (\text{B.0.2})$$

From the commutation relation of the group algebra one can write the structure constants f^{abc} in terms of traces of products of fundamental representation matrices, t^a , as in

$$f^{abc} = -i(\text{Tr}(t^a t^b t^c) - \text{Tr}(t^a t^c t^b)). \quad (\text{B.0.3})$$

Using this trace representation the 3g vertex factor decomposes into two color-oriented vertices both of whose color-oriented factors can be expressed by

$$(T_{c.o.}^1)_{\alpha\beta\gamma}^{abc} = \text{Tr}(t^a t^b t^c)g[g_{\alpha\beta}(p_1 - p_2)_\gamma + g_{\beta\gamma}(p_2 - p_3)_\alpha + g_{\gamma\alpha}(p_3 - p_1)_\beta] \quad (\text{B.0.4})$$

see Fig.(B.1). The above factor is specifically that of the first diagram on the right side. It can simply be read off the graph by turning clockwise. For the

$$\begin{aligned}
 & \text{Diagram 1} = \text{Diagram 2} + \text{Diagram 3} \\
 & \text{Diagram 4} = \text{Diagram 5} + \text{Diagram 6} + \text{Diagram 7} + \text{Diagram 8} + \text{Diagram 9} + \text{Diagram 10} \\
 & \text{Diagram 11} = \text{Tr}(t^a t^b t^c t^d) \left(2 \frac{a}{d} \frac{b}{c} - \frac{a}{d} \frac{b}{c} - \frac{a}{d} \frac{b}{c} \right)
 \end{aligned}$$

Figure B.1: Color-oriented vertices.

second graph the same clockwise rotation rule for color indices and momenta holds and the factor is

$$(T_{c.o.}^2)_{\alpha\beta\gamma}^{acb} = \text{Tr}(t^a t^c t^b) g [g_{\alpha\beta} (p_2 - p_1)_\gamma + g_{\beta\gamma} (p_3 - p_2)_\alpha + g_{\gamma\alpha} (p_1 - p_3)_\beta] \quad (\text{B.0.5})$$

Similarly, using the same replacement for the structure constants, the 4g vertex splits into six different trace combinations, all of which can be expressed by a single color-oriented vertex factor

$$(W_{c.o.})_{\alpha\beta\gamma\delta}^{abcd} = g^2 \text{Tr}(t^a t^b t^c t^d) [2g_{\alpha\gamma} g_{\beta\delta} - g_{\alpha\delta} g_{\beta\gamma} - g_{\alpha\beta} g_{\gamma\delta}], \quad (\text{B.0.6})$$

which represents the color-oriented factor of the first diagram on the right side in Fig.(B.1).

Appendix C

Color decomposition of cut and ordinary Feynman diagrams

As was mentioned in chapter 5, summing up diagrams with color factors is feasible only when they have the same color or their color factor has been decomposed in terms of a basis so that one can sum up the coefficients of the same color basis elements. Here we will work out these color decompositions in a graphical manner.

Let t_a be the generators of $SU(N)$ group satisfying the commutation relation

$$[t_a, t_b] = i f_{abc} t_c \quad (\text{C.0.1})$$

and normalized according to,

$$\text{Tr}(t_a t_b) = \frac{1}{2} \delta_{ab} . \quad (\text{C.0.2})$$

The constants f_{abc} are the group structure constants and are antisymmetric in all the indices. Then it follows that

$$f_{abc} f_{abd} = 2c \delta_{cd} \quad ; \quad i^3 f_{adg} f_{bed} f_{cge} = i c f_{abc} , \quad (\text{C.0.3})$$

which can be represented pictorially as in Fig.(C.1). Combining (C.0.1) and the first equation in (C.0.3) we get $i f_{bad} t_a t_b = c t_d$ which is shown pictorially

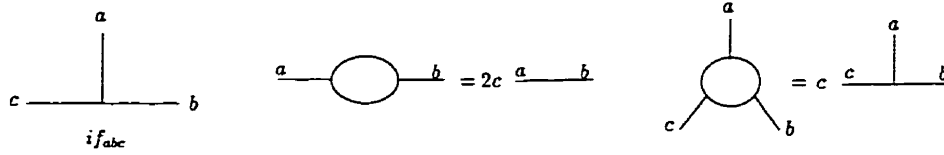


Figure C.1: (a) Triple-gluon color factor, (b),(c) Two identities involving 3g vertex.

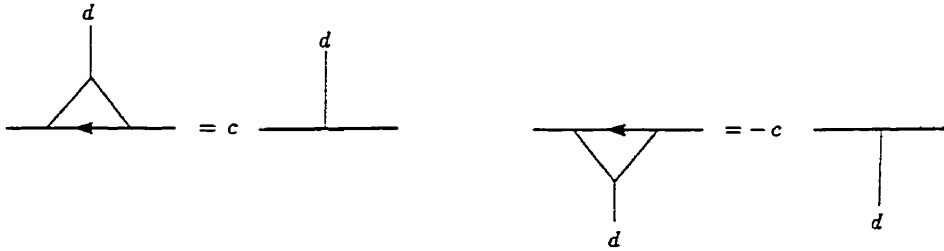


Figure C.2: Two different forms of $if_{bad}t_at_b = ct_d$.

in Fig(C.2). Also, taking a cut on the fermion line to be the commutation of two t_a matrices we can draw the set of relations in Fig.(C.3). Now, using these graphical relations, we can analyze all the color factors that were encountered in chapter 5. Figures (C.4) and (C.5) are examples of a ordinary Feynman diagram and a cut diagram analyzed using graphical relations.

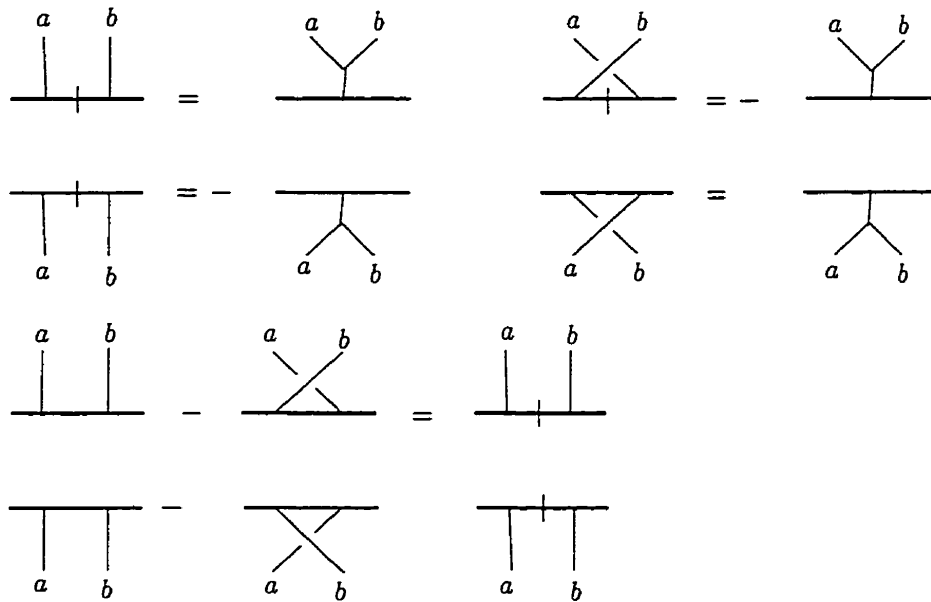


Figure C.3: Final set of graphical relations.

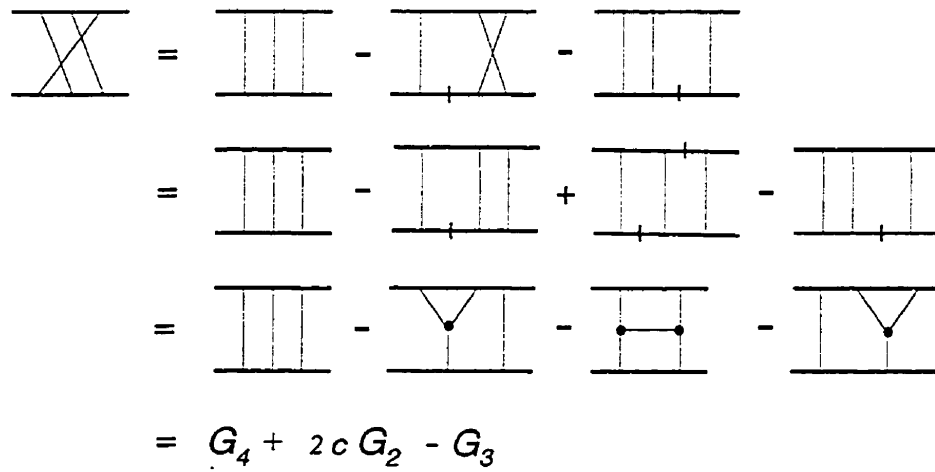


Figure C.4: A sample calculation of the color of a Feynman diagram.

$$\begin{aligned}
\text{Diagram 1} &= - \text{Diagram 2} = - \text{Diagram 3} + \text{Diagram 4} \\
&= - c^2 \text{Diagram 5} - \text{Diagram 6} \\
&= - c^2 \text{Diagram 5} + \text{Diagram 7} = - c^2 \text{Diagram 5} + c^2 \text{Diagram 8} = 0
\end{aligned}$$

Figure C.5: A sample calculation of the color of a cut diagram.

Appendix D

Dimensional Regularization formulas

Below is a list of standard integrals [42] that were used in chapter 6 to regularize the UV divergence of the fermion loop.

$$\begin{aligned}
 \int d^n k \frac{1}{(k^2 + 2k \cdot q - m^2)^\alpha} &= \frac{i\pi^{n/2} \Gamma(\alpha - n/2)}{\Gamma(\alpha) (-q^2 - m^2)^{\alpha - n/2}}, \\
 \int d^n k \frac{k^\mu}{(k^2 + 2k \cdot q - m^2)^\alpha} &= \frac{-i\pi^{n/2} \Gamma(\alpha - n/2)}{\Gamma(\alpha) (-q^2 - m^2)^{\alpha - n/2}} q^\mu, \\
 \int d^n k \frac{k^\mu k^\nu}{(k^2 + 2k \cdot q - m^2)^\alpha} &= \frac{i\pi^{n/2}}{\Gamma(\alpha) (-q^2 - m^2)^{\alpha - n/2}} [q^\mu q^\nu \Gamma(\alpha - n/2) \\
 &\quad + \frac{1}{2} g^{\mu\nu} (-q^2 - m^2) \Gamma(\alpha - 1 - n/2)], \\
 \int d^n k \frac{k^\mu k^\nu k^\lambda}{(k^2 + 2k \cdot q - m^2)^\alpha} &= \frac{i\pi^{n/2}}{\Gamma(\alpha) (-q^2 - m^2)^{\alpha - n/2}} \left[-q^\mu q^\nu q^\lambda \Gamma(\alpha - n/2), \right. \\
 &\quad \left. -\frac{1}{2} (g^{\mu\nu} q^\lambda + g^{\nu\lambda} q^\mu + g^{\lambda\mu} q^\nu) \right. \\
 &\quad \left. \times (-q^2 - m^2) \Gamma(\alpha - 1 - n/2) \right], \\
 \int d^n k \frac{k^\mu k^\nu k^\lambda k^\rho}{(k^2 + 2k \cdot q - m^2)^\alpha} &= \frac{i\pi^{n/2}}{\Gamma(\alpha) (-q^2 - m^2)^{\alpha - n/2}} \left[q^\mu q^\nu q^\lambda q^\rho \Gamma(\alpha - n/2), \right. \\
 &\quad \left. +\frac{1}{2} (q^\mu q^\nu g^{\lambda\rho} + \text{perm}) (-q^2 - m^2) \Gamma(\alpha - 1 - n/2), \right. \\
 &\quad \left. +\frac{1}{4} (g^{\mu\nu} g^{\lambda\rho} + \text{perm}) (-q^2 - m^2)^2 \Gamma(\alpha - 2 - n/2) \right].
 \end{aligned}$$

Bibliography

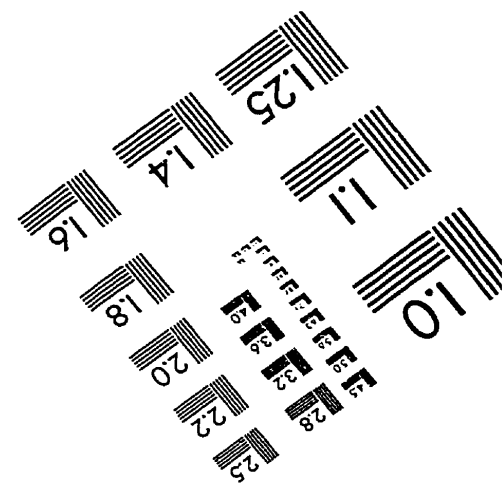
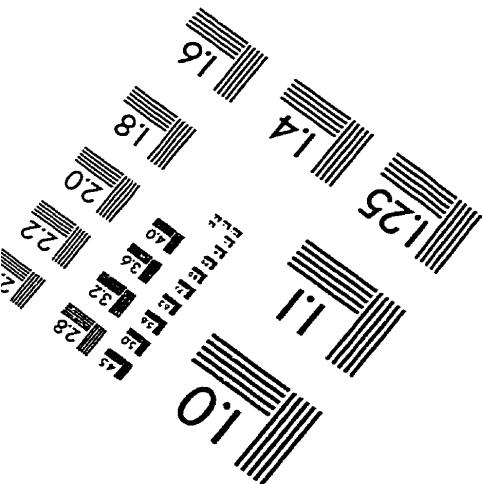
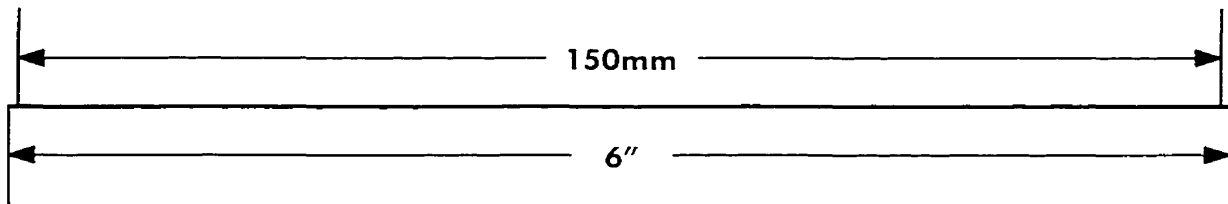
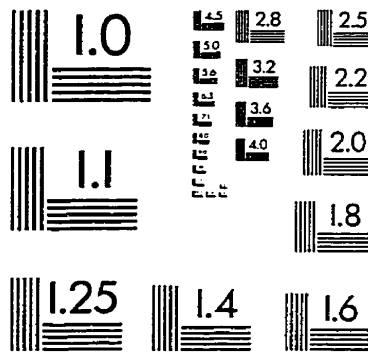
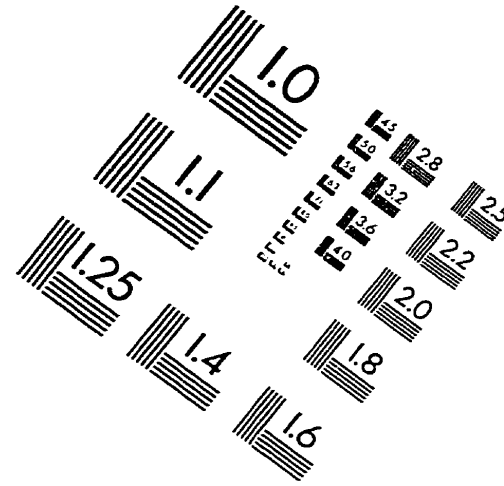
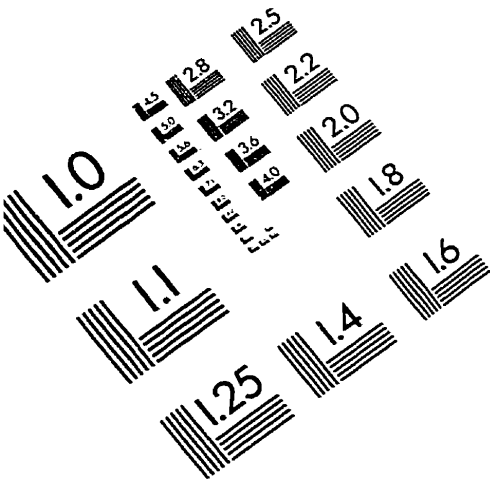
- [1] J. Wess and J. Bagger, *Introduction to Supersymmetry and Supergravity* 2nd edition, World Scientific, Singapore, (1990).
- [2] M.T. Grisaru, H.N. Pendleton and P. van Nieuwenhuizen, *Phys.Rev.* **D15** (1977) 996.
- [3] M.T. Grisaru and H.N. Pendleton, *Nucl.Phys.* **B124** (1977) 81.
- [4] Z. Bern, L. Dixon and D. Kosower, *Nucl.Phys.* **B437** (1995) 259.
- [5] Yu.A. Gol'fand and E.P. Likhtman, *JETP Letters* **13** (1971) 323.
- [6] J. Wess and B. Zumion, *Nucl.Phys.* **B70** (1974) 39.
- [7] P. Goddard, *Nucl.Phys.* **B88** (1975) 429; A. Pais and V. Rittenberg, *J.Math.Phys.* **16** (1975) 2062; **17** (1976) 598.
- [8] S.J. Parke and T.R. Taylor, *Phys.Lett.* **157B** (1985) 81.
- [9] P. Cvitanovic, P.G. Lauwers and P.N. Scharbach, *Nucl.Phys.* **B186** (1981) 165.
- [10] M.L. Mangano and S.J. Parke, *Phys.Rep.* **200**(1991) 301.
- [11] U. Amaldi et al., *Phys.Lett.* **B44** (1973) 112.
- [12] S.R. Amendolia et. al., *Phys.Lett.* **B44** (1973) 119.

- [13] A. Donnachie, P.V. Landshoff, *Nucl.Phys.* **B231** (1983) 189; *Nucl.Phys.* **B244** (1984) 322; *Nucl.Phys.* **B267** (1986) 690; *Phys. Lett.* **B296** (1992) 227.
- [14] ZEUS Collaboration (M. Derrick et al.), *Phys.Lett.* **B315** (1993) 481; *Phys.Lett.* **332** (1994) 228; H1 Collaboration (T. Ahmed et al.), *Nucl.Phys.* **B429** (1994) 477; *Phys.Lett.* **B348** (1995) 681.
- [15] M. Froissart, *Phys.Rev.* **123** (1961) 1053.
- [16] A. Martin, *Nuovo Cimento* **42** (1966) 930.
- [17] P.D.B. Collins. 'An Introduction to Regge Theory and High energy Physics', Cambridge University Press, Cambridge, (1977).
- [18] F.E. Low, *Phys.Rev.* **D12** (1975) 163; S. Nussinov, *Phys.Rev.Lett* **34** (1975) 1286.
- [19] H. Cheng and T.T. Wu, *Expanding Proton: Scattering at High Energies*, M.I.T. Press 1987.
- [20] N.T. Nieh and Y.P. Yao, *Phys.Rev.Lett.* **32** (1974) 1074; *Phys. Rev.* **D13** (1976) 1082; B. McCoy and T.T. Wu, *Phys.Rev.Lett.* **35** (1975) 604; *Phys.Rev.* **D12** (1975) 3257; **D13** (1976) 1076; L. Tyburski, *ibid.* **13** (1976) 1107; L.L. Frankfurt and V.E. Sherman, *Yad.Fiz.* **23** (1976) 1099 [*Sov.J.Nucl.Phys.* **23** (1976) 581]; A.L. Mason, *Nucl.Phys.* **B117** (1976) 493.
- [21] C.Y. Lo and H. Cheng, *Phys.Rev.* **D13** (1976) 1131; **D15** (1977) 2959; H. Cheng, J.A. Dickinson, and K. Olausen, *Phys.Rev.* **D23** (1981) 534.
- [22] C.S. Lam and K.F. Liu, *Nucl.Phys.* **B483** (1997) 514.

- [23] Y.J. Feng and C.S. Lam, *Phys.Rev.* **D55** (1997) 4016.
- [24] C. Ewerz, *Towards an effective theory of small- x QCD*, **hep-ph/9707257**.
- [25] V.S. Fadin and L.N. Lipatov, *Nucl.Phys.* **B477** (1996) 767; G. Camici and M. Ciafaloni, *Phys.Lett* **B386** (1996) 341.
- [26] H. Cheng and T.T. Wu, *Phys.Rev.* **D1** (1970) 2775.
- [27] A. Bottino, A.M. Langoni and T. Regge, *Nuovo Cimento* **23** (1962) 954.
- [28] C.S. Lam *Nonabelian Cut Diagrams*, Lectures given at Pacific Workshop on Strong Interactions. Aug. 1996. **hep-ph/9704240**.
- [29] G.V. Frolov, V.N. Gribov and L.N. Lipatov, *Phys.Lett.* **31B** (1970) 34; *Yad.Fiz.* **12** (1970) 994 [*Sov.J.Nucl.Phys.* **12**, (1971) 543.]
- [30] V. Del Duca, *An introduction to perturbative QCD pomeron and to jet physics at large rapidities*, **hep-ph/9503226**.
- [31] I.S. Gradshteyn and I.H. Ryzhik, 'Table of Integrals, Series and Products', Academic Press, (1965).
- [32] L.N. Lipatov, *Yad.Fiz.* **23** (1976) 642 [*Sov.J.Nucl.Phys.* **23** (1976) 338].
- [33] P. Ramond, *Field theory: A Modern Primer*, Addison-Wesley, 1989 (section 4.9)
- [34] E.A. Kuraev, L.N. Lipatov and V.S. Fadin, *Zh.Eksp.Teor.Fiz* **71** (1976) 840 [*Sov.Phys.JETP* **44** (1976) 443]; J.A. Dickinson, *Phys.Rev.* **16** (1977) 1863.
- [35] Y.J. Feng, O.Hamidi-Ravari and C.S. Lam, *Phys.Rev.* **D54** (1996) 3114.

- [36] H. Cheng and T.T. Wu, *Phys.Rev* **186** (1969) 1611; M. Levy and J.Sucher, *Phys.Rev.* **186** (1969) 1656.
- [37] C.Y. Lo, *Nucl.Phys.* **B157** (1979) 212; *Phys.Rev.* **D23** (1981) 508.
- [38] L.N. Lipatov, *Yad.Fiz.* **23** (1976) 642 [*Sov.J.Nucl.Phys.* **23** (1976) 338]; Ya.Ya. Baliskii and L.N. Lipatov, *Yad.Fiz* **28** (1978) 1597 [*Sov.J.Nucl.Phys.* **28** (1978) 822].
- [39] J. Bartels *Phys.Lett.* **68B** (1977) 258; *Nucl.Phys.* **B151** (1979) 293; J.B.Bronzan and R.L. Sugar, *Phys.Rev.* **D17** (1978) 585; V.N. Gribov, *Zh.Eksp.Teor.Fiz.* **53** (1967) 654; L.V. Gribov, E.M. Levin and M.G. Ryskin, *Phys.Rep.* **100** (1983) 1.
- [40] M. Mangano and S.J. Parke. *Nucl.Phys.* **B299** (1988) 673; *Phys.Rev.* **D39** (1989) 758; *Phys.Rep.* **200** (1991) 301.
- [41] M.F. Sohnius, *Phys.Rep* **128** (1985) 39.
- [42] M. Kaku, '*Quantum Field Theory*', Oxford University Press, (1993).

IMAGE EVALUATION TEST TARGET (QA-3)



APPLIED IMAGE, Inc
1653 East Main Street
Rochester, NY 14609 USA
Phone: 716/482-0300
Fax: 716/288-5989

© 1993, Applied Image, Inc., All Rights Reserved